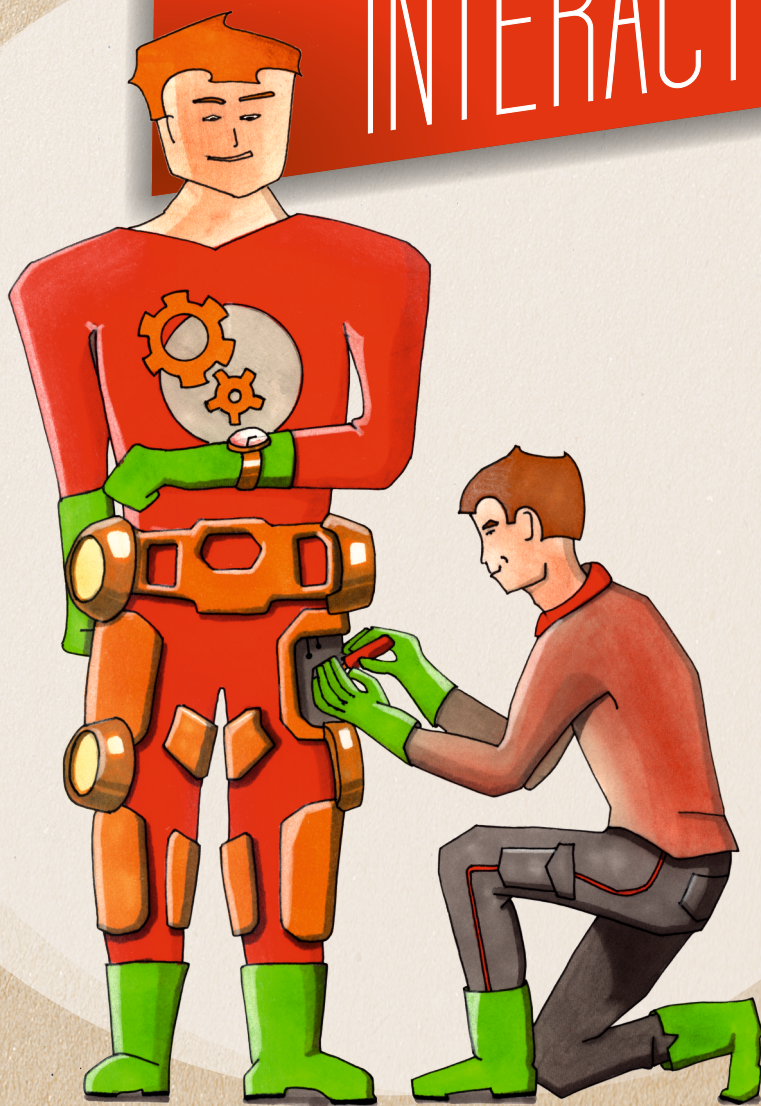


HUMAN-EXOSKELETON

INTERACTION



WIETSE VAN DIJK



# Human–Exoskeleton Interaction

Wietse van Dijk



# Human–Exoskeleton Interaction

Proefschrift

ter verkrijging van de graad van doctor aan de Technische Universiteit Delft op  
gezag van de Rector Magnificus prof. ir. K.C.A.M. Luyben; voorzitter van het  
College van Promoties, in het openbaar te verdedigen op dinsdag 21 april 2015 om  
10:00 uur

door

Willem VAN DIJK  
ingenieur geboren te Goes, Nederland

Dit proefschrift is goedgekeurd door de promotoren:

Prof. dr. ir. Herman van der Kooij

Prof. dr. Frans van der Helm

De promotiecommissie bestaat uit:

Rector magnificus, voorzitter

Prof. dr. ir. Herman van der Kooij 3ME – TU Delft

Prof. dr. Frans van der Helm 3ME – TU Delft

Onafhankelijke leden:

Prof.dr.ir. J. Harlaar

Vrije Universiteit Amsterdam

Prof.dr. D. De Clercq

Universiteit Gent, België

Prof.dr. C.J. Walsh

Harvard University, Verenigde Staten

Prof.dr.ir. H.F.J.M. Koopman

Universiteit Twente

Prof.dr.ir. R.H.M. Goossens

IO – TU Delft

Reservelid:

Prof.dr.ir. P. Breedveld 3ME

3ME – TU Delft

Dit onderzoek is financieel ondersteund door de Europese Unie via het Evryon Project (FP7-ICT-2007-3-231451) en Toyota.

ISBN: 978-94-6186-463-5

A digital copy of this dissertation can be obtained from <http://repository.tudelft.nl>

Author e-mail: [wietsevandijk@gmail.com](mailto:wietsevandijk@gmail.com)

# Contents

Summary	7
Samenvatting	13
1 Introduction	19
2 Background	25
3 Optimization of human walking for exoskeletal support	39
4 Real-time Motion Analysis and Parameter Estimation with a Multibody Kalman Filter	53
5 Improving the transparency of a rehabilitation robot by exploiting the cyclic behavior of walking	73
6 A Passive Exoskeleton with Artificial Tendons: Design and experimental evaluation	89
7 XPED <sub>2</sub> : A Passive Exoskeleton with Artificial Tendons	101
8 The Achilles Ankle Exoskeleton	113
9 Conclusions, Discussion, and Future Directions	139
10 Appendix: MKF and Equations of motion	153
References	169
List of figures	183
Dankwoord / Thanks	185
Publications	189
About the author	191
Propositions	193
Stellingen	195



# Summary

---

Walking is a very efficient way of getting around and covering large distances. Due to impairments or in extreme conditions, such as carrying a heavy load, one might encounter difficulties while walking. In many cases, wheeled vehicles offer a solution. However, wheeled vehicles are often not suitable for indoor environments or heavy outdoor terrain. Furthermore, wheeled vehicles do not exploit the walking capabilities of the human.

As an alternative, exoskeletons have been proposed. These exoskeletons fit around the human body as a portable mechanical suit. The effort and control needed to fulfill a task are shared by the human and the exoskeleton. Human physical effort is measured by metabolism. Metabolism can be measured by recording the intake and exchange of oxygen and carbon dioxide. Many different exoskeletons have been developed in recent decades. Recently experiments showed that walking metabolism can be reduced with an exoskeleton.

The goal of this dissertation is to improve exoskeletons that reduce the metabolic cost of walking. One of the main difficulties in achieving this goal is the difficulty in determining in advance what the effect of the exoskeleton will be on the metabolic energy consumption of walking. As a consequence, the design process is characterized by trial and error. This dissertation contributes to improving the complete design process, which includes the modelling, the hardware and control design, and the evaluation of exoskeletons. Based on a literature review, three challenges were defined that facilitate a more systematic design approach for exoskeletons. These challenges are:

- Improving knowledge of human–exoskeleton interaction
- Improving exoskeleton hardware and control
- Fast and detailed evaluation of exoskeleton concepts

These challenges have been the cornerstones of the research described in this dissertation.

## Improving knowledge of human–exoskeleton interaction

### Walking simulations

The dynamics of human walking are highly non-linear. This has been shown in both simulation studies and experimental studies. The development of exoskeletons requires knowledge of this non-linear behavior. A way to predict this behavior is through biomechanical models. These models predict the kinematics, kinetics, muscle activation, and metabolism of walking (Geyer and Herr, 2010; van den Bogert et al., 2011). Until now, these models have not been used to predict walking with an exoskeleton. This dissertation makes a first attempt to use these models for exoskeleton design. The model developed by Geyer and Herr (2010) is used to simulate human walking with exoskeleton dynamics based on the exoskeleton by (Cain et al., 2007). The model of Geyer and Herr was used since it also has a model of the neuromuscular controller. This controller model has a relatively small number of parameters, which makes it suitable for optimization. Optimization of the control parameters showed that the walking model can adapt to exoskeletal walking. Some experimental trends were captured by the simulation study. However the model does not yet predict the quantitative results that can directly be used in the development process.

### Empirical knowledge

Since biomechanical models have insufficient accuracy to predict the metabolic cost of walking with an exoskeleton, an alternative solution must be found. One of these solutions is to use empirical data that has been obtained with studies with previous exoskeletons. This dissertation has further expanded this empirical knowledge.

The XPED exoskeletons that are described in this dissertation are a realization of the extendon concept of Van den Bogert (2003). This concept makes use of long elastic cables that run parallel to the human leg. These cables have a similar function to the long tendons that are observed in some animals that move very efficiently, like horses. The cables can temporarily store energy and redistribute energy over the joints. In simulation these extendons reduce the human joint moments by 71 percent. This model-based prediction is based on the assumption that the joint angles do not change under the load and also the total joint torques stay are invariant. A second assumption is that a reduction in the human joint moments leads to a reduction in the walking metabolism. This dissertation contradicted both assumptions.

Experiments with the Achilles exoskeleton, an active ankle exoskeleton, have shown that the joint angles are strongly influenced by the support provided by the Achilles exoskeleton. This should be taken into account when designing a support strategy for the exoskeleton. In the XPED and Achilles exoskeleton, the joint angle patterns were assumed to be influenced by the exoskeleton support. When the joint angles changed in the experimental studies, the support decreased. From this result it was concluded that the support should be robust against changes in the walking pattern. It is noted that in other exoskeletons (Malcolm et al., 2013; Sawicki and Ferris, 2008), the support was high despite the changes in the walking pattern. Still it is difficult to make an exact copy of the controllers of these exoskeletons for implementation in the Achilles exoskeleton since an exact description of the dynamics of these exoskeletons is not available. For the exoskeletons described in this dissertation, an exact description of the dynamics is included. The intention of this description is to make the results obtained with these exoskeletons more generally applicable.

## **Improving exoskeleton hardware and control**

Many exoskeletons are not powerful enough or are too heavy to be successful. This follows from regression equations comparing the results of different exoskeletons (Mooney et al., 2014a). In this dissertation, two design methods are presented that can be used to design exoskeletons that can generate much mechanical power and a relatively low weight.

### **Use of passive mechanisms**

If the mechanical power in exoskeletons is delivered directly by motors, these motors are relatively heavy. Analogous to mechanisms found in musculoskeletal systems, passive elements could be used to reduce the required motor power. For specific supports, it is even possible to design exoskeletons without motors. The previously mentioned XPED exoskeletons are an example of these passive exoskeletons.

Passive elements can also be used in combination with active elements. An example in the human body is the combination of the soleus muscle and the Achilles tendon (Ishikawa et al., 2005). In this dissertation, a similar principle is applied in the Achilles exoskeleton. The Achilles exoskeleton supports the ankle push off. In this exoskeleton, a spring in series with an actuator is used. Temporarily storing energy in the spring can generate a higher mechanical peak power than the maximal motor power and reduce the energy consumption.

## **Numerical optimization**

The performance of the exoskeleton is determined by the interaction between many different components. It is difficult to see how changes in one component influence the functioning of other components. This dissertation solves this problem through modelling and optimization. A model of the exoskeleton is made that contains the (electro-)mechanical properties of exoskeletons. The dimensioning and choice for components can be acquired through optimization of the model. This principle has been applied in the design of the XPED and Achilles exoskeletons.

## **Improvement of exoskeleton control**

Walking is a cyclic motion. This dissertation has shown how this property of walking can be used to improve the force control of exoskeletons. The gait phase can be estimated with an adaptive frequency oscillator (AFO). Input to the AFO is a cyclic signal. In the case of walking, the hip angle or ground reaction force are suitable candidates. Based on the phase estimation cyclic signals can be estimated. The estimated signal is build up from primitive function. In this case, these are Gaussian functions. The amplitude of these signals is determined by a non-linear filter. The estimated signals can be used to improve tracking or to attenuate undesired dynamical effects.

## **Fast and detailed evaluation of exoskeleton concepts**

### **Improvement in gait analysis**

The human effort during walking and the change of human metabolic cost due to support with an exoskeleton is measured with respiratory analysis. This measure gives no insight in how changes in metabolic energy emerge. To get this insight, additional measurements are needed. Some of these measurements are kinetic and kinematic measures obtained from gait analysis. This analysis can, for example, be used to see how much mechanical power the human and the exoskeleton absorb and generate. Data is commonly acquired by tracking optical markers placed on the human body and measuring interaction forces with dynamometers such as force plates. Gait analyses are sensitive to errors and in the case of exoskeletal walking, the protocol is hindered due to occlusion of markers by the exoskeleton. The kinematic and kinetic acquired data is redundant. Current data analysis protocols do not make optimal use of this redundancy. This dissertation describes a generic method to process gait data based on an extended Kalman filter. The filter assumes consistent dynamics, and makes it possible to improve the accuracy of estimated joint angles moments, and estimate system parameters (e.g. segment

lengths). The latter makes it possible to eliminate the need for palpation of anatomical landmarks. Since the method can be used in real-time, it can be used to evaluate the effects of changes in control settings of the exoskeletons while walking.

### **Exoskeleton testbeds**

The development of new hardware to evaluate new exoskeleton concepts is very time consuming. It would therefore be beneficial to be able to test multiple concepts on one platform, an exoskeleton testbed. This requires some flexibility in the hardware and control. Also the dynamics of the exoskeleton should be well defined. This makes it possible to generalize the knowledge that is obtained with exoskeletons and use it in new exoskeleton designs. In this dissertation, two exoskeletons are described that could serve as a testbed. The Achilles exoskeleton is an autonomous exoskeleton for support of the ankle. The Achilles exoskeleton is force controlled and different controllers can be implemented on the exoskeleton. Secondly, this dissertation evaluated how existing rehabilitation robots can be used to simulate the design of new exoskeletons. This dissertation specifically focuses on attenuation of the existing exoskeletons dynamics and improvement of the tracking.

### **Conclusion**

The goal of this dissertation was to improve exoskeletons that reduce the metabolic cost of walking. The research has not directly led to such new exoskeletons. One of the main causes is the difficulty of predicting with sufficient accuracy the effect of an exoskeleton on the walking kinetics, kinematics, and metabolism. Some biomechanical models that might be suitable for this are available and have also been used in this dissertation. However, these models have not been validated. Therefore this dissertation paid special attention to the evaluation of exoskeletons to make these validation studies possible. Altogether, this has led to new methods to model, design, and evaluate exoskeletons. Hopefully, these methods will be valuable tools for the design of future exoskeletons.



# Samenvatting

---

Lopen is een efficiënte manier van voortbewegen die kan worden gebruikt om lange afstanden af te leggen. Door ziekte of in extreme omstandigheden, zoals tijdens het dragen van zware bagage, kan het lopen worden bemoeilijkt. Het wiel biedt in veel gevallen uitkomst. Echter voertuigen met wielen zijn vaak ongeschikt voor ongelijk terrein en gebruik in gebouwen, ook maken ze geen gebruik van de loopcapaciteiten van de mens.

Als alternatief zijn exoskeletten bedacht. Deze exoskeletten sluiten om het lichaam als een draagbaar mechanisch pak. De inspanning en aansturing die nodig zijn om de taak uit te voeren worden verdeeld tussen de mens en het exoskelet. De inspanning van de mens wordt uitgedrukt in het metabolisme, dit kan worden bepaald door de omzetting van zuurstof in koolstofdioxide te meten. In de afgelopen decennia zijn er veel verschillende exoskeletten ontwikkeld. Recent is het experimenteel aangetoond dat het metabolisme tijdens het lopen kan worden verminderd door het dragen van een exoskelet.

Het doel van dit proefschrift is om deze exoskeletten te verbeteren. Een van de grote moeilijkheden hierbij is dat van te voren het niet exact te bepalen is welke invloed een exoskelet zal hebben op de menselijke inspanning. Met als gevolg dat het ontwerpproces zich laat karakteriseren door trial-and-error. Dit proefschrift richt zich daarom op het gehele ontwerpproces. Dit omvat de modellering, het ontwerp van de hardware en regelaar en de evaluatie van exoskeletten. Na een beschouwing van dit gehele proces zijn een drietal uitdagingen geformuleerd om tot een meer systematisch ontwerpproces voor exoskeletten te komen. Deze uitdagingen zijn:

- Het verbeteren van het inzicht in interactie tussen mens en exoskelet
- Het ontwikkelen van betere hardware
- Het snel evalueren van exoskeletconcepten

Deze uitdagingen zijn het uitgangspunt geweest voor het onderzoek dat is beschreven in dit proefschrift.

## Verbeteren van het inzicht in interactie tussen mens en exoskelet

### Loopsimulaties

Het menselijk lopen vertoont sterk niet-lineair gedrag. Dit volgt zowel uit simulatiestudies als uit experimenten. Het ontwikkelen van een exoskelet vereist inzicht in dit gedrag. Een mogelijkheid om dit gedrag te voorspellen is door het gebruik van biomechanische mensmodellen. Deze modellen voorspellen de beweging, het krachten spel, de spieractivatie en het metabolisme van het menselijk lopen (Geyer and Herr, 2010; van den Bogert et al., 2011). Tot nu toe zijn deze modellen niet gebruikt om het lopen met een exoskelet te voorspellen. Dit proefschrift doet hier een eerste aanzet toe. Het model van Geyer en Herr (2010) is gebruikt om het lopen met een exoskelet gebaseerd op het exoskelet van Cain et al. (2007) te simuleren. Het model van Geyer en Herr werd geselecteerd omdat het naast het spierskeletmodel ook een neuromusculaire regelaar bevat. Deze regelaar heeft een relatief beperkt aantal parameters waardoor het model geschikt is om optimalisaties mee uit te voeren. Optimalisatie van de parameters van de regelaar heeft laten zien dat het model zich kan aanpassen aan lopen met een exoskelet en dat een aantal experimenteel waargenomen veranderingen ook zichtbaar zijn in het model. De simulaties zijn echter kwalitatief nog niet goed genoeg om direct als ontwerphulpmiddel gebruikt te worden.

### Empirische kennis

Omdat resultaten van simulaties en modellen ontoereikend zijn om exoskeletten mee te ontwerpen wordt er ook veel gebruik gemaakt van empirische kennis die is opgedaan met experimenten met eerdere exoskeletten. Dit proefschrift heeft ook hieraan een bijdrage geleverd.

De XPED exoskeletten zijn een realisatie van het exotendonconcept van Van den Bogert (2003). Dit concept omvat lange elastische kabels die parallel lopen aan het been. Deze kabels zijn analoog aan de lange pezen zoals die voorkomen in onder andere het been van een paard. Deze elementen kunnen tijdelijk energie opslaan en herverdelen over de gewrichten. In simulatie kan dit concept de gewrichtsmomenten verlagen met 71%. Dit getal is uitgerekend onder de aanname dat lopen met zo een exoskelet geen invloed heeft op de gewrichtshoeken en de totale gewrichtsmomenten. Een tweede aanname is gemaakt dat een reductie in de

gewrichtsmomenten leidt tot een reductie in het metabolisme. Dit proefschrift ontkracht beide aannames.

Ook het onderzoek met het Achilles-exoskelet, een geactueerd enkel exoskelet, heeft aangetoond dat gewrichtshoeken sterk afhankelijk zijn van de geleverde ondersteuning door het exoskelet. Dit heeft gevolg voor de aangeboden ondersteuning. In de XPED en Achilles exoskeletten werd een constante enkelhoek aangehouden. In experimenten met deze exoskeletten was, door de veranderde gewrichtshoeken, de ondersteuning lager dan was voorspeld. Hieruit is geconcludeerd dat de ondersteuning robuust moet zijn tegen veranderingen in het looppatroon. Bij andere exoskeletten is waargenomen dat de ondersteuning hoog is ondanks veranderingen in het looppatroon (Malcolm et al., 2013a; Sawicki and Ferris, 2008). Het is echter lastig om resultaten van andere exoskeletten direct over te nemen omdat een exacte beschrijving van de mechanica en aansturing van deze exoskeletten ontbreekt. Dit proefschrift laat verschillende exoskeletten zien waar deze beschrijving wel compleet is om resultaten van het onderzoek algemeen toepasbaar te maken.

## Het ontwikkelen van betere hardware

Veel exoskeletten zijn simpelweg niet krachtig genoeg of te zwaar om succesvol te kunnen zijn. Dit blijkt uit regressievergelijkingen die de prestaties van verschillende exoskeletten hebben vergeleken (Mooney et al., 2014a). In dit proefschrift zijn twee ontwerpmethodes beschreven die het mogelijk maken exoskeletten ontwerpen met een hoog vermogen en relatief laag gewicht

## Gebruik van passieve mechanismes

Als alleen maar motoren worden gebruikt om vermogen te leveren in een exoskelet leidt dit tot relatief zware motoren. Analoog aan het menselijk spier-skeletstelsel kunnen passieve elementen worden gebruikt om het geleverde vermogen te verminderen. Hierdoor kunnen minder zware motoren worden gebruikt. Voor bepaalde types ondersteuning is het zelfs mogelijk om zonder motoren te ontwerpen. De eerder genoemde XPED exoskeletten zijn hier een voorbeeld van.

Passieve elementen kunnen ook worden toegepast in combinatie met actieve elementen. In het menselijk lichaam wordt dit onder andere waargenomen bij de scholspier (soleus) en de achillespees (Ishikawa et al., 2005). In dit proefschrift wordt een vergelijkbaar principe toegepast in het Achilles exoskelet. Het Achilles exoskelet ondersteunt de enkelafzet. In dit exoskelet wordt een veer in serie met een actuator gebruikt. Door tijdelijke opslag van energie kan het maximale vermogen wat de motor moet leveren worden verminderd.

## Numerieke optimalisatie

De werking van een exoskelet wordt bepaald door de interactie tussen veel verschillende componenten. Het is vaak lastig te doorgronden hoe een verandering in een component doorwerkt in andere componenten. Dit proefschrift laat zien hoe dit probleem kan worden opgelost door modelleren en optimaliseren. De (elektro)mechanische eigenschappen van het exoskelet kunnen worden gemodelleerd. In het model kunnen de dimensionering en eigenschappen van onderdelen als modelparameters worden meegenomen. De uiteindelijke keuze voor onderdelen en de dimensionering hiervan kan door optimalisatie van het model worden verkregen. Dit principe is toegepast in het ontwerp van de XPED en Achilles exoskeletten.

## Verbetering van aansturing

Lopen is een cyclische beweging. In dit proefschrift wordt beschreven hoe deze eigenschap kan worden gebruikt om de aansturing van exoskeletten te verbeteren. De fase van het lopen wordt geschat met een adaptieve frequentie oscillator (AFO). De input voor de AFO is een repeterend signaal, in het geval van lopen kan bijvoorbeeld de heuphoek of de grondreactiekracht worden gebruikt. Op basis van de geschatte fase kunnen andere signalen worden geschat. De geschatte signalen worden opgebouwd uit een aantal primitieve functies. In dit geval zijn dit Gaussische functies. De amplitude van deze signalen wordt bepaald door een niet-lineair filter. De geschatte signalen kunnen worden gebruikt om een regelmatig beter een referentiesignaal te laten volgen of om ongewenste dynamische effecten te kunnen wegregelen.

## Snel en nauwkeurig evalueren van exoskeletconcepten

### Verbeteren van loopanalyses

De menselijke inspanning, en de mogelijke vermindering hiervan door ondersteuning met een exoskelet, wordt gemeten met het metabolisme. Deze maat geeft echter geen inzicht in hoe deze verandering tot stand komt. Extra metingen geven hier meer inzicht in. Een van deze metingen is het uitvoeren van een loopanalyse. De loopanalyse geeft de gewrichtshoeken en –momenten weer. Hieruit kan bijvoorbeeld worden afgeleid hoe het mechanisch vermogen is verdeeld tussen de mens en het exoskelet. Data voor het uitvoeren van een loopanalyse wordt meestal verzameld door het plaatsen en volgen van optische markers op het lichaam en het meten van de grondreactiekrachten met dynamometers (zoals krachtplaten). Loopanalyses zijn zeer gevoelig voor fouten en in het geval van het meten met een exoskelet wordt het uitvoeringsprotocol

bemoeilijkt doordat delen van het exoskelet de optische markers in de weg zitten. De data die wordt verzameld is redundant wat de mogelijkheid biedt tot foutdetectie en -reductie, hier wordt echter in gangbare methodes voor dataverwerking geen optimaal gebruik van gemaakt. Dit proefschrift laat een algemene methode zien voor dataverwerking in de vorm van een extended Kalman-filter. Het filter veronderstelt consistente dynamica. Door deze veronderstelling kunnen fouten worden gereduceerd en systeemp parameters worden geschat. Dit laatste maakt kalibratie gebaseerd op de identificatie van anatomische punten overbodig. Deze kalibratie is voor veel andere methodes noodzakelijk. Een voordeel van deze methode is tevens dat data realtime kan worden verwerkt.

### **Testplatformen voor exoskeletten**

Het ontwikkelen van nieuwe hardware om een exoskeletconcept te evalueren neemt veel tijd in beslag. Het is daarom zinnig om een testplatform te ontwikkelen waarop meerdere exoskeletconcepten kunnen worden geëvalueerd. Dit vereist een zekere flexibiliteit in de hardware en regelaar. Ook moet de mechanica van het platform en de regelaar die op het platform is geïmplementeerd goed zijn beschreven. Zo kan kennis die wordt vergaard met het platform worden gegeneraliseerd voor gebruik in nieuwe exoskeletontwerpen. In dit proefschrift worden twee exoskeletten beschreven die kunnen worden gebruikt als testplatform. Het Achilles exoskelet is een autonoom exoskelet voor ondersteuning van de enkel. Dit exoskelet is krachtgestuurd en er kunnen meerdere controllers op worden uitgetest. Ook wordt in dit proefschrift beschouwd hoe bestaande revalidatierobots kunnen worden ingezet om nieuwe exoskeletten te simuleren. Er wordt specifiek gekeken naar het wegeregelen van dynamische effecten en het verbeteren van het volgen van een aansturingssignaal.

### **Conclusie**

Dit proefschrift heeft als doel gehad exoskeletten die het metabolisme van het lopen omlaag brengen te verbeteren. Het onderzoek heeft niet direct geleid tot exoskeletten die het metabolisme ook omlaag brengen. Een van de oorzaken hiervan is geweest dat op dit moment van te voren moeilijk is te voorspellen welke invloed een nieuw exoskelet heeft op het metabolisme van het lopen. Enkele biomechanische modellen zijn beschikbaar en zijn ook toegepast in dit onderzoek. De validatie van deze modellen ontbreekt. Er is daarom in dit proefschrift speciale aandacht uitgegaan naar het evalueren van exoskeletten om deze validatie mogelijk te maken. Dit alles heeft geleid tot een aantal nieuwe methodes om exoskeletten te modelleren, ontwerpen, en evalueren met in de hoop dat deze methodes in de toekomst zullen bijdragen aan nog betere exoskeletten.



# 1 Introduction

---

## 1.1 Motivation

Human walking is energy efficient and can be used to cover long distances. Some people even walk around the world (Johanson, 2011), but most people walk more modest distances. The average Dutchmen walks a distance roughly equal the length of his or her country by foot one time a year (all travel movements excluding vacation and professional travels) (Centraal Bureau voor de Statistiek, 2014).

Walking is an indispensable necessity, which becomes clear when walking is impaired or when extreme working conditions are encountered. Many daily activities require some form of mobility, and these activities might be a challenge for someone with a walking impairment. Carrying a heavy load for a long distance is challenging for everybody. In many cases, a solution is found in the form of a wheeled vehicle, but in indoor environments or rough outdoor terrain wheeled vehicles do not suffice. Furthermore, wheeled vehicles ignore the (remaining) human walking capabilities. The use of an exoskeleton would form a more elegant solution. The exoskeleton, a wearable mechanical device, assists or augments the human motion. This idea has been around for a long time but only recently gained more attention (Figure 1).

Assisting people with a walking impairment and augmenting performance of healthy subjects are closely related. In both cases the load of the task and the control of the task are shared between the human and the exoskeleton. This dissertation will specifically focus on lowering the metabolic cost of walking (i.e. enhanced endurance), but the results can be generalized to other tasks.

Many exoskeletons have been built with the intention of reducing the metabolic cost of walking. Recently it was shown that the metabolic cost of walking could be reduced with an exoskeleton (Malcolm et al., 2013a; Mooney et al., 2014a). Still, exoskeletons technology is in an early stage of development.

## 1.2 Goal and challenges

The goal of this dissertation is to improve exoskeletons that reduce the metabolic cost of walking. The past decades of exoskeleton development have been characterized by trial and error. Many new prototypes were presented. Only a few were evaluated, and even fewer were successful. This led to long development times and has limited the success of exoskeletons.

The success of exoskeletons could be greatly improved if the trial-and-error approach were replaced with more systematic methods. Chapter 2 reviews studies related to exoskeletons and identifies the key challenges that need to be fulfilled in order to come to such methods.

### 1.2.1 Challenge 1: Improve knowledge of human–exoskeleton interaction

The knowledge of human–exoskeleton interaction is insufficient to accurately predict performance results by simulation and to generalize experimental results to be applied to more than one exoskeleton. The human and the exoskeleton are two dynamic systems that interact. Enhanced knowledge of each of these systems would contribute to a better design approach for exoskeletons.

#### *Insight in the human dynamical system*

Neuromuscular models have been shown to capture fundamental characteristics of human gait, estimate metabolic cost, and adapt to new tasks (Geyer and Herr, 2010; Song and Geyer, 2012). So far, these models have not been able to predict the

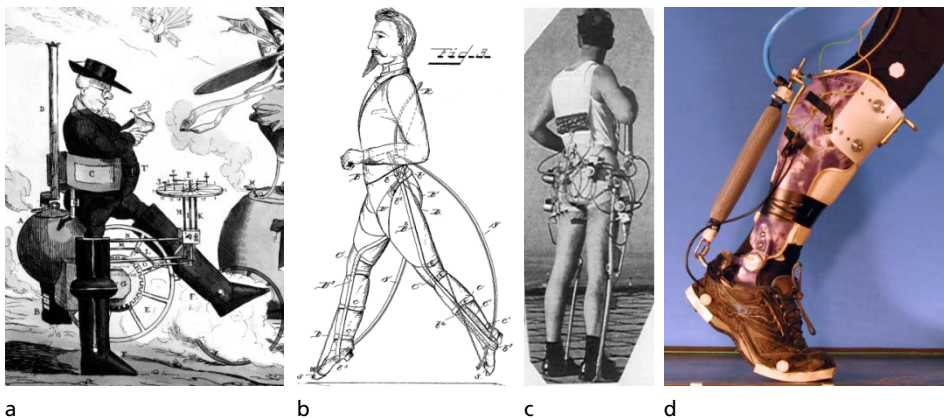


Figure 1: Almost 200 years of exoskeletons. a: (ca. 1830) Detail of the print “Locomotion” by Robert Seymour. The artist envisioned the steam powered pants as one of the applications of the steam engine. b: (1891) A patent by Nicholas Yagn describing a “Apparatus for Facilitating Walking, Running, and Jumping” (Yagn, 1890). c: (1969) First active exoskeleton developed by the Mihailo Pupin Institute (Vukobratovic, 2007). d: (2013) First exoskeleton that reduces the metabolic cost of walking (Malcolm et al., 2013a). Credits are given in the list of figures.

metabolic cost of exoskeletal walking. If such models were available, it would be possible to optimize exoskeleton designs in computer simulation.

### ***Insight in the exoskeleton dynamical system***

Exoskeleton dynamics are often not completely described in publications. Without the exact description, it is impossible to reproduce results. A description of the exoskeleton dynamics makes it possible to generalize the results obtained with a specific exoskeleton, and would therefore make a large contribution to the understanding of human-exoskeleton interaction.

### **1.2.2 Challenge 2: Improving exoskeleton hardware and control**

There are still many opportunities to improve exoskeleton hardware and control. In general, exoskeleton performance increases with power and decreases with weight. It was shown by Mooney et al. (2014a) that many exoskeletons lack the mechanical power (or are too heavy) to achieve an improvement in human performance over normal walking. Improving the hardware with more powerful yet lightweight designs is expected to enhance exoskeleton performance.

### **1.2.3 Challenge 3: Fast and detailed evaluation of exoskeleton concepts**

The experimental evaluation of an exoskeleton concept can take a very long time. Developing the hardware, analysis of results, and tweaking the exoskeletons takes the majority of the time. The challenge is to shorten the time needed to evaluate exoskeleton concepts.

## **1.3 Approach**

This dissertation presents newly developed tools both in software and hardware contributing to overcoming the set challenges. The chapters of this dissertation describe how these challenges have been approached from different angles.

### ***Evaluation of a neuro-muscular model in combination with an exoskeleton***

#### *Challenge 1*

Biomechanical models might be used to simulate walking with an exoskeleton. In Chapter 3, the neuromuscular model of Geyer and Herr (2010) is used to simulate exoskeletal walking. The simulated exoskeleton is based on the ankle exoskeleton with different controllers described by Cain et al. (2007). The neuromuscular controller is re-optimized to walk energy efficiently with the exoskeleton. The simulation results are compared with the experimental results of Cain et al. (2007).

## ***Improved motion analysis***

### *Challenges 1 and 3*

Human–exoskeleton interaction can be evaluated using motion analysis. Traditional motion analysis protocols are sensitive to uncertainties. These uncertainties arise from inaccurate palpation of anatomical landmarks or partially missing data. Both types of uncertainties easily occur during exoskeleton evaluations due to obstruction by the exoskeleton. Chapter 4 presents a general framework that can handle uncertainties from various sources. The framework allows for real-time data analysis, which can be used for fast evaluation and adjustments of exoskeleton concepts.

## ***Learning controller for exoskeleton testbeds***

### *Challenges 1 and 3*

Instead of building a new exoskeleton for each new exoskeleton concept, a testbed can be used to simulate a variety of exoskeleton concepts. The testbed should have a transparent mode on top of which the dynamics of a new exoskeleton can be rendered. A good transparent mode should closely resemble normal walking, which is not always the case. Walking can be influenced by the dynamics of the testbed (e.g. van Asseldonk et al., 2008). The quality of the transparent mode can be improved by designing a controller that compensates for the testbed dynamics. Chapter 5 presents a method with a learning controller that improves the transparent mode of a rehabilitation robot that can be used to simulate exoskeleton concepts. A similar controller is used in Chapter 8 to improve torque tracking.

## ***Lightweight design using passive elements***

### *Challenge 2*

Human and animal legs contain passive elements that contribute to energy-efficient locomotion. The energy storage function of tendons can be mimicked in exoskeleton designs (Hollander et al., 2005; van den Bogert, 2003). This reduces the power requirements and weight of the exoskeleton. Chapters 6–8 describe the design and experimental evaluation of different exoskeletons with passive elements.

## ***Numerical optimization of exoskeleton components***

### *Challenge 2*

The weight of the exoskeleton should be kept minimal. Minimizing the weight of exoskeleton components is difficult since exoskeletons are typically multibody systems where the design of one component influences the requirements on many other components. This dissertation presents methods for modelling the (electro-)

mechanical structure of the exoskeletons. This model can be optimized using numerical simulations to optimize the exoskeleton design (Chapters 6-8).

### ***Autonomous exoskeleton testbed***

#### *Challenge 3*

Chapter 8 presents a new ankle exoskeleton. This exoskeleton uses series elastic actuation and allows the evaluation of different control algorithms. The exoskeleton is autonomous, which allows for experiments on different terrains.



## 2 Background

---

Walking is for many people their principle way of getting around. It is energy efficient and can be used to cover large distances. Still, one might encounter tasks that are beyond his or her capabilities. This might occur in extreme work conditions or when dealing with an impairment. The traditional approach in these situations is to turn to wheeled vehicles such as bicycles, cars and wheelchairs.

The downside of wheeled vehicles is they perform best on flat paved roads. This is problematic since much of our environment is built for people who can walk and doors, stairs, or narrow passages are discovered everywhere. Additionally many vehicles are not suitable for rough outdoor terrains. As an alternative to wheeled vehicles, exoskeletons have been proposed. Exoskeletons (and orthoses) have been defined as:

*“Mechanical devices that are essentially anthropomorphic in nature, are 'worn' by an operator [user] and fit closely to the body, and work in concert with the operator's [user's] movements.”* (Herr, 2009)

Since these exoskeletons fit closely to the human body they are believed to be much more compatible with many of our daily life situations. This review will focus on exoskeletons for walking and running. These exoskeletons can be divided into two groups: 1. Exoskeletons for healthy users and users with partially impaired legs, and 2. Exoskeletons for paraplegic users. In the first group there is usually a form of a shared task where the forces and moments required for the movement are divided between human and the exoskeleton. In the second group the task might be shared in terms of control, but the forces and moments required for the movement are fully provided by the exoskeleton (e.g. Wang et al., 2014). This makes these exoskeletons fundamentally different. This review will focus on exoskeletons for healthy users and in a lesser extend users with partially impaired legs. Furthermore some exoskeletons that have been demonstrated without any information on the design, control or performance (e.g. HAL, Cyberdyne Inc. Tsukuba, Ibaraki, Japan or Hercule, RB3D, Auxerre, France) are not discussed.

A generic model that describes human and exoskeleton interaction is shown in Figure 2. The model describes how a task is shared between the human and the exoskeleton, and how the performance of this task is evaluated. The intention of the shared task is in most cases to improve human performance by either enhancing human strength or endurance for healthy users or neuro-rehabilitation or motion assistance of users with a limb pathology. All these different applications can be described using the same model and sometimes the same exoskeletons are used for these different applications (e.g. endurance and strength (Galle et al., 2014), or endurance and motion assistance (Sawicki and Ferris, 2008; Sawicki et al., 2006))

For a successful exoskeletons design, knowledge of the underlying dynamical systems is essential along with powerful hardware that influences the interaction between these systems. The review is divided in three sections corresponding to different phases of the design cycle; investigation, development, and evaluation. This review aims to come up with general considerations for exoskeleton design rather than a list of all different exoskeletons that exists. The review will conclude with current challenges that exist within exoskeleton design.

## 2.1 Investigate

The investigation step covers the process from problem definition to the design specifications. In exoskeleton design, the problem is in many cases well defined. For healthy subjects this is in most cases either preform the same task at a lower metabolic cost or perform a higher intensity task (faster walking, carrying heavier loads) at the same metabolic cost. For partially impaired patients the problem

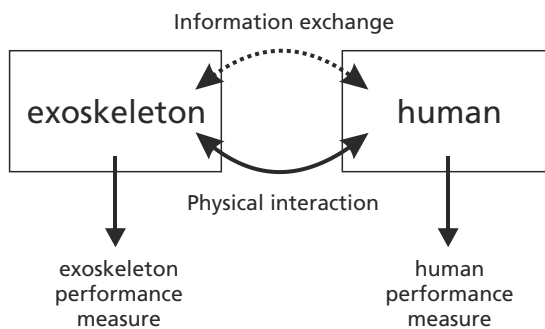


Figure 2: A generic human exoskeleton model. The model describes two dynamical systems, the human and the exoskeleton, that are attached to each other causing physical interaction. Additionally information can flow between the exoskeleton and the human (e.g. electromyographic (EMG) recordings that are used by the exoskeleton controller (Gordon and Ferris, 2007)). This results in a shared load and control task. The intention of this shared task is to enhance the user's performance. In a typical research setup, measures are taken from the human to evaluate its performance. Additionally, measures can be taken from the exoskeleton to evaluate the exoskeleton performance.

definition might focus on a sub-task such as creating foot clearance during swing (Koopman et al., 2013). Translating the objective into a design specification requires knowledge of human locomotion. The knowledge that exists about human locomotion can roughly be divided into two groups: walking models and empirical knowledge.

### 2.1.1 Walking models

#### *Musculoskeletal models*

The metabolic cost of a specific task can be predicted through musculoskeletal models Figure 3. These models include muscular and skeletal properties. Based on the model states an estimate of the metabolic cost can be obtained (Umberger et al., 2003). The model states can be obtained through modelling of the neuromuscular control (Geyer and Herr, 2010) or optimization of open loop muscle activation patterns (van den Bogert et al., 2011). Both models have been successfully used for the simulation of human walking. To become successful design tools for designing of wearable robotics, these models should also successfully predict other tasks, specifically exoskeletal walking. Adaptation to new tasks has been demonstrated by (Song and Geyer, 2012). So far it has not been with validated quantitative results that the metabolic cost is accurately estimated for these new tasks.

#### *Simplified walking models*

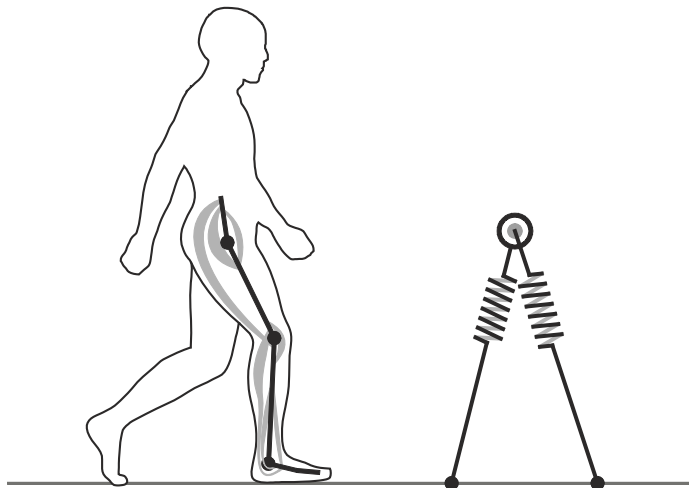


Figure 3: Neuromuscular vs. simple walking models. Left: A representation of the neuromuscular model of Geyer and Herr (2010). The model contains seven segments (Torso, Thigh, Shank, and Foot) and in total fourteen muscles (the segments and muscles of one leg are shown). Right: A simplified walking model, the bipedal spring-mass model of Geyer et al.

Simplified walking models form a contrast with the high-dimensional musculoskeletal models Figure 3. The aim of the simple walking models is to drastically reduce the number of variables while still capturing the essence of walking. The advantage is that these models can be studied with little computational effort. Examples of these models are the simplest walking model of (Garcia et al., 1998), the spring-mass model, and the bipedal spring-mass model (Geyer et al., 2006). Examples of the predictive power of these models are the correlation between impact losses after heel strike with metabolic cost, and the relation between step length and metabolic cost (Donelan et al., 2002) and the correlation between leg stiffness and ground reaction forces (Geyer et al., 2006). A downside of these models is that due to their simplifications they do not give a support strategy for specific joints. This requires additional assumptions when translating model results to exoskeleton design specifications.

### 2.1.2 Empirical knowledge

Studying (exoskeletal) walking resulted in a rich body of empirical knowledge that gives insight in human-exoskeleton interaction. This research can roughly be divided into three groups. *Gait analysis*: Gait analysis has is to investigate the kinetics and kinematics of walking with and without exoskeletons. *Augmentation factor*: The augmentation factor is a measure that compares the performance of different exoskeletons. So far it is the only meta-study carried out to find an empirical relation that predicts the human performance when walking with an exoskeleton. *Adaptation effects*: These studies investigate how humans adapt to walking with an exoskeleton. These studies investigate how changing a specific (exoskeleton) parameter affects the human performance

#### ***Gait analysis***

Gait analysis describes the joint angles and torques over time. The general procedure to obtain this data is to track motions of body segments with an optical tracking system and measure ground reaction forces with dynamometers such as force plates (Cappozzo et al., 2005). It is important to notice that gait analysis cannot be used to predict walking with an exoskeleton in advance.

#### ***Superposition principle***

It is sometimes assumed that exoskeleton specifications can be directly obtained from gait analysis. In this case the superposition principle is used to define the shared load task between the human and the exoskeleton. The superposition principle assumes that that the joint angles and the total torque (human and exoskeleton) are invariant under the load (e.g. van den Bogert, 2003). This assumption is incorrect as will be discussed later on.

### ***Augmentation factor***

The augmentation factor (AF) is an empirical relation that estimates the change in metabolic rate due to walking with an exoskeleton (Mooney et al., 2014a). The relation is based on: the average positive and negative power during one step  $p^+$  [W] and  $p^-$  [W], the apparent efficiency of the exoskeleton  $\eta$  [], the mass  $m_i$  [kg] and the relative cost of carrying this mass  $\beta_i$  [W/kg] on the foot, shank, thigh, and pelvis segment.

$$AF = \frac{P^+ + P_{dis}}{\eta} - \sum_{i=1}^4 \beta_i m_i \quad \text{with } P_{dis} = \min(0, p^- + p^+) \quad (1)$$

The first term of the equation, involving the average power, is based on a meta-study combining results of different exoskeletons. The second part of the equation is based on a parameter sweep where subjects walked with different masses placed on different body segments (Browning et al., 2007). The augmentation factor shows that there exist a clear trade-off between the amount of support the exoskeleton provides and the mass of the exoskeleton. The augmentation factor is solely based on average power and weight. Many other differences in exoskeleton design, such as the control method or measurement protocol, which do have a significant effect on the metabolic cost, are not captured in the augmentation factor. The augmentation factor therefore only provides a course estimate. This is further addressed below.

### ***Adaptation effects***

#### *Joint angle and moment adaptation*

(Kao et al., 2010a; Lewis and Ferris, 2011) investigated how joint angles change under influence of an exoskeleton. One study supported hip flexion torque, another supported ankle plantarflexion torque. Both studies showed that while the total torque stayed the same, the joint kinematics changed significantly. This means that for exoskeletons the superposition principle will not hold and exoskeletons cannot be designed purely on gait analysis data from normal walking.

#### *Support timing*

The effect of timing is investigated by (Malcolm et al., 2013a). Most ankle exoskeletons provide plantarflexion torque starting during the stance phase and ending at toe-off. The onset of the timing influences the metabolic cost of walking. Onsets close to heel strike result in a smaller reduction in metabolic cost than onsets close to toe-off. The optimal support-torque pattern is thereby different from the normally observed ankle torque pattern.

### *Control input signal*

The exoskeleton controller requires some form of control input that let it synchronize its actions with the human. The choice for a specific signal directly influences the exoskeleton performance (Cain et al., 2007).

### *Time and exploration*

Humans adapt their gait to optimize for energy efficiency (Umberger and Martin, 2007). However, when walking with an exoskeleton this adaptation is not instantaneous. Studies with ankle exoskeletons have shown that it can take up to 20 minutes before a plateau is reached. Adaptation effects are also still visible after multiple sessions (Galle et al., 2013; Gordon and Ferris, 2007). It is not given that humans will always adapt their walking pattern to maximize energy efficiency in a reasonable amount of time. For specific examples it has been shown that exploration had to be enforced before a global maximum was found (Selinger et al., 2014).

## 2.2 Development

The development phase covers the design, planning, and creation of the exoskeleton. Different options are available when choosing the joints to be actuated, the level of autonomy, the actuation and support, and the control algorithm. Different solutions that were found in existing exoskeletons are reviewed below.

### 2.2.1 Actuated joints

Exoskeletons can support the ankle, knee, and hip joint or a combination of those. The hip and ankle joint have multiple degrees of freedom. Single-joint exoskeletons typically support only one degree of freedom in the sagittal plane. Multi-joint exoskeletons sometimes provide support for additional degrees of freedom like hip abduction and adduction. Degrees of freedom can be supported in one direction (unidirectional) or both directions (bidirectional).

### *Ankle*

There exists a relative large group of ankle exoskeletons (Figure 4). The rationale for ankle exoskeletons is given by (Sawicki and Ferris, 2008). The ankle provides the majority of the work during push-off work in the trailing leg during double support, and thereby compensates for the energy loss due to impact of the leading leg as discussed above. The push-off torque is unidirectional which is reflected in many exoskeleton designs (Malcolm et al., 2013a; Mooney et al., 2014a; Norris et al., 2007; Sawicki and Ferris, 2008).

## ***Knee***

During a normal gait cycle the knee mostly dissipates energy. The knee has a dual characteristic during walking and running. In the stance phase the stiffness is high and in the swing phase the stiffness is low. Mimicking the dual stiffness characteristics with a locking mechanism has been beneficial for patients (Rietman et al., 2004). A similar approach has also been used to design running exoskeletons (Elliott et al., 2014). The fact that the knee mostly dissipates energy has been used to harvest energy from the human motion. The harvested energy can be used to charge batteries of personal equipment (Donelan et al., 2008).

## ***Hip***

During a normal gait cycle the hip joint exerts both positive and negative power. Different exoskeletons have been designed to partially take over this task. Examples are unidirectional exoskeletons (Lewis and Ferris, 2011) and bi-directional exoskeletons (Kerestes et al., 2014; Lenzi et al., 2013).

## ***Multi joint***

Multi joint exoskeletons can be divided into three sub-categories. The first category contains exoskeletons that combine a number of single joint actuators. Rehabilitation robots (Riener, 2012; Veneman et al., 2007), exoskeletons for paralyzed patients (Ekso Bionics, 2012; Wang et al., 2014; Zeilig et al., 2012) are typical examples within this category. The second category contains exoskeletons that link multiple joints. This is similar to bi- and tri-articular muscles found in nature (van den Bogert, 2003). The coupling of joints is mostly intended to increase



Figure 4a: Exoskeleton by Malcolm et al. (2013a). b: Exoskeleton by Mooney et al. (2014b). c: Exoskeleton Kao et al. (2010b), multiple slightly different versions exist. Credits are given in the list of figures.

the exoskeleton efficiency (Malcolm et al., 2013b). The third category contains exoskeletons that do not have connections at the thigh and shank segment. This can either be for bodyweight support (Krut et al., 2010) or simulate the spring like behavior of the human leg (Elliott et al., 2014) which are closely related.

### 2.2.2 Autonomy

We will define three levels of autonomy: *untethered*, the exoskeleton has no connection to the fixed world; *tethered*, the exoskeleton is connected to the fixed world through a flexible connection that is typically used to transfer power or data; *world fixed*, there is a direct connection between the limbs and the fixed world through a series of rigid elements.

#### ***Untethered***

Untethered exoskeletons are designed for use outside the lab environment. Untethered operation is required for many intended exoskeleton applications, but puts heavy constraints on the weight of the power source and actuators that have to be carried on board.

#### ***Tethered***

Tethered devices are typically used on treadmills in lab environments. The user can move freely in a limited space. The tether can transfer power and data which gives the possibility to place a power source, actuator, or computer off-board. This makes it easier to construct lightweight exoskeletons.

#### ***World fixed***

World fixed exoskeletons are also typically used on a treadmill. Their intended use is in most cases for gait rehabilitation and are therefore also referred to as rehabilitation robots. Examples of such robots are the Lokomat (Riener, 2012) and the LOPES (Veneman et al., 2007). They have the advantage that the weight of the exoskeleton can be transferred to the ground. Often the weight of the user can also be partially supported by a bodyweight support system. These robots are heavy and cannot easily be moved. This is acceptable since they are specifically designed for use within clinics.

### 2.2.3 Actuation and support principle

The actuation and support principle determines what forces and torques are exerted on the human body. Interaction forces between the human and the exoskeleton can be controlled by using impedance (Vallery et al., 2008) or admittance control (Meuleman et al., 2013). Both methods have a feedback controller that regulates the control signal to the actuator. Other exoskeletons lack

such a feedback loop. Since stiff position control is often not desired, they have a compliant actuation mechanism and the actuator is open-loop controlled (e.g. Cain et al., 2007). Impedance controlled and the described open-loop controlled exoskeletons require compliant actuation mechanisms. The different solutions that exist are reviewed.

### ***Pneumatic***

Pneumatic actuators have been used in multiple exoskeletons design (Malcolm et al., 2013a; Norris et al., 2007; Sawicki and Ferris, 2008), mostly in the form of pneumatic muscles. Pneumatic muscles are lightweight and have intrinsic compliance. The compressed air is supplied by a tank or a compressor. These components are typically placed off-board resulting in tethered devices.

### ***Electric***

Electric actuators are suitable for light weight exoskeletons design (Mooney et al., 2014a). To enable force control electric actuators can be used in series with elastic elements, which also makes the actuator compliant (Hitt et al., 2007). The deflection of the elastic element can be measured which makes series elastic actuation a candidate for impedance control.

### ***Passive***

In order to design autonomous lightweight exoskeletons, passive exoskeletons have been proposed. In these exoskeletons the support torque is provided by passive components like springs and dampers. This has the advantage that passive exoskeletons can be constructed that are extremely lightweight (Wiggin et al., 2011). Sometimes the term quasi-passive is used for exoskeletons that contain active components to control components that are mechanically passive, like actuated clutches or magnetorheological dampers (Walsh et al., 2007).

## **2.2.4 Control algorithm**

Actuated exoskeletons require a controller to regulate the signals sent to the actuator. This review will discuss the high level control algorithms that exist, but will skip the details of low level feedback controllers. The latter is broadly reviewed in other literature (e.g. Vallery et al., 2008). The intention of exoskeletons is to give a certain amount of support. The best type of support is open for debate, and different support algorithms exist. To synchronize the support with the motions of the user some support algorithms rely on a gait phase estimator. Gait phase estimators will be separately discussed.

### ***Support algorithms***

The most straightforward control signal is an on/off signal that activates the actuator for certain parts of the gait. This type of controller is popular in ankle exoskeletons with pneumatic muscles. The support torque provided by these exoskeletons is not an on/off signal. The non-linear properties of this actuator can result in a torque pattern that is close to the human ankle torque pattern observed in walking (Cain et al., 2007; Malcolm et al., 2013a). Similar are exoskeletons that define a reference pattern for the actuator. This pattern is again a function of the gait phase and feedback control is used to track this pattern (Hitt et al., 2007).

Support algorithms can also depend on the gait phase in combination with the system state (joint angles and angular velocities). In prosthetics such a controller has been implemented by that simulates different sprig characteristics for different phases of the gait (Caputo and Collins, 2014). A control signal can also be generated independent of the gait phase. The controller of (Gordon and Ferris, 2007) uses a modified EMG signal of the soleus muscle to control the exoskeleton.

Rehabilitation robots are intended for training of patients with (partially) impaired legs. Rehabilitation strategies can focus on a subtask of walking. Therefore specialized controllers are developed that for example increase foot-height during swing (Koopman et al., 2013) or couple the motion of the left and right leg (Vallery et al., 2009b).

### ***Gait phase estimation***

Different exoskeletons define their support as a function of the gait phase. This requires some form of synchronization for which multiple solutions exist. The property that walking is cyclic can be used in this case. A solution that is used for multiple exoskeletons is to define the support as a function of time. The time is reset when heel strike is detected (Malcolm et al., 2013a; Mooney et al., 2014a). The heel strikes can be detected by footswitches under the foot. The gait phase can also be learned with an adaptive frequency oscillator. This approach online fits sinusoidal functions to one or more measured periodic signals, which are typically joint angles. An advantage of this method is that it can learn the frequency of a signal (Righetti et al., 2006; Ronsse et al., 2011). A last approach is to directly map joint angles and angular velocities to a reference signal. The phase of this reference signal can be used to define the support (Karssen and Wisse, 2008).

## **2.3 Evaluate**

In the identification of exoskeletons we discriminate between primary and secondary measures. The primary measures investigate if the original objective was

met. To gain additional knowledge of the underlying dynamical systems additional measurements are needed.

### **2.3.1 Primary measures**

The primary measures are the measures for the human effort and the overall task intensity (the task to be performed by the human and the exoskeleton). A common method is to measure metabolic rate with an open respirometry system. The relation between the oxygen uptake and carbon dioxide production with the metabolic rate is given by an empirical relation (Collins, 2008). Alternative measures that have been used are heart rate and blood lactate measurements (Galle et al., 2014). In many studies the overall task intensity is kept at a constant level, typically by walking on a treadmill at a fixed speed. The overall task intensity can be varied in different ways, walking speed (Kerestes and Sugar, 2014) and carried weight (Galle et al., 2014) are two typical examples of which the quantities can be easily measured.

### **2.3.2 Secondary measures**

#### ***Kinetics kinematics***

The calculation of kinematics and kinetics is commonly based on the measurement of body movements with a marker tracking system and ground reaction forces through dynamometers such as force plates or instrumented treadmills. This data is often combined with motion or force sensors within the exoskeleton. The kinematic and kinetic analysis commonly serves two purposes. One is to determine the kinematic and kinetic effects of human-exoskeleton interaction (e.g. Kao et al., 2010a). A second is to determine the performance of the exoskeleton (e.g. Malcolm et al., 2013a).

#### ***Muscle activation***

Muscle activation is measured in different exoskeletons through electromyography (EMG) with surface electrodes. The advantage is that the signal can be obtained for individual muscles at a high sampling rate. This gives insight in how the task is shared between the human and the exoskeleton. Downside is that EMG cannot be directly linked to metabolic cost.

#### ***Muscular dynamics***

If the muscular dynamics are known it can be investigated how individual muscles contribute to an increase or decrease in the metabolic cost. The muscular dynamics can be directly or indirectly studied. The muscle-fiber velocity has been measured with ultrasound by (Farris et al., 2013). The muscular dynamics can also be

indirectly studied. In this case the muscle activations are found through optimization. In this case the muscular dynamics are optimized to match the experimentally obtained kinematics and kinetics (Delp et al., 2007). So far the latter approach has not been applied in exoskeleton research.

## 2.4 Challenges

So far, this chapter reviewed the state-of-the-art of walking and running exoskeletons for healthy users and users with a limb pathology. The review was separated into three sections that covered the investigation, development, and evaluation phase of exoskeletons. The principal findings of each section will be briefly summarized. Essential improvements in each section will be formulated in the form of a challenge.

### 2.4.1 Investigate

It is difficult to predict the metabolic cost of walking with an exoskeleton. While musculoskeletal models have predicted the metabolic cost of normal walking, it has not been shown yet with validated quantitative results that these models can adapt to other tasks. Alternatively, simplified walking models and empirical relations have been formulated to predict the metabolic cost of exoskeleton walking. Their scope is more limited, and they cannot be used for any arbitrary exoskeleton.

#### ***Challenge 1: Improve the knowledge of human–exoskeleton interaction***

Since no estimate of the metabolic cost of exoskeletal walking can be made, the design process is often characterized by trial-and-error. Improved knowledge of human–exoskeleton interaction could lead to a more systematic approach for exoskeleton design. The human and the exoskeleton are two dynamical systems that interact, the challenge is split into improved knowledge of the human dynamical system and improved knowledge of the exoskeleton dynamical system.

##### *Insight in the human dynamical system*

A thorough insight in the human dynamical system would make it possible to estimate human performance before human experiments have been carried out. This can either be through walking models or expanding the empirical knowledge.

##### *Insight in the exoskeleton dynamical system*

Some examples are found where the exoskeleton dynamics are described in full detail (Koopman et al., 2013; Witte et al., 2015), but this is not common practice. In many cases the dynamics are not straight forward, e.g. when pneumatic muscles

are used which are highly non-linear. Without this description it is not possible to repeat experimental results with a different exoskeleton. A description of the exoskeleton dynamics makes it possible to generalize the results obtained with a specific exoskeleton, and would therefore make a large contribution to the understanding of human-exoskeleton interaction.

### **2.4.2 Development**

There exist a wide variety of exoskeleton designs. The variety can partly be explained by the intended application, e.g. design considerations for a clinic based rehabilitation robot are different than for an exoskeleton that augments walking in outdoor terrains. Another part could be explained by the fact that the best hardware configuration has not yet been found.

#### ***Challenge 2: Improving exoskeleton hardware and control***

Hardware requirements are very strict. In general, exoskeleton performance increases with power and decreases with weight. It was shown by (Mooney et al., 2014a) that many exoskeletons lack the power (or are too heavy) to achieve a performance better than normal walking. Improving the hardware with more lightweight designs should therefore enhance exoskeleton performance.

### **2.4.3 Evaluation**

Exoskeleton concepts are typically evaluated by building a prototype and do an experimental evaluation. This method is very time consuming. Building and tuning the exoskeleton takes a lot of time while performing the actual measurement takes only a little.

The evaluation of exoskeletons is often performed by using a primary measure that measures human effort or task intensity. These measures provide quantitative results that make it possible to compare the performance of different exoskeletons. It is in many cases not sufficient to explain the differences between experimental results obtained with different exoskeletons. Additional insights in the human-exoskeleton interaction can be obtained with a gait analysis that provides kinematic and kinetic data. Performing a gait analysis with an exoskeleton has some specific difficulties. For many protocols the data analysis takes a lot of time and cannot be processed in real-time. Furthermore the exoskeleton might interfere with the measurement equipment (e.g. optical markers of a motion tracking system could be blocked by the exoskeleton).

***Challenge 3: Fast and detailed evaluation of exoskeleton concepts***

Exoskeleton designs could be greatly improved if the time it takes to evaluate exoskeleton concepts could be severely reduced. Most progress could be made by reducing (or eliminating) the time it takes to build and tune the exoskeleton and perform data analysis. Data analysis methods should be adapted so that they are better compatible with exoskeletal walking making measurements easier to conduct.

# 3 Optimization of human walking for exoskeletal support

---

Wietse van Dijk

Herman van der Kooij

*Published as: W. van Dijk and H. van der Kooij, "Optimization of human walking for exoskeletal support.," IEEE Int. Conf. Rehabil. Robot., vol. 2013, pp. 1–6, Jun. 2013.*

*Abstract—It is hypothesized that healthy humans can reduce their energy expenditure during walking by wearing an exoskeleton. Exoskeletons are often designed for mechanical efficiency at joint level. This approach disregards the energy savings mechanisms in the human leg like bi-articular muscles and tendons. We use the muscle-reflex model to simulate the experiments by Cain et al. with an ankle exoskeleton actuated by a pneumatic muscle that supports plantarflexion. The muscle-reflex model predicts muscle activations and metabolic rate. The reflex-control parameters of the model were optimized for walking with and without support from an exoskeleton. The simulated exoskeleton uses either the EMG signal from the soleus muscle (proportional myoelectric control), or a footswitch to trigger the actuation of the pneumatic muscle. Cain et al. did find an experimental reduction in soleus muscle activation of 41.4 percent for the proportional myoelectric control and 13.0 percent for the footswitch control, where the optimization outcomes of simulated walking predicted a reduction of 42.8 percent and 25.9 percent respectively.*

## 3.1 Introduction

It is hypothesized that healthy humans can improve their walking performance by wearing an exoskeleton (Ferris et al., 2007). During the last decade the number of exoskeleton prototypes with the intention of doing this has greatly increased. Theoretical and experimental results give no conclusive answer on how humans can be most effectively supported during walking. One of the proposed strategies

for multiple exoskeletons is to partially match the support with the torque patterns normally observed in human gait. Joint torques and powers are calculated using inverse dynamics. Exoskeletons that use this principle can be (quasi) passive systems (van den Bogert, 2003; van Dijk et al., 2011; Walsh et al., 2007; Wiggin et al., 2011), or active systems (Cain et al., 2007; Norris et al., 2007). The assumption made for the design of these systems is that if the gait kinematics and joint torques stay the same, the joint torques that the human has to provide will decrease, what will make the human walking effort, in mechanical terms, more efficient. However, in metabolic terms, these systems, as well as other systems (Herr, 2009; Malcolm et al., 2013a), have not or only slightly reduced energy expenditure during walking.

A problem with exoskeletons solely focusing on reducing joint torque or power is that they do not take into account the following effects: 1. Humans will adapt to the support, which results in different gait kinetics and kinematics (Kao et al., 2010a) and 2. Tendons provide temporal energy storage and bi-articular muscles transfer energy between joints (Ishikawa et al., 2005; Wiggin et al., 2011). We assume that due to this focus on mechanical efficiency, exoskeleton performance is often overestimated, and thereby leads to the poor results with reducing metabolic cost in exoskeletal walking studies.

More advanced walking models that take into account the human adaptation, and the effects of tendons and bi-articular muscles might better predict the effectiveness of an external support offered by an exoskeleton. This requires forward dynamical simulations to evaluate kinetic and kinematic adaptation effects and modeling of the musculoskeletal system to predict the effect of tendons and bi-articular muscles. Examples of such models are (Geyer and Herr, 2010; van den Bogert et al., 2011). The model we used in this study is the muscle-reflex model of (Geyer and Herr, 2010). The model is suitable for forward simulation of human walking, models musculoskeletal dynamics and control, and has a limited number of control parameters. The model has the flexibility to represent different gaits as has been shown by the optimization of the model for different walking speeds (Song and Geyer, 2012). The model has been extended and optimized for walking and running in 3D (Wang et al., 2012), however this was done mainly for animation purposes and out of plane movements were not generated by a muscle model, but controlled by a PD-controller instead.

Aim of this study is to investigate if this model can be used for exoskeletal walking and if it can make predictions for the metabolic cost of walking. This requires the control parameters of the model to be optimized which is a highly non-linear

optimization problem. A particle swarm optimization (PSO) is used to perform this optimization.

To test the model and the optimization two different types of external support that mimic the behavior of an exoskeleton were implemented in the walking simulation. The supports were modeled after the controllers used by (Cain et al., 2007) on a pneumatic ankle exoskeleton (Ferris et al., 2005; Gordon et al., 2006).

The first implemented controller is the ankle torque feedforward (AFF) controller. The AFF controller plays back a fraction of a pre-recorded ankle torque pattern normally observed in human gait. This controller is modeled after the footswitch (FS) controller of (Cain et al., 2007) where the amount of support is controlled by a footswitch. A similar controller was also evaluated by (Norris et al., 2007). The second implemented controller is the soleus activation feedback (SFB) controller. The SFB controller amplifies the soleus muscle activation signal generated by the muscle-reflex model. This controller is modeled after the proportional myoelectric controller (PM) of (Cain et al., 2007). The PM controller measures the EMG of the soleus muscle and scales the support of the exoskeleton with this signal.

The study of (Cain et al., 2007) was selected since the results with this exoskeleton are well documented and different controllers have been applied on the same exoskeleton. In terms of mechanical power these two controllers offer a similar support, however the measured performance of the two controllers is different in terms of EMG, kinematics and adaptation time.

We hypothesize that the optimization of the muscle-reflex model for different exoskeletal supports can predict the experimental outcomes. Additionally the prediction of the metabolic cost (Umberger et al., 2003) can be used to determine the metabolic advantage of the exoskeletal supports.

## 3.2 Methods

### 3.2.1 Walking and exoskeleton model

The walking model which was used is the muscle-reflex model (Geyer and Herr, 2010; Song and Geyer, 2012). The walking model consists of seven body segments with fourteen muscles. Each muscle has its own controllers that generate a muscle stimulation signal. Via the muscle dynamics this results in joint torques. The walking simulation is extended with an external support that acts around the ankle and mimics the support of the controllers implemented on the pneumatic ankle exoskeleton by (Cain et al., 2007). Our support offers a torque directly at the ankle

joint. Effects from the mass or actuator dynamics are not taken into account (Figure 5).

### **Ankle torque feed forward (AFF)**

This controller plays back a fraction of the ankle torques ( $\tau_{REF}$ ) normally observed in human gait and that were acquired from an internal gait database. The ankle torques are defined as a function of the gait phase ( $\phi(t)$ ). The gait phase is detected by an adaptive frequency oscillator that synchronizes the gait frequency with the right and the left hip angle (Righetti et al., 2006). Zero phase ( $\phi(t) = 0$ ) is synchronized with the heel strike. The reference torques are scaled with a gain ( $G_{AFF}$ ) and the control torque ( $\tau_{AFF}$ ) becomes:

$$\tau_{AFF}(t) = G_{AFF} \tau_{REF}(\phi(t)) \quad (2)$$

### **Soleus activation feedback (SFB)**

This controller exerts an ankle torque ( $\tau_{SFB}$ ) that is proportional to the soleus activation ( $A_{SOL}$ ) with a gain ( $G_{SFB}$ ).

$$\tau_{SFB} = G_{SFB} A_{SOL} \quad (3)$$

The muscle activation signal of the muscle-reflex model is analogous to the rectified and filtered EMG signal measured in humans.

## **3.2.2 Simulations**

The walking model has been implemented in a custom-made simulator for 2D rigid body dynamics for Matlab (Natick, Mass., USA). The simulator uses a fourth order Runge-Kutta integrator with a fixed time step of  $5 \cdot 10^{-4}$  s. The software including the simulation results is available under a BSD license ([dbl.tudelft.nl/exoskeleton/simulation/](http://dbl.tudelft.nl/exoskeleton/simulation/)). Our simulations ran on 12 cores of a server with two Intel Xeon E5 2665 processors.

## **3.2.3 Optimization algorithm**

The optimization algorithm which was used is a particle swarm optimization

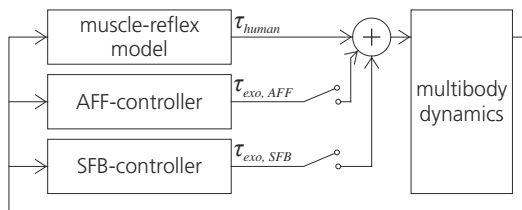


Figure 5: Schematic overview of the simulation. The muscle reflex model and exoskeleton controllers generate input torques for the multibody dynamics module that simulates the motion of the human body segments.

(PSO). A variant of the particle swarm optimization is used where each particle is influenced by its own best position over all the past iterations ( $x_{pbest}$ ) and a local best position of the previous iteration ( $x_{localbest}$ ). The local particles are determined by a ring topology, where each particle receives information of its  $n$  left and right neighbors. Additionally the velocity is damped with a factor ( $\omega = 0.95$ ). The velocity ( $v$ ) of particle  $j$  at iteration  $k + 1$  is adjusted as follows:

$$v_{jk+1} = \omega v_{jk} + r_1 (x_{pbest} - x_{jk}) + r_2 (x_{socialbest} - x_{jk}) \quad (4)$$

where  $r$  is a random number between 0 and 1, and  $x_{jk}$  the position of particle  $j$  at iteration  $k$ . The positions of the particles are limited by  $x_{min}$ ,  $x_{max}$  that are the bounds on the control parameters by (Geyer and Herr, 2010). The velocity of the particles  $v_{min}$ ,  $v_{max}$  is limited as follows.

$$v_{min} = -v_{max} = 0.015 \cdot (x_{max} - x_{min}) \quad (5)$$

### Staged optimization

The PSO uses a staged optimization criterion. First the fitness of the first stage is calculated, if a desired fitness value is reached the particle moves to the next stage and the fitness of this next stage is calculated, until a final stage is reached. This can be interpreted as a constrained optimization problem where the stages are the constraints. In the optimization the following stages are used:

First stage is maximizing the simulation time close to its set maximum ( $t_{max}$  [s]). The simulation is terminated if the model falls. Maximizing the simulation time is in this case similar to ensuring that the model does not fall. The second criterion is a coarse matching of the walking speed. Third stage is the minimization of the standard deviation of the step time. This is a coarse measure for stability and it ensures a regular gait pattern. The fourth step is a fine matching of the gait speed. The fifth, and final, step is the optimization of the product of: average muscle power, the RMS of the muscle activation averaged over the muscles, and average absolute ligament torques. The first two terms are introduced to optimize for an energy efficient gait pattern. The last term prevents for overstretching of ligaments

Stage	Fitness	Criterion next stage
1	Simulation time [s]	> $t_{max} - 0.01s$
2	abs(Speed – Desired speed) [m/s]	< 0.5m/s
3	SD(Step time) [s]	< 0.05s
4	abs(Speed – Desired speed) [m/s]	< 0.1m/s
5	Average muscle power [W/kg] x muscle activation RMS [] x average absolute ligament torques [Nm/kg]	--

Table 1: Fitness criteria

and might be interpreted as a pain factor (Song and Geyer, 2012). To determine the best particle out of a group of particles they are first sorted by their achieved stage and secondly on their fitness within that stage. The values choices for the fitness criteria are summarized in Table 1.

### ***Muscle noise***

To achieve more stable results muscle noise ( $e$ ) was added to the model. For every stage and fitness evaluation by the PSO the simulation was repeated three times with different random initialized noise. Of the three acquired stages and fitness values the lowest was passed to the optimization algorithm. The noise is a piecewise polynomial fit through data points with random time intervals between 0.1 s and 0.2 s with random values between 0 and 1. The muscle stimulations ( $S$ ) were adapted as follows:

$$S = (1 + 0.02e) \cdot S \quad (6)$$

### **3.2.4 Optimization experiments**

Two optimization experiments were performed. The first optimization was used to optimize the initial conditions. The second optimization was walking with different types and levels of support. The settings of the PSO for the different experiments are given in Table 2. During all the experiments we optimized all the muscular control parameters of the reflex model. For the optimization of the initial conditions the lean angle of the torso (applied to the torso element and the shank of the stance leg), the angle of the swing leg and the speed of the swing leg were optimized as well, since the muscle-reflex model cannot start from every possible pose.

#### ***Optimizing initial conditions***

The muscle-reflex model and the phase detection of the AFF controller require a few seconds of simulation before they reach steady state. Since the optimizations of supported walking require a long computation time, a series of optimizations were performed to optimize the initial conditions, so further simulations can start from a steady state walking cycle. These optimizations optimized walking without the support from the controllers. The maximal simulation time was 15 seconds. To

	Initial conditions	Supported walking	
Step	--	1 <sup>st</sup> step	2 <sup>nd</sup> to 8 <sup>th</sup>
Population	50	60	40
Population 1 <sup>st</sup> iteration	100	120	80
Iterations	60	75	50
Particle neighbours (n)	2	7	5

Table 2: Settings used for the PSO

check the convergence of the results the optimization was repeated five times. The state of the walker at  $t = 10$  s of the optimization with the best fitness was used as the initial state for the further experiments. The computation time for this experiment was two hours per repetition.

### ***Optimizing supported walking***

After the initial conditions were determined walking with and without the different controllers was optimized. We optimized for different walking conditions: walking with SFB controller, walking with AFF controller, and walking without support. The amount of support was gradually increased over eight optimizations, indicated by the optimization step ( $i_{step}$ ). This was done to obtain results for different levels of support. For the SFB controller the gain ( $G_{SFB}$ ) is:

$$G_{SFB} = (30 \cdot i_{step} - 1) \quad i_{step} = 1..8 \quad (7)$$

For the AFF controller the gain ( $G_{AFF}$ ) is a function of the body mass ( $m$ ) and the step:

$$G_{AFF} = 0.06 \cdot m \cdot (i_{step} - 1) \quad i = 1..8 \quad (8)$$

For the normal walking there is no change in the support. Still the same multistep approach was chosen for walking without support, so all optimizations have a similar number of iterations of the PSO.

The initial population of each optimization step, except for the first optimization step, is a random population around the best particle from the previous step. The position of each new particle is seeded within +/-15% of the search space size around the best particle of the previous step (respecting the bounds on the search space). In order to evaluate the convergence of the results the experiment was repeated ten times. The computation time for this experiment was approximately twenty hours per repetition.

### **3.2.5 Data processing**

For each optimization result an average step was calculated from the last five steps of each simulation. The amount of support was characterized by the maximal support power in an average step. For the experimental results by (Cain et al., 2007) this was 1.23 and 1.18  $\text{Wkg}^{-1}$  for the FS and PM controller respectively. The average of 1.20  $\text{Wkg}^{-1}$  was used as the target support power for our optimization. From the different optimization steps, the results from the optimization step where the maximal support powers were closest to this target were selected.

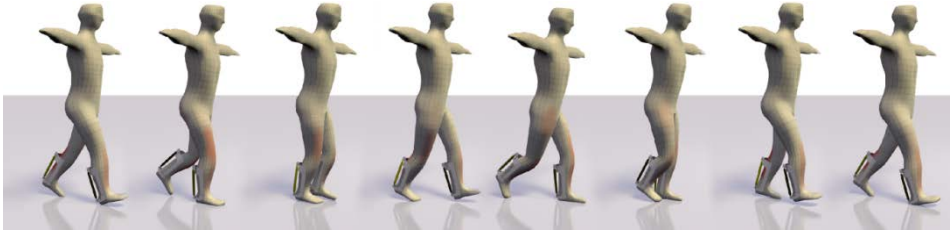


Figure 6: Typical example of a walking cycle with an ankle exoskeleton.

Three different energy related measures for the evaluation of walking performance are used. 1. Average absolute joint power. The average was taken over the time and summed over the joints. 2. Average muscle power. This is the power from the contractile element of the muscle averaged over time and summed over the muscles. 3. Estimated metabolic cost. The estimated metabolic cost using the model of (Umberger et al., 2003) takes into account the muscle activation and maintenance heat, the shortening and lengthening heat, and the mechanical work. All these measures are normalized with the body weight. Results for the different controllers are compared to each other. Statistics are performed with a single sided ANOVA-test over all the results from the different repetitions of the experiment.

### 3.3 Results

#### 3.3.1 Optimization

During all optimizations on average 31.9% and at least 7.5% of the particles reached the final stage of the five fitness stages in the last iteration of the optimization. This means that for all optimizations, solutions were found that fulfilled the criteria for optimization stages one to four. A typical example of a walking cycle that was optimized is shown in Figure 6. For both controllers the simulation step where the maximal support power ( $P_{max}$ ) was closest to the maximal support power of (Cain et al., 2007) was selected (Figure 7). For the SFB controller this was the fourth optimization step ( $G_{SFB} = 90 \text{ Nm}$ ,  $P_{max} = 1.18 \text{ W/kg}$ ) and the fifth optimization step for the AFF controller ( $G_{AFF} = 0.24 \text{ Nmkg}^{-1}$ ,  $P_{max} = 1.04 \text{ Wkg}^{-1}$ ). Further results will describe the data acquired from these optimization steps.

#### 3.3.2 Support vs. joint power, muscle power and energy expenditure

Different energy measures were calculated from the results. The average absolute joint power, the average power of the contractile elements in the muscle, and the estimated metabolic cost calculated using the model of (Umberger et al., 2003) are given in Table 3. The results are given for all the joints together and for the ankle only.

### 3.3.3 Ankle kinematics and kinetics

The average ankle angle, ankle torque, and ankle power are shown in Figure 8. The ankle kinematics for walking with and without the support are compared with the cross correlation coefficient. For the SFB controller the correlation with unsupported walking is 0.98. For the AFF controller the correlation with unsupported walking is 0.99.

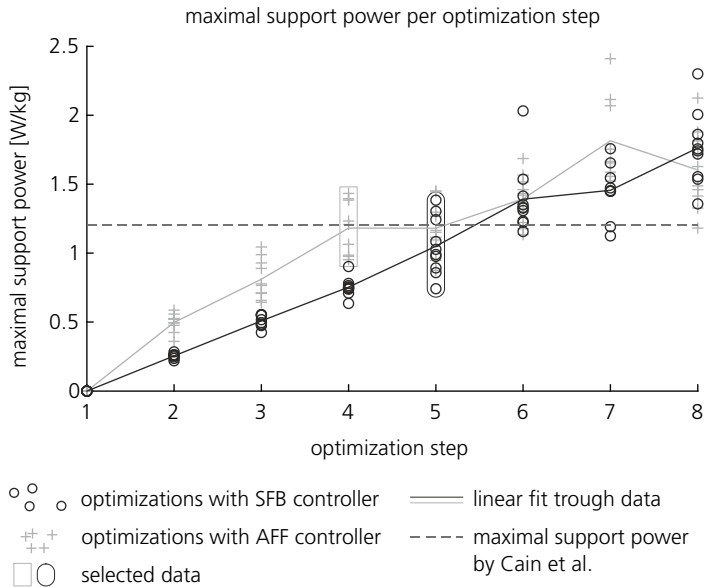


Figure 7: Optimization step vs. the maximal support power. The different markers for each optimization step represent the data acquired from the different repetitions of the experiment.

	All joints			Ankle only		
	No support	SFB	AFF	No support	SFB	AFF
Metabolic rate [Wkg <sup>-1</sup> ]	2.82 (0.05)	2.82 (0.13)	2.63 (0.13)*	0.486 (0.058)*	0.378 (0.024)*	0.340 (0.051)*
Muscle power [Wkg <sup>-1</sup> ]	1.12 (0.06)	1.23 (0.07)*	1.12 (0.06)	0.157 (0.008)*	0.147 (0.014)*	0.149 (0.010)*

Table 3: Different measures for the human energy expenditure. Results are shown for all joints together and for the ankle only. The muscle energy expenditure and the muscle power for the ankle only was based in data from, the soleus, tibialis anterior and gastrocnemius muscles. Values between brackets denote standard deviations over the repetitions of the experiment. \* denotes a significant difference between the results with controller from results for unsupported walking (single sided ANOVA,  $p < 0.05$ )

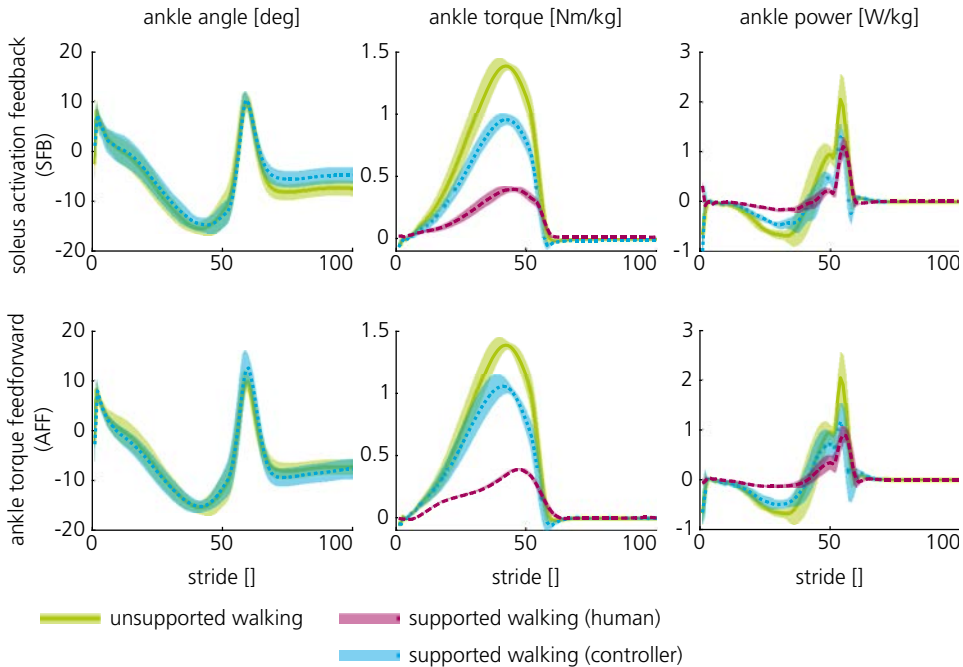


Figure 8: Comparison of kinetics and kinematics for the different controllers. The upper row shows the ankle angle, the middle row shows the ankle torque, the bottom row shows the ankle power. Plantarflexion is positive.

### 3.3.4 Support work vs. muscle activation

The muscle activations for the different controllers are compared in Figure 9. Significant decreases of 42.8% and 25.9% in soleus activation were found for the SFB controller and AFF controller respectively (experimentally found reductions were 41.4% and 13.0%). For the SFB controller we found a significant increase for the tibialis anterior and the gluteus muscles of respectively 16.0% and 5.4%, in the experiment by Cain et al. these changes were not significant. For the AFF controller we found a significant reduction of 37.9% and 10.0% in respectively the activation of the gastrocnemius and vastus muscles. Cain et al found a decrease in the gastrocnemius muscles of 27.7% and 9.77% for the PM and FS controller respectively.

## 3.4 Discussion

### 3.4.1 Optimization

The used optimization algorithm was able to find stable gait patterns for the different controllers and the different levels of support. This is a first indication that the muscle-reflex model is able to simulate walking with exoskeletons or orthoses.

### 3.4.2 Gait kinematics

The different conditions led to very similar gait kinematics for the ankle. Cain et al. have shown in their experiments that the initial gait kinematics showed more plantar flexion and converged to a gait pattern closer to that of normal walking. This adaptation process cannot be captured with the optimizations. The PM controller of Cain et al. and the results for the SFB controller both show a gait pattern very similar to that of unsupported walking. Cain et al. showed that the gait kinematics of the footswitch controller even after convergence showed large

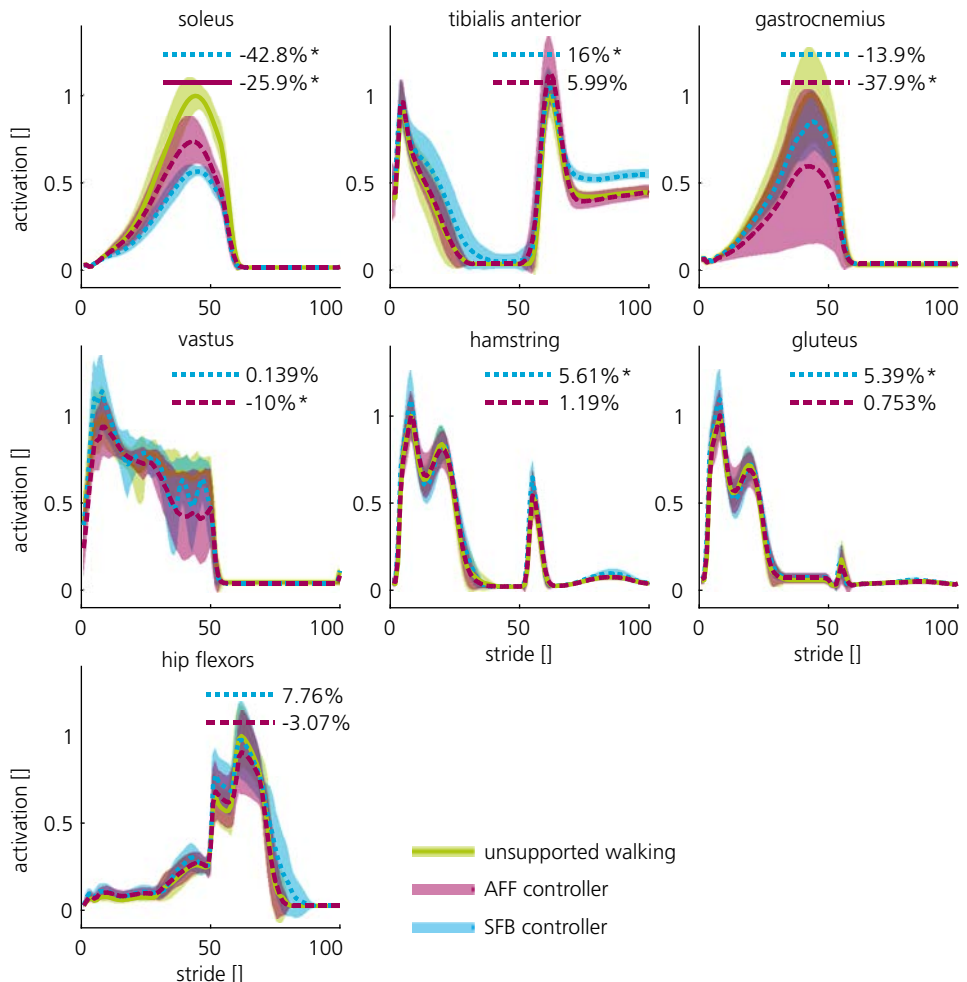


Figure 9: Muscle activations for the different walking conditions. Lines denote the mean, shaded areas denote the standard deviations taken over the last five steps of the different optimizations. The data is normalized to the walking condition without support. The percentages show the difference in RMS between no support and walking with the controllers. \* denotes a significant difference between the results with controller from results without controller (single sided ANOVA,  $p < 0.05$ )

deviations from a normal gait pattern, where this was not observed with the AFF controller we evaluated. The FS controller of Cain et al. produces a weaker resemblance to a normal ankle torque signal since it is controlled by an on/off signal coming from the footswitch, which might have contributed to the different gait pattern.

### 3.4.3 Muscle activation

The studies from Cain showed that both controllers have the biggest effect on the activity of the soleus muscle, which was confirmed by our simulation results. We also found a big reduction in gastrocnemius activation for the AFF controller that was not found by Cain et al. It should be noted that the standard deviation in the gastrocnemius activation over the different repetitions of the optimization was large. Cain et al. did find a significant reduction in gastrocnemius EMG for the SFB controller that we did not find, but in another study with the same controller by (Gordon et al., 2006) this reduction was not found. Additionally we found numerous smaller differences that were significant, but not reported in the experimental study. These effects are small and they might not be noticed in experiments due to inter-subject differences.

### 3.4.4 Energy expenditure

Of the different energy measures (absolute joint power, muscle power, and metabolic rate) evaluated over all the joints, only the metabolic rate for the AFF controller decreases significantly. A possible explanation might be that reductions in energy expenditure at the ankle are counteracted by increases in energy expenditure at the knee and hip. Additionally the muscle-reflex model tends to overestimate the hip and knee power, making the relative contribution of the ankle smaller. To rule out these effects the ankle was also evaluated in isolation. For the ankle alone all performance measures predicted a decrease in energy consumption. Experimental data with the proportional feedback controller showed reductions in metabolic rate of  $0.39 \text{ Wkg}^{-1}$  ( $3.39 \text{ Wkg}^{-1}$  with the unpowered device,  $3.00 \text{ Wkg}^{-1}$  with the powered device) (Sawicki, 2009). The simulations with the SFB controller only predicted savings of  $0.108 \text{ Wkg}^{-1}$ . The prediction of the reduction in muscle power showed the smallest gain in energy efficiency by the controllers. The predictions of reductions in joint power and metabolic rate were on a comparable scale. For the AFF controller the relative reduction in metabolic rate was larger, for the SFB the relative reduction in joint power was larger.

Our research has some limitations that might be addressed in future research. Although the muscle reflex model has a good resemblance of human walking the model is not validated. Our research considers only the torque exerted by the

exoskeleton. The mass of the exoskeleton was not taken into account. However, added mass to the leg does have a significant influence on the walking performance (Browning et al., 2007; Malcolm et al., 2013a; Sawicki, 2009).

### 3.5 Conclusion

We have shown that the muscle-reflex model adapts to an external support. Muscle activation patterns showed similar changes as the experimental recordings of EMG when an ankle support is provided. In general, changes in muscle activation and metabolism predicted by the simulation were lower than the observed changes in the experiment. For this study we only used experimental data from one exoskeleton as reference. Based on this reference we conclude that the simulations give a conservative estimation of the reduction in human energy expenditure. Estimated metabolic rate and joint power showed similar reductions. Our hypothesis that reductions in estimated metabolic rate would be lower than reductions in joint power was not confirmed. Still the estimated metabolic rate is a physiologically sounder estimate of the human energy expenditure than absolute joint power.



## 4 Real-time Motion Analysis and Parameter Estimation with a Multibody Kalman Filter

---

*Wietse van Dijk*

*Shiqian Wang*

*Herman van der Kooij*

*In review*

*Abstract— In motion analysis, the errors that are made in the processing of measurement data are much larger than the measurement errors. Protocols for data processing are prone to errors caused by: incorrect model parameters, imprecise palpation of anatomical landmarks, poor estimates of the accelerations, soft tissue artifacts, and missing data. Motion analysis data often contains redundant information that can be used to reduce these errors. We developed the multibody Kalman filter (MKF) for real-time motion analysis that considers uncertainties from various causes. The MKF simultaneously estimates kinematics and kinetics from force and motion data. This makes the MKF suitable for real-time applications. The MKF eliminates the need to palpate anatomical landmarks, which is labor intensive and prone to errors.*

*The performance of the MKF was evaluated in two experiments. In the first experiment the MKF was used on synthetic data generated with a simplified walking model. This experiment showed the advantage of simultaneously handling force and motion data. In the second experiment the gait of four subjects was analyzed with the MKF and the calibrated anatomical systems technique (CAST). The RMS difference in estimated joint angles between these two methods ranged from  $1.72^\circ$  to  $6.41^\circ$ . The RMS difference in joint moments ranged from 0.07 to 0.30 Nm/kg.*

Estimation errors for the position, force, and moment showed that the MKF is as reliable as the CAST.

Keywords: Motion analysis, gait, multibody dynamics, Kalman filter, real-time, parameter estimation

### 4.1.1 Nomenclature

#### **Latin (lower case)**

$f()$	time update function
$f_{int}$	internal forces and moments
$f_{ext}$	external forces and moments
$g()$	measurement function
$q_{fix}$	generalized coordinates (not time varying)
$q_{flo}$	generalized coordinates (time varying)
$r$	measurement noise
$s$	state vector
$u$	velocities
$w$	process noise
$z$	measurement vector

#### **Latin (upper case)**

$A$	$df(x, w)/dx'$
$B$	projection of the state update function on the state
$C$	topology matrix
$D$	measurement noise covariance matrix
$G$	$dg(x, r)/dx'$
$I$	identity matrix
$O$	zero vector or matrix
$P$	error covariance matrix

$Q$  process noise covariance matrix

$W$   $df(x, w)/dw$

#### **Other**

$\square_i$  vector index

$\square_{i,j}$  vector sub-index

$\square_k$  time frame  $k$

$\tilde{\square}$  *a priori* estimate

$\hat{\square}$  *a posteriori* estimate

$\|\square\|$  Euclidian norm/distance

## 4.2 Introduction

Movement analysis has a wide range of applications in research, clinics, and sports. Data is acquired by measuring motions and interaction forces with the environment. Motion is captured with optical or electromagnetic tracking systems or with body-mounted motion sensors (Wong et al., 2007). Interaction forces with the environment can be acquired with force plates, an instrumented treadmill (Riley et al., 2007), or force shoes (Veltink et al., 2005).

Measurement data is commonly processed in three sequential steps. The first step is to determine the location of the joints and define a reference frame for each segment. In most conventional methods for data processing, the joint centers and segment reference frames are defined with respect to anatomical landmarks (Ferrari et al., 2008). This can be done by placing the markers directly on the anatomical landmarks (e.g. the Conventional Gait Model, CGM) or by using a calibration trial (e.g. the calibrated anatomical systems technique, CAST, Cappozzo et al., 1995; Davis et al., 1991). In a calibration trial, anatomical landmarks are palpated with an instrumented so that their relative positions to other markers are known. The second step is to calculate the segment and joint angles by comparing the orientation of markers clusters during movement with their orientation in a reference pose. Velocities and accelerations are obtained by differentiating the angles with respect to time. The third step is to calculate the kinetics, i.e. joint moments and joint powers. Joint moments are usually derived from Newton-Euler equations.

### 4.2.1 Estimation errors

In general, estimation errors in joint angles and moments due to processing of measurement data are much larger than the measurement errors (Baker, 2006). Conventional methods that use tracking of optical markers, such as the CGM and CAST, have some common problems that are the cause of these estimation errors:

*Incorrect model parameters:* The relation between anatomical landmarks, joint locations, joint orientations, and mass distributions often depend on regression analysis and inter-subject differences are ignored (Davis et al., 1991; Leva, 1996; Reinbolt et al., 2005; Winter, 1990).

*Imprecise palpation of anatomical landmarks:* The identification of anatomical landmarks on the subject depends on the experimenter and might be inaccurate. Differences in the joint angles can be more than 20° between different sites and experimenters (Della Croce et al., 2005; Gorton et al., 2009).

*Poor estimate of the accelerations:* The acceleration signal tends to be noisy due to the numerical differentiation of the angles. This is commonly suppressed by applying a low-pass filter.

*Soft tissue artifacts:* The methods assume that every segment is rigid. However, soft tissue deformation causes markers to move relative to the true segment reference frames causing an error in the estimation of the joint centers and the segment reference frames (Leardini et al., 2005).

*Missing data:* The methods are vulnerable to missing data that commonly occurs due to marker occlusion. If one marker is missing, a segment reference frame cannot be reconstructed, and kinetics and kinematics for one or more joints cannot be calculated. This can be partially compensated with interpolation techniques.

### 4.2.2 Countermeasures

Different countermeasures are introduced to reduce the estimation errors due to processing of measurement data. Different approaches can be separated into methods that solely focus on an improved estimation of the kinematics and methods that improve both kinematics and kinetics.

#### *Improved kinematics*

Different studies focus on estimating joint rotation centers directly from marker data instead of indirectly from anatomical landmarks. In the former case, the joint centers are estimated from the relative movements of markers on both sides of the joint (Reinbolt et al., 2005; Schwartz and Rozumalski, 2005).

The segment kinematics can be determined for every segment and time step individually (segmental optimization method, SOM). In reality the segment kinematics are constrained at the joints. Global optimization methods (GOMs) make use of these constraints to reduce the estimation error. GOMs describe the body as a multilink system and estimate all joint angles at the same time (Lu and O'Connor, 1999). Requiring motion smoothness can further improve this estimate, for example by using a Kalman filter (Cerveri et al., 2003), possibly in combination with a smoother (De Groot et al., 2008).

Obtaining the joint positions and finding the segment trajectories is an estimation problem with different kinds of uncertainties. This estimation problem can be captured in an universal framework (Todorov, 2007). In this framework all unknown quantities (including model parameters) are treated as variables and all prior knowledge is encoded probabilistically. This framework is a Gauss-Newton generalization of an extended Kalman filter, and has been tested for both synthetic

and experimental kinematic data. With this filter, the model parameters and kinematics can be reliably estimated, also when input data is partially missing (Todorov, 2007).

### ***Improved kinematics and kinetics***

In many cases, the force-plate data and the motion data contain redundant information, since the forces and accelerations are coupled via the mass matrix. Solving the equations of motions is thereby an over-constrained problem. In conventional methods, the over-constrained problem is solved by simply ignoring some of the force and moment equilibrium constraints, which results in residual forces and moments. Alternatively, finding the joint torques and moments might be formulated as an optimization problem (Chao and Rim, 1973; Delp et al., 2007; Kuo, 1998; Remy and Thelen, 2009; van den Bogert and Su, 2008). By doing so, joint toques are more accurately estimated, and measurement biases can be identified. So far these methods were not suitable for real-time applications.

#### **4.2.3 Goal**

The goal of this paper is to develop a general framework for motion analysis and parameter estimation that considers uncertainties from various causes and makes an optimal estimation of kinematics and kinetics simultaneously. The framework we developed is an extension of Todorov's framework to the kinetic domain. This leads to a Kalman filter that estimates the state of a multibody dynamical system, hence the name multibody Kalman filter (MKF). This integral approach allows for real-time analysis of gait data.

To justify the use of the MKF we will conduct two experiments. In the first experiment the MKF is used on a set of synthetic data. This experiment shows advantage of the extension of Todorov's framework to the kinetic domain. In the second experiment the gait of four subjects is analyzed. This experiment shows the applicability of the MKF for motion analysis. The kinematics and kinetics calculated with the MKF and the CAST are compared. The latter is an example of common practice in gait analysis.

## **4.3 Methods**

### **4.3.1 The MKF**

The MKF is a special application of the extended Kalman filter, and an extension of the filter developed by Todorov (2007). This section will generally describe the MKF. A detailed description of the MKF equations can be found in the appendix. The MKF performs alternating time and measurement updates. The time update

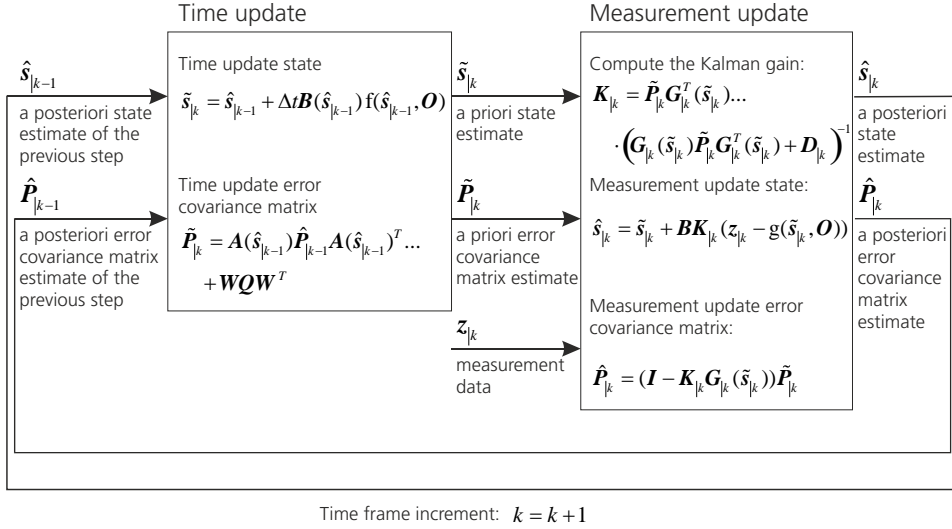


Figure 10: Schematic overview of the workings of the MKF which is a special application of the extended Kalman filter. First, the filter makes a time update that leads to an a priori estimate of the state and the error covariance matrix. Secondly, the filter makes a measurement update that lead to an a posteriori estimate of the state and the error covariance matrix. After the measurement update the time frame is incremented with one and the cycle restarts.

predicts ahead, resulting in an *a priori* estimate (denoted with  $\tilde{\cdot}$ ). The measurement update corrects the estimates when new measurements are available, resulting in an *a posteriori* estimate (denoted with  $\hat{\cdot}$ , Figure 10). The extended ( $\mathbf{s}$ ) state vector is defined by:

$$\mathbf{s} = \begin{Bmatrix} \mathbf{q}_{fix} \\ \mathbf{q}_{flo} \\ \mathbf{u} \\ \mathbf{f}_{int} \\ \mathbf{f}_{ext} \end{Bmatrix} \quad (9)$$

$\mathbf{q}_{fix}$  is a vector with time-invariant spatial variables. These are the model parameters such as segment lengths and local joint orientations of which the value is unknown. Therefore, they are modeled as variables as well.  $\mathbf{q}_{flo}$  is a vector with time-variant spatial variables (e.g. joint angles).  $\mathbf{u}$  and  $\mathbf{f}_{int}$  are vectors with generalized velocities and forces (e.g. joint velocities and moments).  $\mathbf{f}_{ext}$  is a vector with external moments and forces acting at the center of mass of each segment in the multibody system (e.g. ground reaction forces).

### Time update

The time update function ( $f(\mathbf{s}_{|k-1}, \mathbf{w})$ ) of the state  $\mathbf{s}_{|k-1}$  is given by:

$$\mathbf{s}_{|k} = \mathbf{s}_{|k-1} + \Delta t \mathbf{B}(\mathbf{s}_{|k-1}) f(\mathbf{s}_{|k-1}, \mathbf{w}), \quad \mathbf{w} = \mathbf{N}(\mathbf{O}, \mathbf{Q}) \quad (10)$$

With:

$$f(\mathbf{s}_{|k-1}, \mathbf{w}) = \left\{ \begin{array}{c} \mathbf{O} \\ \mathbf{u}_{|k-1} \\ \bar{\mathbf{M}}(\mathbf{q}_{|k-1})^{-1} \bar{\mathbf{f}}(\mathbf{q}_{|k-1}, \mathbf{u}_{|k-1}, \mathbf{f}_{int|k-1}, \mathbf{f}_{ext|k-1}) \\ \mathbf{w}_{int|k} \\ \mathbf{w}_{ext|k} \end{array} \right\} \quad (11)$$

Where  $\Delta t$  is the time step,  $k$  and  $k-1$  are, respectively, the indices of the current and previous time frame.  $\mathbf{q}_{fix}$  is unchanged because it is time invariant.  $\mathbf{q}_{flo}$  is updated with the velocity.  $\mathbf{u}$  is updated with the acceleration. The acceleration is calculated with the equations of motion.  $\mathbf{f}_{int}$  and  $\mathbf{f}_{ext}$  are updated with the process noise  $\mathbf{w}$ .  $\mathbf{w}$  is assumed to have a normal distribution with zero mean and covariance  $\mathbf{Q}$ . The matrix  $\mathbf{B}$  accounts for the quaternion constraints. The *a priori* estimates  $\tilde{\mathbf{s}}_{|k}$  and  $\tilde{\mathbf{P}}_{|k}$  are made using the *a posteriori* estimate  $\hat{\mathbf{s}}_{|k-1}$  and  $\hat{\mathbf{P}}_{|k-1}$  while assuming zero process noise:

$$\hat{\mathbf{s}}_{|k} = \tilde{\mathbf{s}}_{|k-1} + \Delta t \mathbf{B}(\tilde{\mathbf{s}}_{|k-1}) f(\tilde{\mathbf{s}}_{|k-1}, \mathbf{O}) \quad (12)$$

$$\tilde{\mathbf{P}}_{|k} = \mathbf{A}(\hat{\mathbf{s}}_{|k-1}) \hat{\mathbf{P}}_{|k-1} \mathbf{A}(\hat{\mathbf{s}}_{|k-1})^T + \mathbf{W} \mathbf{Q} \mathbf{W}^T \quad (13)$$

With:

$$\mathbf{A}(\mathbf{s}) = \mathbf{I} + \Delta t \frac{d f(\mathbf{s}, \mathbf{w})}{d \mathbf{s}} \mathbf{B} \quad \text{and} \quad \mathbf{W} = \frac{d f(\mathbf{s}, \mathbf{w})}{d \mathbf{w}} \quad (14)$$

### Measurement update

The measurement function ( $g(\mathbf{s}, \mathbf{r})$ ) provides a new measurement ( $\mathbf{z}_{|k}$ ) at each time frame. The measurement is a function of ( $\mathbf{s}$ ) and the measurement noise ( $\mathbf{r}$ ):

$$\mathbf{z} = g(\mathbf{s}, \mathbf{r}), \quad \mathbf{r} = \mathbf{N}(\mathbf{O}, \mathbf{D}) \quad (15)$$

Where  $r$  is assumed to be normally distributed with zero mean and covariance  $D$ . It is not required that every time frame all signals are measured, this accommodates for missing data. The Kalman gain ( $K$ ) is calculated as follows:

$$\mathbf{K}_{|k} = \tilde{\mathbf{P}}_{|k} \mathbf{G}_{|k}^T (\tilde{\mathbf{s}}_{|k}) \left( \mathbf{G}_{|k} (\tilde{\mathbf{s}}_{|k}) \tilde{\mathbf{P}}_{|k} \mathbf{G}_{|k}^T (\tilde{\mathbf{s}}_{|k}) + \mathbf{D}_{|k} \right)^{-1} \quad (16)$$

With:

$$\mathbf{G}(\mathbf{s}) = \frac{d \mathbf{g}(\mathbf{s}, \mathbf{r})}{d \mathbf{s}} \mathbf{B}(\mathbf{s}) \quad (17)$$

The Kalman gain is used to perform the measurement update resulting in the *a posteriori* estimate  $\hat{\mathbf{s}}_{|k}$  and  $\hat{\mathbf{P}}_{|k}$ :

$$\hat{\mathbf{s}}_{|k} = \tilde{\mathbf{s}}_{|k} + \mathbf{B} \mathbf{K}_{|k} (\mathbf{z}_{|k} - \mathbf{g}(\tilde{\mathbf{s}}_{|k}, \mathbf{O})) \quad (18)$$

$$\hat{\mathbf{P}}_{|k} = (\mathbf{I} - \mathbf{K}_{|k} \mathbf{G}_{|k} (\tilde{\mathbf{s}}_{|k})) \tilde{\mathbf{P}}_{|k} \quad (19)$$

### **Implementation**

The MKF was implemented in Matlab (MathWorks, Natick, MA, USA) and ran on a laptop (Intel Core2Duo T9600).

#### **4.3.2 Synthetic data experiments**

This experiment shows the workings of the filter on a simple model. Synthetic data was used so the ground truth was available, the noise on the model could be controlled, and the noise covariance was exactly known. Synthetic data was generated by using the bipedal spring-mass model of (Geyer et al., 2006) shown in Figure 12. The kinematics of the model were estimated with the MKF that used both the position and force input, and with a simple Kalman filter (SKF). The SKF used only the position inputs and assumed constant accelerations with a noise term to account for the errors introduced by this assumption. In this particular case the SKF was effectively the same as the MKF without force inputs.

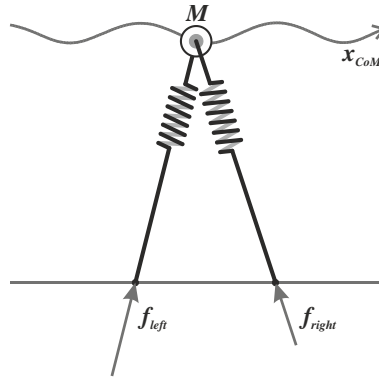


Figure 12: Two dimensional bipedal spring mass model (Geyer et al., 2006). The model consists out of a point mass representing the body and two massless linear springs representing the legs. The springs deform during stance and thereby exert forces on the center of mass, during swing the leg moves to a fixed angle with respect to the ground. The properties are chosen to represent human like walking (mass = 80 kg, leg length = 1 m,  $g = 9.81\text{m/s}^2$ ). The system has a constant energy and has many stable gait patterns. We selected a system energy of 819 J, a leg stiffness of 14 N/mm, and an initial leg angle of  $69^\circ$ . This specific example is also shown in (Geyer et al., 2006). The simulated measurements are the position of the center of mass and the sum of the ground reaction forces with a sampling rate of 100Hz.

To investigate the effect of a smoother the filter output was processed by a Rauch-Tung-Striebel smoother (Rauch et al., 1965). Gait analysis methods that do not apply special smoothing, like SOMs and GOMs, often use a low pass filter to eliminate measurement noise and obtain smooth signals that can be numerically derived to obtain velocities and accelerations (e.g. Riley et al., 2007). The results of the MKF and SKF were therefore also compared with the marker kinematics after

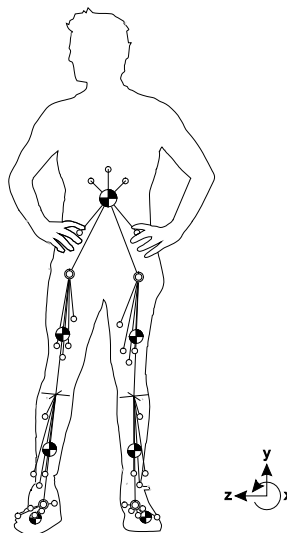


Figure 11: Front view of the human model and definition of axes used in the experiments. The subjects walked in the positive x-direction.

forward and backward filtering the center of mass position ( $\mathbf{x}_{CoM}$ ) with a fourth-order Butterworth filter with a cut off frequency of 15 Hz. Note that a smoothers and backward filters cannot be used in real-time applications since they require estimates from future time frames.

The filters were used multiple times with input signals containing different amounts of white noise. The standard deviation of the noise on the  $\mathbf{x}_{CoM}$  ranged between 0.001 m and 0.1 m. The standard deviation of the noise on the ground reaction forces, only used by the MKF, was 1%, 10%, and 20% of the amplitude of the force signal. The process noise covariance was determined by taking the covariance of the high pass filtered (fourth-order Butterworth filter, 0.25Hz crossover frequency)  $\mathbf{x}_{CoM}$  and force signals without noise. The measurement noise was set to its actual value. The filter performance was evaluated by calculating the variance accounted for (VAF) of the absolute position (high pass filtered, 4<sup>th</sup> order Butterworth filter, 0.25Hz crossover frequency) and absolute acceleration of the CoM. The VAF is given by:

segment name	segment parent	joint type	Time variant?	estimated during DCT	estimated during WT
HAT position	--	T	Yes	Yes	Yes
HAT orientation + CoM*	HAT position	B	Yes	Yes	Yes
HAT markers (5x)	HAT orientation + CoM	T	No	Yes	No
Right hip location	HAT orientation + CoM	T	No	Yes	No
Right hip joint	Right hip location	B	Yes	Yes	Yes
Right thigh CoM	Right hip joint	S	No	No	No
Right thigh markers (4x)	Right hip joint	T	No	Yes	No
Right knee location	Right hip joint	S	No	Yes	No
Right knee orientation	Right knee location	H	No	Yes	No
Right knee joint	Right knee orientation	H	Yes	Yes	Yes
Right shank CoM	Right knee joint	S	No	No	No
Right shank markers (4x)	Right knee joint	T	No	Yes	No
Right ankle location	Right knee joint	S	No	Yes	No
Right ankle joint	Right ankle location	B	Yes	Yes	Yes
Right foot CoM	Right ankle joint	S	No	No	No
Right foot markers (5x)	Right ankle joint	T	No	Yes	No

Table 4: Human model. Segment name: The name of the segment, Segment parent: The name of the proximal segment it is attached to, Joint type: The type of joint (B: ball joint 3DoF, H: hinge joint 1DoF, T: translational joint 3DoF, S: sliding joint 1DoF). Time variant: yes: variable is time variant, no: variable is time invariant, Estimated during DCT: The variables are estimated while processing the dynamic calibration trial (kinematics only), Estimated during WT: The variables are estimated while processing the walking trial. The model is symmetric so that for every right segment there is an equivalent left segment. \*CoM = Centre of mass, HAT = Head, arms and trunk, DoF = Degree of freedom.

$$\text{VAF}(\mathbf{y}) = 1 - \frac{\text{var}(\|\mathbf{y} - \hat{\mathbf{y}}\|)}{\text{var}(\|\mathbf{y}\|)} \quad (20)$$

Where  $\mathbf{y}$  is the true signal and  $\hat{\mathbf{y}}$  is the signal estimate.

### 4.3.3 Human data

#### *Subjects*

Four healthy subjects (two males, two females, age: 21 years 5 months  $\pm$  1 year 10 months, height: 1.76  $\pm$  0.12 m, weight: 73.4  $\pm$  11.9 kg) participated in this experiment. The Human Research Ethics Committee of the Delft University of Technology approved the study, and all subjects gave written informed consent to participate.

#### *Human model*

A 3D seven-segment model was used to describe the human body (Figure 11, Table 4).

#### *Experimental apparatus and recordings*

Ground reaction forces and moments were recorded with a dual belt instrumented treadmill (Y-Mill, Forcelink B.V., Culemborg, The Netherlands). Marker trajectories were recorded by an optical tracking system (VZ4000, Visualeyex, Burnaby, BC, Canada). Data was sampled at 100 Hz.

#### *Experimental protocol*

Markers were placed on the subject according to Figure 11 and the subject's weight and height were recorded. For the CAST, the following anatomical landmarks were palpated with a pointer: The anterior/posterior superior iliac spine, the trochanter major, lateral/medial epicondyle, the caput fibulae, the tuberositas tibiae, the lateral/medial malleolus, the calcaneus, the caput metatarsale I/V. All landmarks were palpated on the left and right side. A static trial was recorded where the subject stands upright. A dynamic calibration trial (DCT) was recorded where the subjects performed a motion moving each leg joint through its whole range of motion. After these initial trials, a walking trial (WT) was recorded. The subject walked at a constant speed of 5 km/h for three minutes. All measurements were performed barefoot.

#### *Data analysis*

The data was analyzed with the MKF and the CAST. For the CAST, BodyMech (VUMC, Amsterdam, The Netherlands) was used. The joint angles and force data

were filtered with a fourth-order low-pass Butterworth filter with a cut-off frequency of 15 Hz.

Theoretically, all variables could be estimated at the same time. Preliminary tests revealed that the estimate of  $\mathbf{q}_{fix}$  greatly improved if the subject moved within a large part of its range of motion. This was accounted by processing the data in two steps. In the first step the DCT trial was processed. During processing of the DCT only kinematics ( $\mathbf{q}_{fix}$  and  $\mathbf{q}_{flo}$ ) were estimated (similar to Todorov's filter), since no force data was available for this trial. In the second step the WT was processed, in which both joint kinetics and kinematics ( $\mathbf{q}_{flo}$ ,  $\mathbf{u}$ ,  $\mathbf{f}_{int}$ , and,  $\mathbf{f}_{ext}$ ) were estimated. During the processing of the WT,  $\mathbf{q}_{fix}$  was kept constant, and left out the state vector (Table 4). The filter parameters are given in Table 5. Anthropometric data from (Leva, 1996; Winter, 1990) were used as an initial state of the filter in the DCM trial.

Both the MKF and CAST were used to estimate the joint centers, joint angles, and joint moments. For both methods, the angles during the static trial were defined as zero. The data was split into individual strides separated by the heel strike of the right foot. The steps from a 60-second sample of each trial were used to calculate a

	DCT	WT		DCT	WT
	$\sigma^2$	$\sigma^2$		$\sigma^2$	$\sigma^2$
$\mathbf{Q}_{flo}$ $\mathbf{Q}_{flo}$ [m, rad] <sup>2</sup>	100 <sup>2</sup>	--	$\mathbf{P}_{fix o}$ $\mathbf{P}_{fix o}$ (marker segment s) [m, rad] <sup>2</sup>	1 <sup>2</sup>	--
$\mathbf{Q}_{fint}$ $\mathbf{Q}_{fint}$ (ankle joints) [Nm] <sup>2</sup>	--	10 <sup>2</sup>	$\mathbf{P}_{fix o}$ $\mathbf{P}_{fix o}$ (other segment s) [m, rad] <sup>2</sup>	0.2 <sup>2</sup>	--
$\mathbf{Q}_{fint}$ $\mathbf{Q}_{fint}$ (other joints) [Nm] <sup>2</sup>	--	20 <sup>2</sup>	$\mathbf{P}_{flo o}$ $\mathbf{P}_{flo o}$ [m, rad] <sup>2</sup>	100 <sup>2</sup>	1 <sup>2</sup>
$\mathbf{Q}_{fext}$ $\mathbf{Q}_{fext}$ [N, Nm] <sup>2</sup>	--	50 <sup>2</sup>	$\mathbf{P}_{u o}$ $\mathbf{P}_{u o}$ [m/s, rad/s] <sup>2</sup>	--	10 <sup>2</sup>
$\mathbf{D}_{marker}$ $\mathbf{D}_{marker}$ [m] <sup>2</sup>	0.02 <sup>2</sup>	0.02 <sup>2</sup>	$\mathbf{P}_{fint o}$ $\mathbf{P}_{fint o}$ (ankle joints) [Nm] <sup>2</sup>	--	10 <sup>2</sup>
$\mathbf{D}_{fext}$ $\mathbf{D}_{fext}$ [N, Nm] <sup>2</sup>	--	50 <sup>2</sup>	$\mathbf{P}_{fint o}$ $\mathbf{P}_{fint o}$ (other joints) [Nm] <sup>2</sup>	--	20 <sup>2</sup>
			$\mathbf{P}_{fext o}$ $\mathbf{P}_{fext o}$ [N, Nm] <sup>2</sup>	--	50 <sup>2</sup>

Table 5: Filter parameters of the MKF filter used in the human experiments. Q, D and  $\mathbf{P}_0$  are diagonal matrices. The coefficients ( $\sigma^2$ ) on the diagonal are mentioned in the table. Ideally these parameters are known, but a course estimate often suffices. Parameters that are similar are grouped and have all the same value. Standard deviation of the marker noise, including soft tissue artifacts, was assumed to be 20mm (Leardini et al., 2005). Standard deviation of the noise in the ground reaction forces and moments was assumed to be respectively 50N and 50Nm. For the DCT trial  $\mathbf{P}_{flo|o}$  was chosen much larger than  $\mathbf{P}_{fix|o}$  so the MKF favored changing joint angles over model parameters. For the same reason  $\mathbf{P}_{fix|o}$  for the marker segments was larger than for the other segments, since the other segments had a reasonable initial estimate adapted from (Leva, 1996; Winter, 1990). For all other values a course estimate was made based normal gait kinetics and kinematics. After this initial guess some filter parameters required manual tuning to improve the filter performance.

median step. The presented results were averaged over the subjects and standard deviations were calculated.

#### 4.3.4 Error measures

##### ***Position estimation error***

For both methods, a position estimation error is defined. The MKF constrains the segment movements at the joint. As a consequence, the estimated marker positions differ from the observed marker positions. The marker estimation error ( $e_{mkr}$ ) is defined as the RMS of the Euclidian distance between observed ( $\mathbf{p}_{mkr,i}$ ) and the estimated ( $\hat{\mathbf{p}}_{mkr,i}$ ) marker position averaged over all markers ( $n$ ) on the segment.

$$e_{mkr} = \frac{1}{n} \cdot \sum_{i=1}^n rms \left( \left\| \mathbf{p}_{mkr,i}(t) - \hat{\mathbf{p}}_{mkr,i}(t) \right\| \right) \quad (21)$$

In the CAST, the segment movement is not constrained by joints. Joints locations are estimated from the segment distal and proximal of the joint. During movement, these estimates may move relative to each other. The joint estimation error ( $e_{jnt}$ ) is defined as the RMS of the Euclidian distance between the estimate from the proximal ( $\hat{\mathbf{p}}_{prox}$ ) and distal ( $\hat{\mathbf{p}}_{dist}$ ) segment.

$$e_{jnt} = rms \left( \left\| \hat{\mathbf{p}}_{prox}(t) - \hat{\mathbf{p}}_{dist}(t) \right\| \right) \quad (22)$$

The proximal and distal joints are defined to coincide during the static trial. The marker and joint estimation errors are defined at different locations and cannot be directly compared. However, their order of magnitude is an indication of the performance.

##### ***Residual moments and forces***

The residual forces and moments ( $f_{res}$ ) are additional forces and moments that are required to maintain the force and moment equilibrium at the HAT-segment. In reality  $f_{res}$  does not exist, and the smaller the forces the more feasible the solution. Therefore the residual force error is defined as:

$$\mathbf{e}_{res} = \begin{Bmatrix} e_{res,Fx} \\ e_{res,Fy} \\ e_{res,Fz} \\ e_{res,Mx} \\ e_{res,My} \\ e_{res,Mz} \end{Bmatrix} = \frac{\text{mean}(\mathbf{f}_{res}(t))}{m} \quad (23)$$

Where  $m$  is the mass of the subject.

## 4.4 Results

### 4.4.1 Synthetic data

Figure 13 shows the performance of the different filters. Up to 3 mm marker noise, all filters gave good position estimates (VAF > 0.9). MKF performed better than the SKF and smoothed estimates are better than unsmoothed estimates. The Butterworth filter only gave good estimates for small amounts of noise. The acceleration estimates were generally poorer than the position estimates. Only the MKFs (except the unsmoothed MKF with 20% force noise) gave an acceptable (VAF > 0.75) estimate for all tested position noise levels.

### 4.4.2 Human data

#### *Estimated joint centers*

The locations of the joint centers in the static trial were both estimated with the MKF and the CAST. The differences between the two estimates were calculated by subtracting the estimates of the CAST from the estimates of MKF. The largest differences were found at the y-position of the hip, knee, and ankle (all between 13.2 mm and 24.6 mm) and the z-position of the hip (left -18.4 mm, right 19.8 mm), see Table 6.

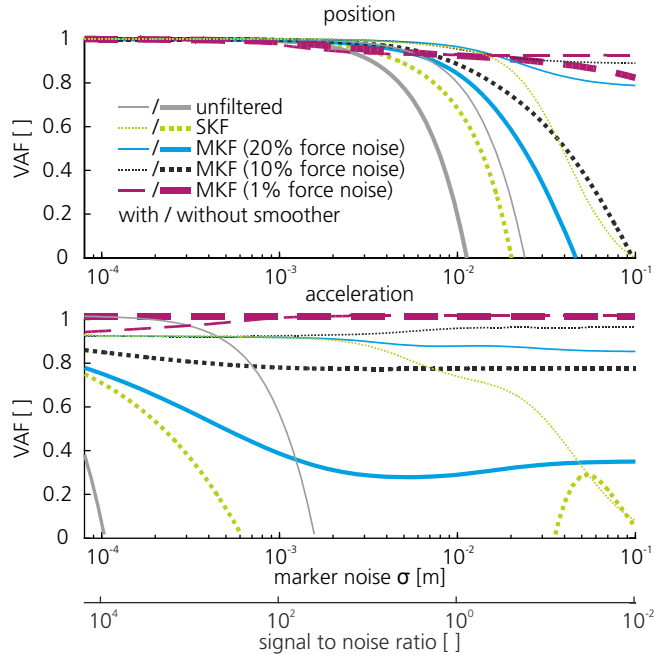


Figure 13: The VAF for the different filters and different noise levels. The smoothed signals were obtained with a Rauch-Tung-Striebel smoother for the MKF and the SKF and with a Butterworth filter for the unfiltered signal. The horizontal axes show the standard deviation ( $\sigma$ ) of the marker noise and the correspondent signal to noise ratio of the CoM position.

	x [mm]		y [mm]		z [mm]	
	mean	$\sigma$	mean	$\sigma$	mean	$\sigma$
left ankle	-9.5	11.0	-20.8	9.6	3.2	6.8
left knee	0.8	9.6	-13.2	3.0	7.8	7.9
left hip	11.5	14.6	-20.5	18.2	-18.4	15.2
right ankle	-4.5	5.8	-20.0	8.1	-2.1	13.2
right knee	6.6	6.8	-22.8	9.0	15.4	15.2
right hip	13.4	10.8	-24.6	10.7	19.8	10.7

Table 6: Differences in the estimation of the joint centers in the static trial with the MKF method and the CAST. The mean values and standard deviations ( $\sigma$ ) are given.

### Gait kinetics and kinematics

The joint angles and moments averaged over the subjects are shown in Figure 14. The largest differences in joint angles were found for the right knee with a RMS of  $6.41^\circ$  (left =  $6.04^\circ$ ). All other differences in joint angles were smaller (Table 7). Table 5 shows that the largest differences in estimated moments were found for the hip flexion/extension and ab/adduction (RMS between  $0.23 \text{ Nm/kg}$  and  $0.30 \text{ Nm/kg}$ ).

### ***Position estimation errors***

Table 9 gives the RMSE of the marker and the joint estimation error. The marker estimation errors (MKF) were between 4.18 (pelvis segment) and 9.28 mm (left foot). The joint estimation errors (CAST) were between 8.18 mm (left ankle) and 22.93 mm (left hip).

### ***Residual moments and forces***

Table 10 gives the residual forces and moments around the CoM of the HAT-segment for both methods. Both methods had a relatively large error in the y- and z-moment (0.21-0.22 Nm/kg).

### ***Computation time***

On the used hardware, the processing of the data was performed 2.2 times faster than real time.

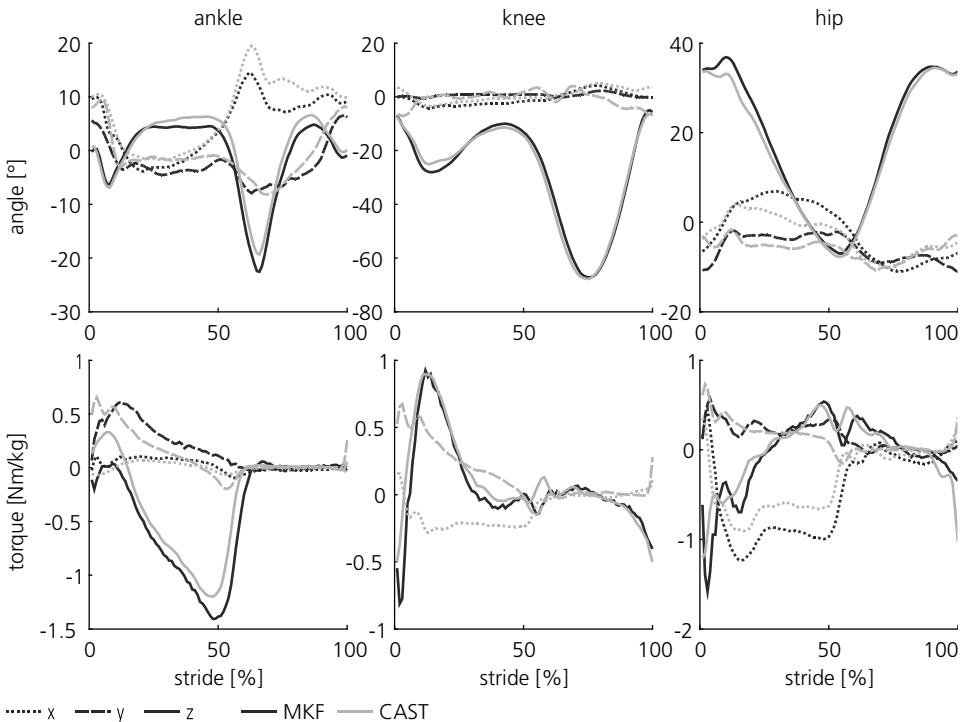


Figure 14: Joint angles and moments calculated with the MKF and the CAST. The joint angles are given as ZXY Euler angles. The lines represent the average over the subjects. Note that since the MKF had a hinge joint at the knee, x- and y-moments were not estimated by the MKF

joint	x [°]		y [°]		z [°]	
	mean	$\sigma$	mean	$\sigma$	mean	$\sigma$
left ankle	4,15	2,27	3,69	1,51	1,72	0,27
left knee	3,17	1,00	6,04	1,07	3,42	1,55
left hip	5,19	0,32	4,96	1,21	4,10	2,88
right ankle	3,91	1,77	3,36	1,56	2,20	0,86
right knee	2,82	0,70	6,41	1,37	2,38	0,79
right hip	4,28	0,30	4,32	1,46	3,15	1,73

Table 7: RMS of the difference in calculated angles. The mean values and standard deviations ( $\sigma$ ) are given.

joint	x [Nm/kg]		y [Nm/kg]		z [Nm/kg]	
	mean	$\sigma$	mean	$\sigma$	mean	$\sigma$
left ankle	0,07	0,04	0,17	0,03	0,22	0,10
left knee	--	--	--	--	0,17	0,01
left hip	0,30	0,16	0,18	0,01	0,28	0,03
right ankle	0,08	0,06	0,15	0,05	0,19	0,06
right knee	--	--	--	--	0,15	0,02
right hip	0,28	0,07	0,16	0,03	0,23	0,02

Table 8: RMS of the difference in calculated moments. The mean values and standard deviations ( $\sigma$ ) are given. Note that since the MKF had a hinge joint at the knee, x- and y-moments were not estimated by the MKF.

## 4.5 Discussion

### 4.5.1 Synthetic data

In the experiment with synthetic data the MKF outperformed the SKF. The addition of a smoother generally improved the estimate. A smoother performs a backward operation and can therefore not be used for real-time applications.

The bipedal spring-mass model only described the hip motion which only made small deviations from a linear movement. In human walking, these deviations are much larger for other joints like the ankle joint. The VAF of the estimates was low for some filter conditions, but it needs to be considered that the signal covariance was already low in the first place. In this example all forces were known from measurements, thereby the MKF made a large improvement over the SKF. If not all forces are measured, like it is the case in gait analysis, this improvement could be more modest. Given the superior performance of the MKF in the simplified model, its use is justified.

### 4.5.2 Human data

The joint angle and moment patterns estimated with the MKF and CAST were compared. The RMS difference in estimated joint angles between both methods ranged from 1.72° to 6.41°. The RMS difference in estimated joint torques ranged

marker estimation error (MKF)			joint estimation error (CAST)		
segment	RMSE [mm]		joint	RMSE [mm]	
	mean	$\sigma$		mean	$\sigma$
left foot	9.28	0.63	left ankle	8.18	3.12
left shank	6.90	0.76	left knee	15.91	4.11
left thigh	5.66	0.61	left hip	22.93	6.53
right foot	4.11	0.62	right ankle	9.66	5.29
right shank	6.39	0.43	right knee	20.97	8.80
right thigh	6.02	0.75	right hip	19.89	5.11
pelvis	4.18	0.63			

Table 9: Position estimation errors. RMSE of the marker estimation error for the MKF and joint estimation error for the CAST. The mean values and standard deviations ( $\sigma$ ) are given.

	MKF		CAST	
	mean	$\sigma$	mean	$\sigma$
Mx [Nm/kg]	0.07	0.02	0.05	0.06
My [Nm/kg]	0.22	0.02	0.21	0.02
Mz [Nm/kg]	-0.22	0.21	-0.21	0.21
Fx [N/kg]	0.11	0.07	-0.03	0.06
Fy [N/kg]	-0.03	0.04	-0.01	0.04
Fz [N/kg]	-0.01	0.01	0.00	0.02

Table 10: RMS of the residual moments and forces at the CoM of the HAT-segment. The mean values and standard deviations ( $\sigma$ ) are given.

from 0.07 to 0.30Nm/kg. Differences of this magnitude are not uncommon when comparing different gait protocols (Ferrari et al., 2008). The differences in joint torque are closely related to the differences in estimated joint centers. Horizontal differences in the joint centers are multiplied with the dominant vertical component of the ground reaction force, this causes that small differences in joint centers have a relative large effect on the joint moments. Additionally the MKF introduces a small phase lag that is partly responsible for the found errors. For non-real-time applications this phase lag could be removed by the use of a smoother algorithm.

In the experiment with human data, the true kinematic and kinetic data was not accessible. The force and moment residuals, except  $F_y$ , at the HAT-segment were similar for the CAST and the MKF. The marker estimation errors for the MKF were generally lower than joint estimation errors for the CAST. This comparison should be interpreted with caution since definition of marker estimation and joint estimation errors differ, and the differences between methods are small. Based on our comparison, we conclude that the MKF performs at least as well as the CAST.

The MKF intrinsically handles uncertainties from multiple sources and makes more optimal use of all available data. This favors the method over the CAST and other conventional methods. The MKF might suffer from errors in the model representation, which is also the case for GOMs (Duprey et al., 2010; Lu and O'Connor, 1999).

The MKF does not use the regression equations to determine the joint centers this might be an advantage for specific subject groups (e.g. children with cerebral palsy (Della Croce et al., 2005)). The identification of anatomical landmarks is more difficult for obese subjects. The MKF eliminates the requirement of this identification and might therefore give more accurate results, although soft tissue artefacts can influence the results. Calibration trials, as needed for the MKF, might be perceived as too difficult for patient. But there are examples where similar calibration trials have been conducted with patients and the benefit might outweigh the difficulty (Baker, 2006).

## 4.6 Conclusion

In this paper we developed an extended Kalman Filter that simultaneously estimates the kinematics and kinetics in real-time. Experiments with synthetic data show that the inclusion of force data largely improves motion estimates. Experiments with human data show that the MKF gives as reliable estimates as with a conventional and commonly used technique in gait analysis (CAST).

One of the main advantages of the MKF is that it estimates model parameters and eliminates the need to palpate anatomical landmarks, which is labor intensive and prone to errors. The MKF is fast enough for real-time motion analysis.



# 5 Improving the transparency of a rehabilitation robot by exploiting the cyclic behavior of walking

---

*Wietse van Dijk\**

*Bram Koopman\**

*Edwin van Asseldonk*

*Herman van der Kooij*

*\*Equal contributors*

*Published as: W. van Dijk, H. van der Kooij, B. Koopman, and E. H. F. van Asseldonk, "Improving the transparency of a rehabilitation robot by exploiting the cyclic behaviour of walking.," IEEE Int. Conf. Rehabil. Robot., vol. 2013, p. 6650393, Jun. 2013.*

*Abstract— To promote active participation of neurological patients during robotic gait training, controllers, such as "assist as needed" or "cooperative control", are suggested. Apart from providing support, these controllers also require that the robot should be capable of resembling natural, unsupported, walking. This means that they should have a transparent mode, where the interaction forces between the human and the robot are minimal. Traditional feedback-control algorithms do not exploit the cyclic nature of walking to improve the transparency of the robot. The purpose of this study was to improve the transparent mode of robotic devices, by developing two controllers that use the rhythmic behavior of gait. Both controllers use adaptive frequency oscillators and kernel-based non-linear filters. Kernel-based non-linear filters can be used to estimate signals and their time derivatives, as a function of the gait phase. The first controller learns the motor angle, associated*

*with a certain joint angle pattern, and acts as a feed-forward controller to improve the torque tracking (including the zero-torque mode). The second controller learns the state of the mechanical system and compensates for the dynamical effects (e.g. the acceleration of robot masses). Both controllers have been tested separately and in combination on a small subject population. Using the feed-forward controller resulted in an improved torque tracking of at least 52 percent at the hip joint, and 61 percent at the knee joint. When both controllers were active simultaneously, the interaction power between the robot and the human leg was reduced by at least 40 percent at the thigh, and 43 percent at the shank. These results indicate that: if a robotic task is cyclic, the torque tracking and transparency can be improved by exploiting the predictions of adaptive frequency oscillator and kernel-based nonlinear filters.*

## 5.1 Introduction

Robot-aided gait training is an emerging clinical tool for gait rehabilitation of neurological patients. These patients benefit from task oriented, high intensity, and repetitive training, to regain functional mobility (Bayona et al., 2005; Kwakkel et al., 2004, 1997; Teasell et al., 2005). Due to the repetitive behavior of gait training, rehabilitation robots are introduced. Robots can be used to provide more frequent, and more intensive training sessions, while reducing the workload of the therapist, compared to conventional forms of manual assisted (and body weight supported) gait training.

Despite the mentioned advantages of robotic-assisted gait training a large



Figure 15: The Lopes is a bilateral exoskeleton with eight degrees of freedom. The actuators are detached from the exoskeleton and connected to the joints via Bowden cables and springs. The robot is impedance controlled via series elastic actuation.

multicenter randomized clinical trial among stroke survivors suggested that the diversity of conventional gait training results in greater improvements in functional recovery than robotic-assisted gait training (Hidler et al., 2009). This emphasizes that robotic-assisted training needs to be further optimized in order to improve therapeutic outcome. Active patient participation is thought to be the key in achieving this improvement.

To encourage active participation, more and more robotic devices control the interaction forces with impedance or admittance control algorithms. Control strategies that promote active participation are often referred to as: “assist-as-needed” (AAN), “cooperative”, “adaptive” or “interactive” controllers, and make the robot’s behavior more flexible and adaptive to the patient’s capabilities, progress and current participation. These types of controllers potentially increase the motivation of the patient since additional effort by the patient is reflected in their gait pattern. Additionally, depending on the impedance levels, small errors are still possible, which have been suggested to promote motor learning in mice (Cai et al., 2005; Ziegler et al., 2010) as well as humans (Emken and Reinkensmeyer, 2005; Jezernik et al., 2003).

A prerequisite of these control strategies is that the robot should have a transparent mode. When the patient does not require any support during specific subtasks or gait phases of walking, or when he increases his capabilities or effort, the robot should reflect normal unassisted walking. Due to the mass and inertia of the device, and/or imperfections in the controller for the transparent mode, unassisted walking is often different from free walking (Emken et al., 2007; van Asseldonk et al., 2008).

In a perfect transparent mode there are no interaction forces between the subject and the robot. In our gait rehabilitation robot, Lopes (Figure 15), the transparent mode consists of a zero-torque mode, where torques at the robot joints are controlled to zero. This does however not result in a perfect transparent mode and causes small gait alterations (van Asseldonk et al., 2008). These imperfections are partly due to sensor noise and friction in the actuation that limit the gains of the PI-controller, resulting in torque tracking errors. Additionally, the forces that occur due to joint friction, gravity, and inertias of the moving segments of the Lopes, are not compensated for in the current implementation. It is possible to compensate for these forces by an additional controller (Vallery et al., 2009a).

As mentioned before, Lopes, like many other rehabilitation robots, is specifically designed to assist a cyclic task, in this case walking. Robotic performance of cyclic

tasks can be improved by repetitive control or adaptive control (Wang et al., 2009). The latter has been implemented on the Lokomat rehabilitation robot in order to increase the compliance and transparency of this robot. One of the proposed controllers for this robot minimizes human-robot interaction forces by online optimization of a limited number of gait characteristics (angle offset, amplitude, and cycle time) of the reference angle trajectory used by their impedance controller (Riener et al., 2005). Thus, the robot motion gets entrained with the desired human motion. In this paper we present a more general framework for improved torque control, and improved transparent control. Therefore we developed two new controllers. Both controllers use a framework of adaptive frequency oscillators and kernel-based non-linear filters to learn a control signal (Gams et al., 2009; Ronsse et al., 2011).

The first controller is intended to improve the limited torque tracking of the currently implemented PI-controller. As suggested by Kuo the control of rhythmic movements can be improved by combining feedback and feed-forward control (Kuo, 2002). In general, feed-forward control requires a precise model of the dynamic system. To establish this model, precise system identification is required which is, for many applications, a limitation to implement feed-forward control strategies. In this special case however we can use the information from previous cycles to learn the feed-forward signal in a model-free manner, and gradually learn the feed-forward signal over multiple cycles.

The second controller compensates for the passive dynamics of the system that exist between the actuator and the user. This includes: gravitational, inertial and frictional forces. Forces that emerge from these effects are not sensed, and therefore not compensated, in the zero-torque mode. Compensation of these forces is achieved by the implementation of an inverse model, which in this case is an inverse dynamical model of the Lopes exoskeleton legs. The forces calculated by the inverse model are opposite to the existing forces. Application of the calculated forces should, theoretically, cancel out the interaction forces between the robot and the human.

Both controllers are tested separately and in combination on a small group of healthy test subjects ( $N=4$ ). To evaluate the performance of both control strategies the applied torques, the human-robot interaction forces, as well as the joint angles, are tracked. Here the suggested control strategies are specifically applied and tuned for the Lopes gait rehabilitation robot, but both approaches can be applied to other applications as well, as long as it concerns cyclic movement.

## 5.2 Experimental setup and methodology

### 5.2.1 Subjects

Four healthy subjects (4 males, age:  $28 \pm 2$  years, height:  $1.80 \pm 0.03$  m, weight:  $74.5 \pm 11.2$  kg) participated in this experiment. All subjects gave written informed consent prior to participation.

### 5.2.2 Experimental apparatus and recordings

To test both controllers the Lopes was used. The Lopes (Figure 15) is a treadmill-based lower-limb exoskeleton type robotic gait trainer. The Lopes is impedance-controlled and has eight actuated degrees of freedom (DoF) (flexion/extension at the hip and knee, hip abduction/adduction and horizontal pelvis translations). The robot was initially designed to provide supported treadmill training for stroke patients. Torque control was achieved by Bowden-cable-driven, PI-controlled, series-elastic actuators (Veneman et al., 2007). The actuators themselves were controlled with an inner velocity feedback loop (Vallery et al., 2007). Every DoF of the Lopes was fitted with potentiometers that record the kinematics, and potentiometers on the springs of the SEA that record the applied torque. Matlab xPC (Mathworks, Natick, Mass., USA) was used to control the applied torques by the exoskeleton joints at 1000 Hz. The performance of the used PI controller is described in (Vallery et al., 2007).

Additionally the interface between the subject's legs and the exoskeleton legs was sensorized using three (six DoF) force sensors (ATI-Mini45-SI-580-20, ATI Industrial Automation, Apex, N.C., USA, Figure 16). The cuffs (Hocoma, Volketswil, Switzerland) used in the Lopes were made of a rigid carbon fiber shell with Velcro straps and secure the subject's legs to the robot. One cuff connected to the upper leg and two cuffs connected to the lower leg of the subject. Only the interface of the right leg was fitted with force sensors. The analog signals coming from the force sensors were sampled at 1000 Hz using a data acquisition system (NI usb-6259, National Instruments, Austin, Texas, USA) and sent to the computer, where the data was stored for further processing. For clarity, the force sensors were only used to quantify the human-robot interaction forces, which were used as a measure for the transparency, and not as an input to the controller.

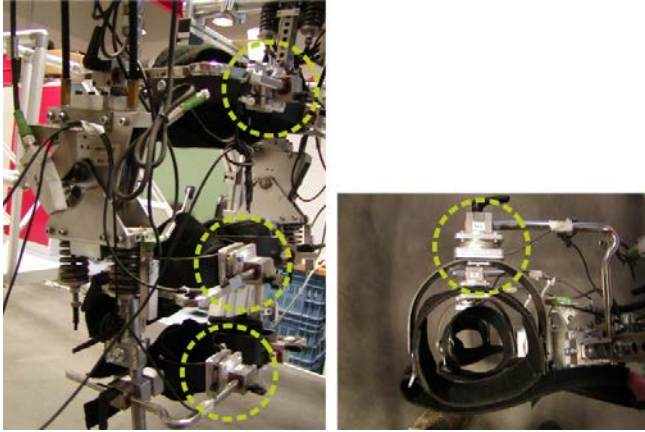


Figure 16: Six DoF force sensors (encircled). The force sensors are, via carbon shells and Velcro straps, attached to the human at one side and to the robot on the other side. Interaction forces are measured at the thigh (1 connection) and the shank (2 connections, high, and low)

### 5.2.3 Controller design

For the controllers that are presented in the next sections, an estimate of the position signals and their first and second order derivatives are required. To learn these signals the approach as suggested by (Gams et al., 2009) was used, which uses adaptive frequency oscillators in combination with kernel-based non-linear filters.

#### *Adaptive frequency oscillator*

Positions and their time derivatives can be expressed as a function of the gait phase. To acquire the gait phase, an adaptive frequency oscillator (Righetti et al., 2006) matches a sinusoidal signal to an input signal. The phase of the sinusoidal signal was used as the gait phase ( $\phi$ ) that runs from 0 to  $2\pi$ . In our application the right and left hip angle were used as input signals, since they show a sinusoidal like profile. The right and left hip angle ( $\theta_{right}$  and  $\theta_{left}$ ) were estimated with the following sinusoidal functions:

$$\hat{\theta}_{right}(t) = k + a \cdot \sin(\phi(t)), \quad \hat{\theta}_{left}(t) = k + a \cdot \sin(\phi(t) + \pi) \quad (24)$$

Of which  $k$ ,  $a$ , and  $\phi$  are the offset, amplitude and the phase of the signal respectively and  $t$  is the time in seconds, the circumflex ( $\hat{\cdot}$ ) denotes a signal estimate by the adaptive frequency oscillator. The left and right hip motions were assumed identical, with only a phase shift of  $\pi$ . The signal parameters were continuously updated using two error functions ( $e$ ).

$$\begin{aligned} e_{right}(t) &= \theta_{right}(t) - \hat{\theta}_{right}(t) \\ e_{left}(t) &= \theta_{left}(t) - \hat{\theta}_{left}(t) \end{aligned} \quad (25)$$

The following differential equations are governing the update process of the sinusoidal signal parameters:

$$\begin{aligned}
 \dot{\varphi}(t) &= \omega + \varepsilon e_{\text{right}}(t) \cos(\varphi(t)) + \varepsilon e_{\text{left}}(t) \cos(\varphi(t) + \pi) \\
 \dot{\omega}(t) &= \varepsilon e_{\text{right}}(t) \cos(\varphi(t)) + \varepsilon e_{\text{left}}(t) \cos(\varphi(t) + \pi) \\
 \dot{a}(t) &= \eta (e_{\text{right}}(t) \sin(\varphi(t)) + e_{\text{left}}(t) \sin(\varphi(t) + \pi)) \\
 \dot{k}(t) &= \eta (e_{\text{right}}(t) + e_{\text{left}}(t))
 \end{aligned} \tag{26}$$

The parameter  $\omega$  [rad s<sup>-1</sup>] estimated the frequency of the stride. Constants  $\eta$  and  $\varepsilon$  were used to regulate the learning rate of the signal. Pre-trials showed that with a  $\eta$  and  $\varepsilon$  of respectively 0.4 and 2 the adaptive frequency oscillator was synchronized within approximately ten steps.

### ***Kernel-based non-linear filters***

Subsequently, the position signals and their first and second order time-derivatives were estimated. The obtained gait phase of the adaptive frequency oscillator was used to learn the joint angles and the motor angles as a function of the phase. We used kernel-based non-linear filters as presented by (Gams et al., 2009) to learn the signal as a sum of  $n$  Gaussian functions ( $\psi(t)$ ):

$$\psi_i(t) = \exp\left(h\left(\cos(\varphi(t) - c_i) - 1\right)\right) \quad i = 1..n \tag{27}$$

with

$$c_i = \frac{2\pi i}{n} \tag{28}$$

where  $h$  is a parameter that determines the width of the Gaussian function. Pre-trials showed that with  $n$  is 20 and an  $h$  of 15 the learned signal matched the angular pattern of the hip and knee well. The learned signal ( $\tilde{\theta}(t)$ ) was estimated on time ( $t$ ) with:

$$\tilde{\theta}(t) = \frac{\sum_{i=1}^n w_i(t) \psi_i(t)}{\sum_{i=1}^n \psi_i(t)} \tag{29}$$

The tilde ( $\tilde{\cdot}$ ) denotes the signal estimated by the non-linear filter. The weights ( $w$ ) were adapted according to:

$$\dot{w}(t) = P\psi(\theta(t) - \tilde{\theta}(t)) \tag{30}$$

Where  $P$  had a value of 3 and is the learning gain, determining how fast the filter adapted its prediction. When the non-linear filter had learned the characteristics of the signal the filter can be locked by setting  $\dot{w}$  to zero. A nice feature of this filter is that analytical derivatives of the signal estimate can be obtained, which provided the velocity and acceleration estimate that was needed for the improved torque tracking and the improved transparency. The frequency and weights were only changing relatively slow and therefore assumed constant:

$$\dot{\varphi}(t) = \omega \text{ and } \dot{w}(t) = 0 \quad (31)$$

Additionally it was assumed that:

$$\frac{d}{dt} \left( \sum_{i=1}^n \psi_i(t) \right) = 0 \quad (32)$$

This is approximately true if a sufficient large number of kernels is chosen. The first time derivative is:

$$\tilde{\dot{\theta}} = \frac{\sum_{i=1}^n w_i(t) \dot{\psi}_i(t)}{\sum_{i=1}^n \psi_i(t)} \quad (33)$$

with

$$\dot{\psi}_i(t) = -\psi_i(t) h \omega \sin(\varphi(t) - c_i) \quad (34)$$

And the second time derivative is:

$$\tilde{\ddot{\theta}} = \frac{\sum_{i=1}^n w_i(t) \ddot{\psi}_i(t)}{\sum_{i=1}^n \psi_i(t)} \quad (35)$$

with

$$\ddot{\psi}_i(t) = -\dot{\psi}_i(t) h \omega \sin(\varphi(t) - c_i) - \psi_i(t) h \omega^2 \cos(\varphi(t) - c_i) \quad (36)$$

### ***Feed-forward velocity learning controller***

In the Lopes the series-elastic actuators were originally PI-controlled. In this setup sensor noise and friction in the actuation limited the maximal feedback gains that can be used, resulting in tracking errors. The cyclic behavior of walking provides the possibility to estimate a feed-forward signal. The feed-forward signal was obtained with a non-linear filter. This filter learned the motor angles, ( $\theta_{motor}$ , from the motor encoder) as a function of the phase, according to eq. 0.6. The analytical derivative (eq. 0.10) of the estimated signal ( $\tilde{\theta}_{motor}$ ) was used as the feed-forward

	Thigh	Shank
Mass [kg]	5.9	4.2
Inertia [kg m <sup>2</sup> ]	0.079	0.044
Length [m]	0.44	--
Centre of mass [m]	0.2	0.2
Damping [Nm <sup>2</sup> s <sup>-1</sup> ]	0.98	0.54
Strap position [m]	0.32	0.15 and 0.29

Table 11: Dynamical properties of the Lopes rehabilitation robot. Distances are measured from the proximal joint of the segment.

signal in the Lopes torque control loop (which is velocity controlled). This signal was added to the motor-velocity command ( $\dot{\theta}_{pi}$ ) from the PI-controller and was sent to the actuators. Figure 17 shows this control strategy.

### ***Dynamics compensation controller***

In the original transparent mode the joint torques were regulated to zero (zero-torque mode). Even if this control works perfectly this does not mean that the human, who walks in the Lopes, does not experience any interaction forces ( $F$ ). Friction, gravity and inertia will still result in reaction forces that are felt via the connections with the Lopes. An inverse dynamics module can be used to calculate the torques ( $\tau_{ID}$ ) required to cancel these interaction forces.

The inverse dynamics module described two planar double pendulums. Each double pendulum represented one leg of the Lopes in the sagittal plane, consisting of an upper and lower leg segment. Each segment of the pendulums had a mass (located at a certain distance from the proximal joint) and inertia. Additionally, each joint had rotational damping, which represented friction in each joint. The parameters corresponding to the different Lopes segments were estimated using multi-input-multi-output (MIMO) system identification (Koopman et al., 2010). Table 11 provides an overview of the system parameters. The input of the inverse model consisted of the hip and knee angle, angular velocity, and angular acceleration. The Lopes was not fitted with accelerometers that measure the required signals directly. Therefore, the joint angles and their first and second order derivatives were also obtained with the non-linear filter.

Figure 17 shows this control strategy.

## **5.2.4 Experimental protocol**

Before the subject was positioned in the Lopes, different anthropometric measurements were taken to adjust the exoskeleton segment lengths. Additionally, the positions of the cuffs were adjusted to align the subject's knee and hip axis with the exoskeleton joints. Next, the subject was positioned into the Lopes and the

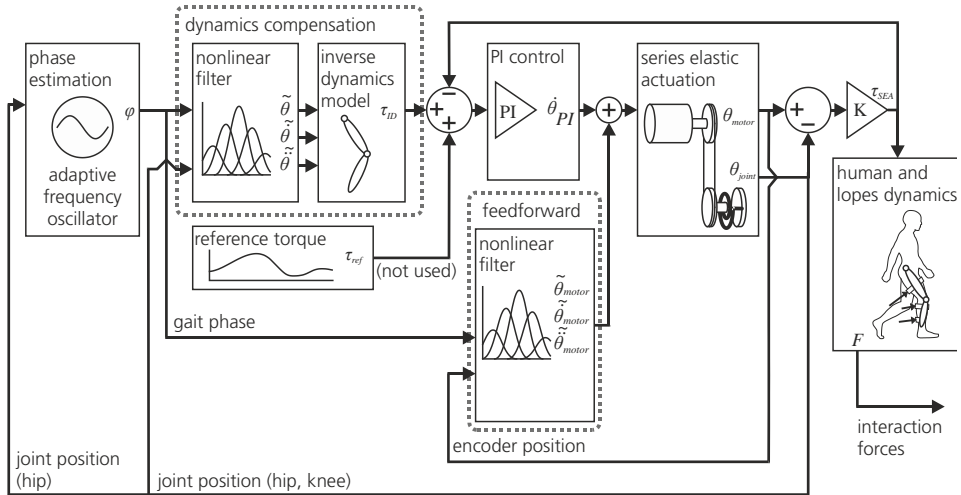


Figure 17: A schematic overview of the implemented controllers on the Lopes rehabilitation robot. The dynamics compensation module and the velocity learning module can be switched off so their output becomes zero. In the experiments described here the transparent mode was evaluated so the reference torque is set to zero.

trunk, thigh, and upper- and lower shank were strapped to the exoskeleton (Figure 16).

After a 5 minute familiarization period, to get used to walking in the Lopes, each subject performed two trials. The trials were performed at a slow walking ( $0.5 \text{ ms}^{-1}$ ) and fast walking speed ( $1.0 \text{ ms}^{-1}$ ). First the subjects walked for ninety seconds in the device using only the PI-controller (the conventional zero-torque mode). During this period the subject's cadence was recorded. The interaction forces scale with the cadence and the walking speed. At higher walking speeds the exoskeleton legs are accelerated and decelerated more, resulting in higher interaction forces. To cancel this effect out, the different controllers were tested at a fixed treadmill speed and a fixed cadence. The fixed cadence was achieved by asking the subjects to synchronize their walking tempo with a metronome that was set to the average of the subjects' pre-recorded cadence. This first condition (90 seconds of PI-controller) was also used to learn the signals that were required for the dynamics compensation. After 90 seconds the non-linear filters, that learn the hip and the knee angle (and their derivatives), were locked. Subsequently the different controllers were tested. The non-linear filter for the feed-forward controller was not locked. The different walking conditions and their duration are listed in Table 12. All conditions (at one speed) were evaluated directly after each other at the same cadence, without interruptions. In the second trial this protocol was repeated for the fast walking speed.

Condition	Duration for each speed (s)
PI	90
PI + velocity learning	90
PI + dynamics compensation	90
PI + velocity learning + dynamics compensation	90

Table 12: Walking conditions

### 5.2.5 Data analysis

All signal processing was done with custom-written software in Matlab (Natick, Mass., USA). The measured forces from the three force sensors were resampled at 100 Hz and synchronized with the potentiometer data from the Lopes.

Of all the recorded conditions only the last 60 seconds were used for data processing. Performance of the controllers was calculated based on the root mean square (RMS) of different signals. The evaluated signals were: 1) the torque tracking error, 2) the interaction force in the sagittal plane (perpendicular to the exoskeleton legs), and 3) the interaction power. The interaction power was calculated by taking the product of the moment of the interaction forces around their proximal joint and the velocity of their proximal joint. Results for the upper and lower shank force were summed. The power provides a measure for the flow of energy between robot and human, that is: it shows how much the robot is supporting, or resisting, the movement of the human.

Average steps were calculated by splitting the data into individual strides, based on the heel-contact event. Next, the different data blocks were normalized as a percentage of the gait cycle and averaged. Paired t-tests were performed to test for significant differences between the conditions. The level of significance was defined at  $p=0.05$ .

## 5.3 Results

### 5.3.1 Torque tracking

	Dynamics compensation off		Dynamics compensation on	
	Slow	Fast	Slow	Fast
Hip	52% (49%-56%)	59% (51%-60%)	56% (53%-64%)	58% (51%-62%)
Knee	61% (55%-68%)	64% (55%-70%)	65% (63%-67%)	62% (61%-63%)

Table 13: Reductions in RMS of the difference between desired and recorded torque (tracking error), averaged over the subjects. All reductions were significant with  $p < 0.01$  (paired t-test). The values between brackets show the range of the data over the different subjects.

The torque tracking was improved by the feed-forward controller. The RMS of the torque tracking error (RMSE) significantly reduced (Table 13, Figure 18). Reductions in tracking error were similar in the zero-torque mode and with the dynamics compensation switched on (Table 3). The small standard deviation

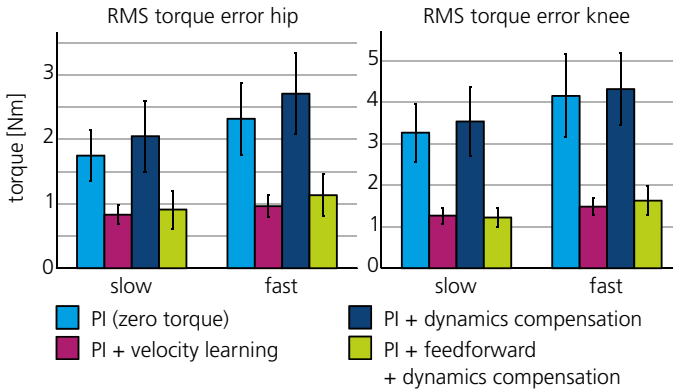


Figure 18: RMS of the tracking error at the hip (left) and knee (right). The bars are the results, averaged over the subjects. The error bars denote the standard deviations.

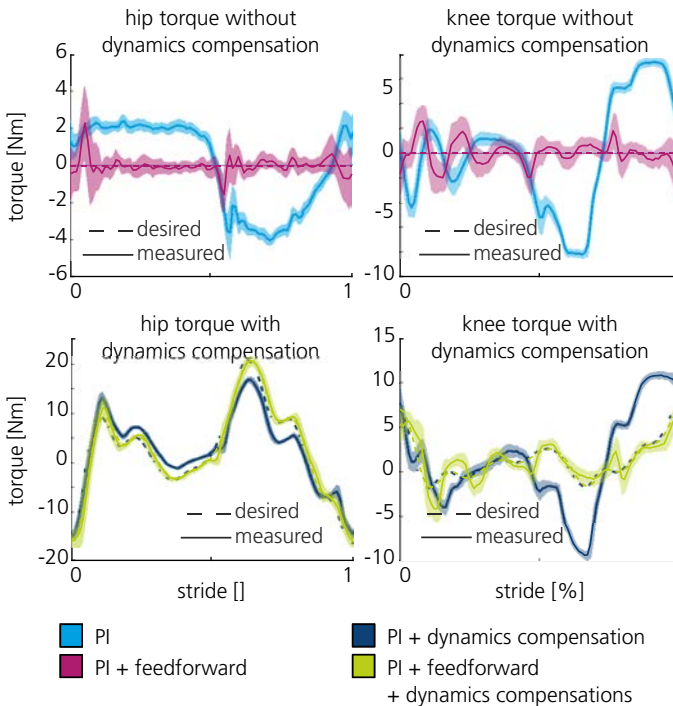


Figure 19: Top: difference between the desired and the measured torque without dynamics compensation (zero-torque mode) Bottom: difference between both signals with dynamics compensation. The figure shows the results for a typical subject. All signals are presented as a function of the gait cycle, starting at heel strike. Left: results for the hip. Right: results for the knee.

indicates that all subjects showed similar reductions. In general the knee joint had the largest reduction in RMSE. No clear effect of the walking speed on the tracking error was observed. A typical example of the tracking error as a function of the gait cycle, with and without the dynamics compensation, is shown in Figure 19.

### 5.3.2 Interaction forces

For the thigh, the interaction forces were reduced when the feed-forward controller was switched on, compared to the zero-torque mode (Figure 20). The dynamics compensation also resulted in a reduction in thigh interaction forces compared to the zero-torque mode. An additional decrease was observed when the feed-forward controller was switched on in combination with the dynamics compensation, leading to a total reduction of interaction forces of 39% ( $p = 0.001$ ) for slow walking and 35% ( $p = 0.009$ ) for fast walking. Walking at higher speed showed the same trends. In general: a higher walking speed resulted in higher interaction forces between subjects and robot.

For the interaction forces on the lower leg (shank high and shank low) the dynamics compensation did not result in a reduction of the forces, compared to the zero-torque mode (Figure 20). In fact: the interaction forces increased slightly. In contrast, the feed-forward controller did reduce the interaction forces. When it was switched on in the zero-torque mode, as well as in combination with the dynamics compensation, it resulted in reduced interaction forces.

### 5.3.3 Interaction power

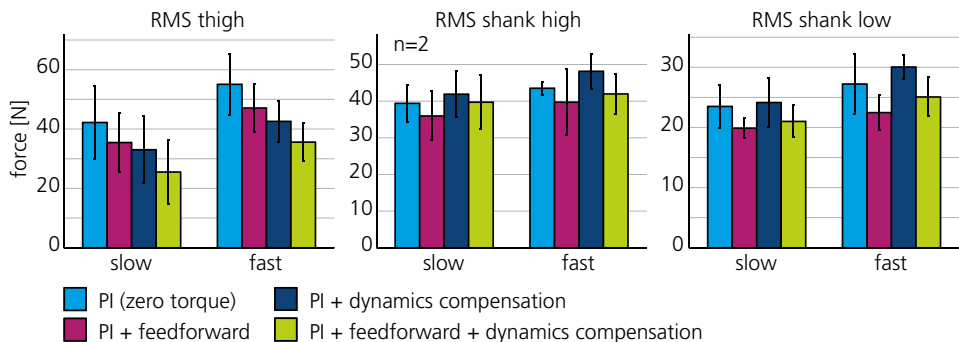


Figure 20: RMS of the interaction forces at the thigh (left) and shank (right). The bars are the results, averaged over the subjects. The error bars denote the standard deviations.

The interaction power (Figure 21) showed the same trends as observed in the interaction forces (Figure 20). At the thigh the dynamics compensation resulted in a reduction in power compared to the zero-torque mode. An additional decrease was observed when the feed-forward controller was switched on (Figure 21). Combining both controllers led to a total reduction of interaction power of 40.9% ( $p = 0.002$ ) for slow walking and 40.2% ( $p = 0.007$ ) for fast walking. Looking solely at the effect of walking speed, walking at higher speeds resulted in larger powers.

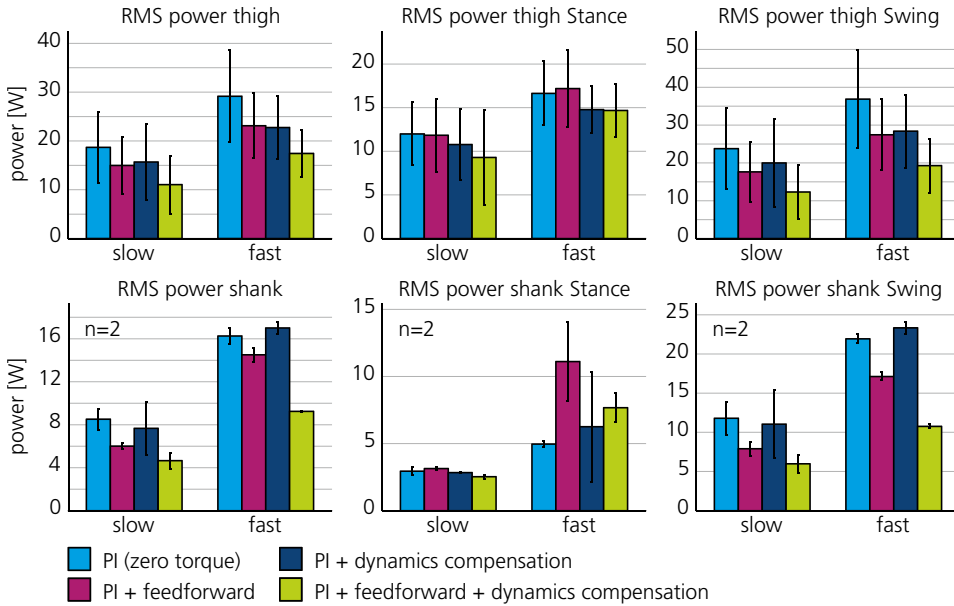


Figure 21: RMS of the power at the thigh (left) and shank (right) over the total gait cycle (top) and divided in stance (middle) and swing phase (bottom). The bars are the results, averaged over the subjects. The error bars denote the standard deviations.

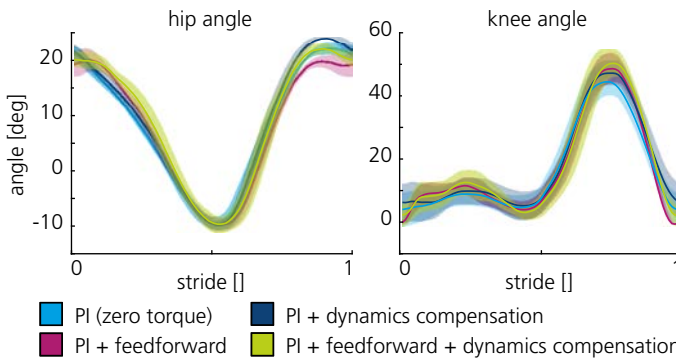


Figure 22: Gait kinematics averaged over the subjects (flexion is positive), and presented as a function of the stride, starting at heel strike. Shaded areas show the standard deviations between the subjects.

For the lower leg the dynamics compensation alone did not result in a clear reduction of the interaction power, compared to the zero-torque mode (Figure 21), but the feed-forward controller did reduce the interaction power. In contrast to the interaction force (Figure 20), combining both controllers resulted in a large reduction in the power at the shank (slow walking 45.3%, fast walking 43.2%).

Figure 7 also shows that the dynamics compensation resulted in a larger reduction in interaction power during the swing phase than during the stance phase.

### 5.3.4 Kinematics

The recorded joint angles are compared for the different controllers in Figure 22. Gait kinematics show only subtle differences. The most prominent difference is the increase in knee flexion angle. If the feed-forward controller and the dynamics compensation are on simultaneously the maximal knee angle is 5.8 degrees larger than the condition where both controllers are off ( $p = 0.003$ ).

## 5.4 Discussion

The purpose of this study was to investigate how the cyclic nature of many rehabilitation tasks could be exploited to improve the control and transparency of rehabilitation robots. The results for the two tested controllers are discussed below.

### 5.4.1 Feed-forward velocity learning controller

The RMS of the torque tracking error showed a large improvement. Still, our approach can only filter out errors that are cyclic, with the same cycle time as the gait cycle (Figure 19). Errors that are not a function of the gait phase cannot be captured by the non-linear filter. The remaining error in the torque tracking is partly due to tracking errors that are not cyclic. However, in our study the cyclic effects were dominant and the RMSE could be reduced by more than half.

### 5.4.2 Dynamics compensation

The effect of the dynamics compensation was measured by the interaction power. When the dynamics compensation was switched on the interaction power reduced, especially for the thigh (Figure 21). Our results also indicate that the effect of the dynamics compensation controller is larger if the feed-forward velocity controller is active in parallel, which clearly improved the torque tracking (Figure 18). This indicates that a good torque tracking is a prerequisite for the dynamics compensation controller to work, especially since the desired torques are relatively small (Figure 19).

In general the dynamics compensation controller showed a larger reduction in interaction power during the swing phase than during the stance phase (Figure 21). This might be due to larger joint accelerations during the swing phase, than during the stance phase. Larger accelerations correspond to larger forces that can be compensated for with this controller. Indeed, Figure 21 shows higher interaction powers during the swing phase compared to the stance phase.

An additional possible explanation is that the interaction forces, during the stance phase, have a source that cannot be compensated for by either one of the controllers. As a safety measure the Lopes has a mechanical end-stop at the knee joint to prevent hyperextension. At initial heel contact, at the beginning of the stance phase, the subject is likely to hit that end-stop and the Lopes cannot reduce the interaction forces by further extending.

Some of the remaining interaction forces might emerge from a misalignment between the human and the robot leg. This cannot be compensated for by the controllers, but can only be solved with a more ergonomic design.

Evaluation of the kinematics showed an increase in maximum knee angle during the swing (Figure 22). This suggests that, in our specific case, the previous observed reduction in knee flexion (van Asseldonk et al., 2008) (in de zero-torque mode) was compensated for by our controllers. This might indicate that the subjects have a more natural gait when the controllers are switched on. Up to this point we did not investigate the changes in human performance in terms of the kinematic resemblance of natural walking, energy expenditure or muscle activation. This will be part of further research.

## 5.5 Conclusion

If a robotic task is cyclic, the performance of this task can be improved by exploiting the predictions of adaptive frequency oscillator and kernel-based nonlinear filters. These filters predict signals for the upcoming steps. This prediction can be used to compose a feed-forward signal to increase robotic control accuracy. We showed that for our rehabilitation robot we improved the torque tracking and reduced the interaction forces between the robot and the human, and thereby improved the transparency of our robot. Still we need to evaluate how the controllers react to sudden gait changes and irregular gait patterns.

# 6 A Passive Exoskeleton with Artificial Tendons: Design and experimental evaluation

---

*Wietse van Dijk*

*Edsko Hekman*

*Herman van der Kooij*

*Published as: W. van Dijk, H. van der Kooij, and E. Hekman, "A passive exoskeleton with artificial tendons: Design and experimental evaluation," in Rehabilitation Robotics (ICORR), 2011 IEEE International Conference on, 2011, pp. 1–6.*

*Abstract— We developed a passive exoskeleton that was designed to minimize joint work during walking. The exoskeleton makes use of passive structures, called artificial tendons, acting in parallel with the leg. Artificial tendons are elastic elements that are able to store and redistribute energy over the human leg joints. The elastic characteristics of the tendons have been optimized to minimize the mechanical work of the human leg joints. In simulation the maximal reduction was 40 percent. The performance of the exoskeleton was evaluated in an experiment in which nine subjects participated. Energy expenditure and muscle activation were measured during three conditions: Normal walking, walking with the exoskeleton without artificial tendons, and walking with the exoskeleton with the artificial tendons. Normal walking was the most energy efficient. While walking with the exoskeleton, the artificial tendons only resulted in a negligibly small decrease in energy expenditure.*

## 6.1 Introduction

Different exoskeletons have been developed for medical or military use like the IHMC exoskeleton or the BLEEX (Kwa et al., 2009; Zoss et al., 2006). The high

power requirements of these exoskeletons negatively influences their operation radius and weight (the IHMC exoskeleton requires an external power supply; the BLEEX has a 30kg on board power supply). Although other, lighter, exoskeletons have been developed, like ReWalk and eLegs (Argo Medical Technologies Ltd, 2010; Berkeley Bionics, 2010), the problem of limited energy resources still persists. Alternatively passive exoskeletons have been developed that aim for energy efficient walking. By using only passive elements, the power requirement reduces to zero. For passive exoskeletons lightweight design is even more important. The mass and inertia of the exoskeleton results in a higher energy expenditure (Browning et al., 2007) that can only be compensated by the passive elements of the exoskeleton. Some of these passive exoskeletons aim at walking in reduced gravity, like the Gravity-Balancing Leg Orthosis and the MoonWalker (Banala et al., 2006; Krut et al., 2010). Another approach is the use of a mechanism that minimizes the mechanical work at the joints. It is assumed that that by minimizing mechanical joint work the metabolic energy expenditure decreases. During a typical human gait cycle the leg joints perform positive as well as negative work. If the energy dissipated due to the negative work is stored, transferred, and reused, a more efficient gait cycle is possible. In humans and animals multiarticular tendons act as an elastic energy buffer and link between the joints (McNeill Alexander, 1991; Voronov, 2004). This mechanism lowers the net joint work. However, the tendons are acting in series with a muscle. Muscular effort is required to tension the tendon. This means that the system cannot be used without energy expenditure. The use of elastic elements (artificial tendons) in parallel with the muscle tendon system circumvents this problem. Such a mechanism has been theoretically studied for human walking (van den Bogert, 2003) and robotic walking (Dean and Kuo, 2009), but the principle has not been applied in an exoskeleton. Goal of this study was to investigate if it is possible to lower the energy expenditure of walking by applying artificial tendons. This is done by designing and evaluating an exoskeleton with artificial tendons.

## 6.2 Design Concept

### 6.2.1 Working principle

The model for the artificial tendons is similar to (van den Bogert, 2003; van Dijk, 2010). The artificial tendon is an elastic cable that spans multiple joints. In this study a configuration was chosen where the artificial tendon spans the hip, knee, and ankle joint. This particular configuration was chosen as a tradeoff between efficiency and complexity (van Dijk, 2010). Additionally this configuration is interesting since it has no equivalent muscle tendon combination in the human



Figure 23: Left: Schematic drawing of the exoskeleton concept with artificial tendons (black). Right: A photo of the exoskeleton

leg. The artificial tendon is on one end attached to the foot and at the other end to the pelvis (Figure 23). At the joints in between, the artificial tendon has an offset by a lever at the ankle ( $d_{ankle}$ ) and the hip ( $d_{hip}$ ), and by a lever with an attached pulley at the knee ( $d_{knee}$ ,  $r_{knee}$ ). These offsets cause the artificial tendon to change length when the joint angles change. The elongation and the stiffness ( $k$ ) of the tendon introduce a force in the artificial tendon. A torque is introduced by the force and the offset from the joint rotation center. For some joint angles the artificial tendon is shorter than its slack length ( $l_{slack}$ ) in which case no torques are exerted. The human effort of walking is influenced by the artificial tendons, since the joint torques the human has to provide equal the joint torques required for walking minus the joint torques provided by the artificial tendons. The torque characteristics of the artificial tendon can be changed by altering the joint offsets and the spring characteristics (spring stiffness and slack length).

### 6.2.2 Optimization

The artificial tendons are tuned to minimize the effort of walking. This is done by optimization of the spring characteristics. To perform the optimization the assumptions are made that: 1.) A cost function can be formulated that scales with the energy expenditure of walking, and 2.) The gait kinematics do not change under influence of the artificial tendons. The chosen cost function to minimize is the absolute residual human joint work during one gait cycle:

$$J = \sum_{i=hip,knee,ankle} \int_{t=0}^T |P_i(t)| dt \tag{37}$$

The interval  $[0, T]$  is one gait cycle and  $P_i$  indicates the power at joint  $i$ . The efficiency ( $\eta$ ) of the artificial tendons based on the cost function with no support ( $J_o$ ) and with support ( $J_s$ ) has been defined as:

$$\eta = 1 - \frac{J_s}{J_o} \tag{38}$$

The optimization was done by a genetic algorithm derived from (Houck et al., 1995). For the optimization gait data from an internal gait database was used. The database includes overground walking data of eight subjects (4 male, 4 female, age  $24 \pm 1$ ) walking at 1.2 m/s. Joint torques and work from the database are normalized

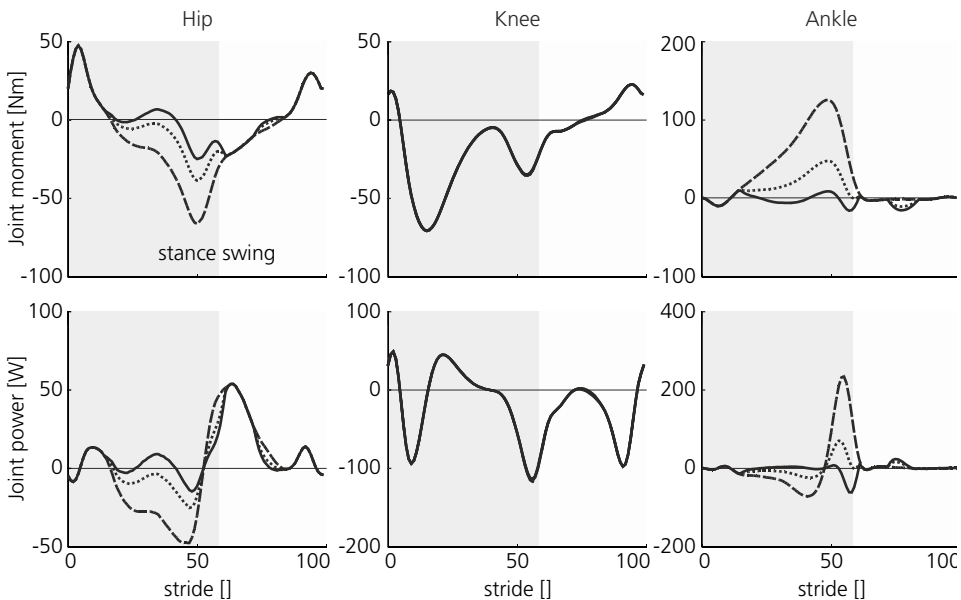


Figure 24: Optimization results. The upper graphs shows the joint moments for one gait cycle, the lower graph shows the joint powers for one gait cycle. The table gives the values for the exoskeleton parameters. The gait cycle starts at heel strike and ends at the next heel strike of the same leg. The data is scaled to a subject mass of 80kg. The knee offset was fixed at zero. The dashed line (---) shows normal gait data. The solid line (—) shows residual joint moments and powers when the artificial tendons offer optimal (100%) support. The dotted line (.....) shows residual joint moments and powers with partial (66%) support.

Support ratio	Efficiency	Exoskeleton parameters					
	$\eta$ [%]	$d_{hip}$ [mm]	$d_{knee}$ [mm]	$r_{knee}$ [mm]	$d_{ankle}$ [mm]	$k$ [Nm <sup>-1</sup> ]	$l_{slack}$ [mm]
66% support	29.9%	50.9	-20	20	143	15000	-862.3
100% support	40.9%	50.9	-20	20	143	10000	-862.3

Table 14: Exoskeleton parameter setting for 66% support and 100% support.

to the subject's weight ( $m$  [kg]). From this data the average torque profile during one step was calculated. An optimization of the parameters gave a maximum theoretical efficiency of 40.9% (Figure 24, Table 14). If 100% of these optimized torques were to be provided, the ankle torque would change sign. As a result, the human might need to recruit different, antagonistic, muscle groups while walking with assistance from the artificial tendons if compared to normal walking. Therefore the exoskeleton torques were reduced to 66% of the optimal torques, so this problem no longer occurred. Additionally for the experiments the knee offset was fixed at zero to prevent locking of the exoskeleton in slight hyperextension. Maximum efficiency given these two constraints was 29.9% (Figure 24, Table 14). During all optimizations the spring stiffness was fixed since all joint torques can already be individually adapted by changing the lever arms.

### 6.2.3 Exoskeleton Design

The artificial tendons were implemented in a lower extremity exoskeleton (Figure 23). The joint offsets and the slack length of the artificial tendons are tunable. The exoskeleton is anthropomorphic so that the movements of the exoskeleton pelvis, thigh, shank, and foot segments match their human equivalents. The exoskeleton was attached to the wearer by a backpack resting on the pelvis, straps at the thigh and shank, and shoes at the feet. The thigh and shank are adjustable in length and different straps can be fitted to accommodate users of different sizes. The exoskeleton provides flexion/extension at the hip and knee, dorsi-/plantarflexion at the ankle, and hip ab/adduction. The range of motion of these joints is sufficient to provide walking. The weight of the exoskeleton is approximately 12kg.

## 6.3 Data Collection

The performance of the exoskeleton was evaluated by experimental testing on human subjects. Goal of the experiment was: 1.) To evaluate the effect of the mass and inertia of the exoskeleton; 2.) To evaluate the effect the artificial tendons. This was done by comparing different walking conditions with and without the exoskeleton and artificial tendons. The comparison was made based on energy expenditure and muscle activation. Additionally the force in the tendons was measured and the feet of the subjects were tracked with optical markers.

### 6.3.1 Subjects

Nine healthy subjects (8 male, 1 female) between the age of 23 and 64 (mean  $31 \pm 13$ ) participated in this study. The weight of the subjects was  $75.1 \pm 6.5$ kg and their length was  $1.79 \pm 0.04$ . All subjects had no symptoms of orthopedic or neurological disorders and gave informed consent before participating in the experiments.

Subjects were selected based on length and shoe size since the exoskeleton fitted only a part of the population.

### 6.3.2 Experimental Apparatus and Recordings

*Artificial tendon force:* The tension force in the artificial tendons was measured by two load cells (Futek LTH 300, Irvine, CA).

*Energy expenditure measurement:* An open circuit respirometry system (Jaeger Oxycon Pro, Viasys Health Care, Warwick, UK) was used to measure the oxygen consumption ( $\dot{V}_{O_2}$  [ml·s<sup>-1</sup>]) and carbon dioxide production ( $\dot{V}_{CO_2}$  [ml·s<sup>-1</sup>]).

*Muscle activation measurement:* During all trials EMG from eight muscle groups of the left leg was recorded. These muscle groups were: gluteus maximus, gluteus medius, biceps femoris, gastrocnemius medialis, rectus femoris, adductor longus, vastus lateralis, and tibialis anterior. The electrodes were placed according to the Seniam guidelines (Hermens et al., 1999). The data were recorded using a Delsys Bagnoli EMG system (Delsys Inc., Boston, MA).

*Heel position:* The position of both heels was recorded using reflective markers. The position of the markers was tracked using a motion capture system (Vicon, Oxford Metric Group, Oxford, UK)

### 6.3.3 Experimental protocol

First the subject's energy expenditure in rest was determined. This was done in a five-minute trial where the subject had to stand still. After the standing trial the exoskeleton was adjusted to the subject size. The artificial tendons were attached to the exoskeleton and the lever arms and slack lengths were adjusted to the values determined in advance by the optimization procedure, based on physical properties of the individual test person. After that, the subject walked two or three practice trials to make sure the exoskeleton had a comfortable fit to the body and the artificial tendons were tuned as planned. During these practice trials small adjustments could still be made. Next, the different walking trials were recorded. The duration of each trial was ten minutes. The last five minutes of the trial were used to determine the median energy expenditure and the last 30 seconds to

Acronym	Order	Description
EA1,EA2	1 <sup>st</sup> , 3 <sup>rd</sup>	walking with the exoskeleton and the artificial tendons attached to the exoskeleton.
E1,E2	2 <sup>nd</sup> , 4 <sup>th</sup>	walking with the exoskeleton without the artificial tendons attached to the exoskeleton
NW5	5 <sup>th</sup>	walking without the exoskeleton (normal walking)

Table 15: Walking conditions

determine the mean muscle activation. After each trial the subject had a five minute break. In between the trials the exoskeleton was not removed. All trials were performed on a treadmill at a fixed speed of 1.1m/s (4km/h). Three different walking conditions were evaluated during five trials. The different trials are summarized in Table 15. Data processing

*Energy expenditure:* The energy expenditure per kg mass ( $\dot{E}$  [W/kg]) for each condition is estimated by a formulae derived from (Collins, 2008):

$$\dot{E} = \frac{16.48V_{O_2} + 4.48V_{O_2}}{m} \quad (39)$$

To estimate the metabolic cost of walking the median value of a condition is taken and the rest rate is subtracted.

*Muscle Activation:* The EMG signal is filtered. First notch filters are applied to remove grid noise (50, 150, 250, 350Hz). Subsequently, the signal is band pass filtered with a second order Butterworth filter between 10 and 400Hz to remove movement artifacts. After that the signal is rectified and low pass filtered (zero phase) at 4Hz. From the last 30 seconds of each condition for each subject an average step is calculated. For each subject the EMG data is normalized to the normal walking condition.

*Average step:* For the analog signals (EMG and tendon force) an average step cycle is calculated. The cycle starts at heel strike and ends at the subsequent heel strike of the same leg. Heel strikes are detected using the data from the optical markers according to the method proposed by (Zeni Jr et al., 2008).

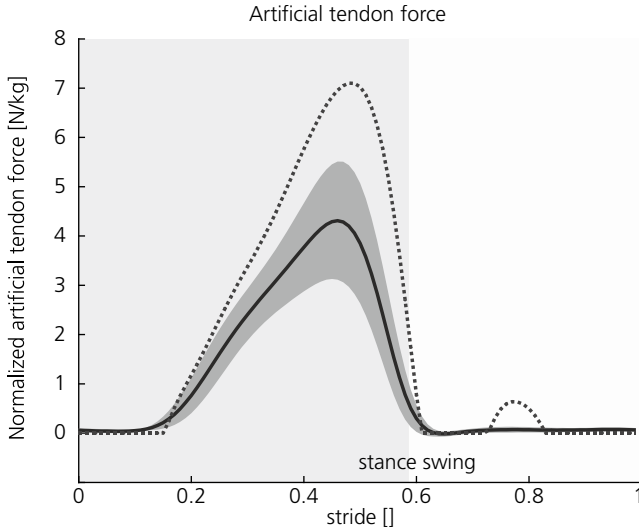


Figure 25: Artificial tendon force normalized to the weight of the subject. The dashed line showed the artificial tendon force predicted in simulation. The solid line shows the artificial tendon force averaged over the subjects measured in experiment. The dark grey area shows the standard deviation.

### 6.3.4 Statistical analysis

Energy expenditure: Different conditions are compared by performing a paired t-test on the median of the energy expenditure values for each subject.

## 6.4 Results

### 6.4.1 Artificial tendon force

The tensioning of the cable starts and ends at the instants which were well predicted by the optimization. The measured tendon force is lower than the value predicted by the optimization (Figure 25).

### 6.4.2 Energy expenditure

Figure 26 shows the energy expenditure during the different trials. The energy expenditure of all the trials with the exoskeleton was higher than that of the trials without the exoskeleton. Compared to normal walking, the average increase in energy expenditure of walking with the exoskeleton without the artificial tendons ( $E_2$ ) was  $35.9 \pm 10.6\%$ . When the conditions with the exoskeleton are compared with each other, the energy expenditure averaged over the subjects for every next trial is lower than the previous ones. This decreasing trend is significant for every combination of trials ( $p < 0.05$ ). To partially eliminate this effect the average of the conditions without the artificial tendons  $E_1$  and  $E_2$  is taken, and compared to the second condition with the artificial tendons ( $EA_2$ ). Here the worst performing

subject has been excluded. The performance of this subject was outside the 99% confidence interval and considered as an outlier. A small significant benefit of the artificial tendons is found (-2.14%, significance  $p = 0.014$ ). For the best subject a higher benefit was measured (-7.12%).

### 6.4.3 Muscle activation

Generally, when walking with the exoskeleton, the EMG values increase when compared to normal walking. The largest difference is noticed in the activation of uniarticular muscles around the hip (gluteus medius, gluteus maximus, and adductor longus) during early stance. The different walking conditions with the exoskeleton are compared to determine the effect of the artificial tendons. Most noticeable is the decrease in the activation of the gastrocnemius muscle (Figure 27).

## 6.5 Discussion

### 6.5.1 Artificial tendon force

The measured artificial tendon force differs with a roughly constant factor from the simulated artificial tendon force. The measured artificial tendon force is in all cases lower than the value calculated in the simulation. Apparently the subjects received

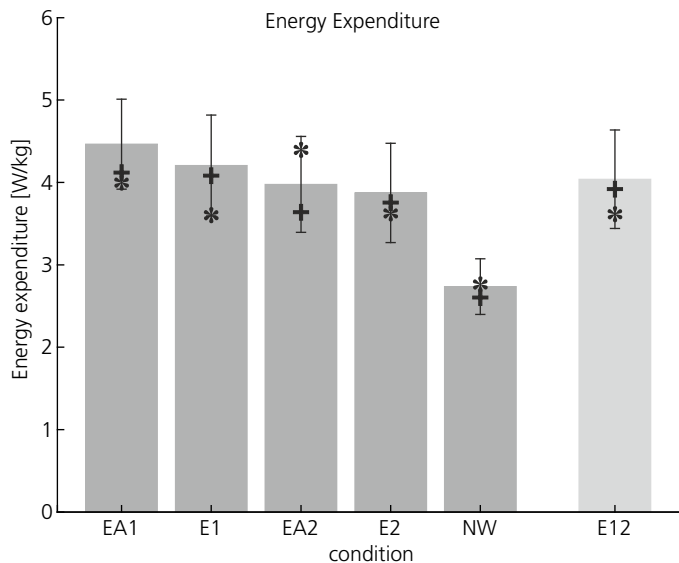


Figure 26: Energy expenditure. Five conditions are shown: Normal treadmill walking (NW), Walking with the exoskeleton and with the artificial tendons 1st and 2nd trial (EA1, EA2), and walking with the exoskeleton without the artificial tendons (E1 and E2). The rightmost column (E12) depicts the average value of E1 and E2. All differences are significant with a paired t-test ( $p < 0.05$ ). + indicates the best performing subject, \* indicates the worst performing subject in terms of energy expenditure.

a smaller support torque than expected. Possible explanations are: the subjects adapt their gait under influence of the exoskeleton with the artificial tendons, and/or the flexible or compressible parts of the exoskeleton (e.g. the foam in the backpack) or soft tissue deform under the loads and act as a serial spring.

### 6.5.2 Energy expenditure

The energy expenditure while walking with the exoskeleton (regardless of the artificial tendons) is generally higher than for normal walking. This is to be expected, since the exoskeleton adds mass and inertia to the legs. The subjects were also restrained in their motion since the exoskeleton has no mechanism for endo-/exorotation. When the conditions with exoskeleton are compared a strong effect of time was notable. This might indicate that there is a learning effect. This learning effect seems to overshadow the effect of the artificial tendons. For only one

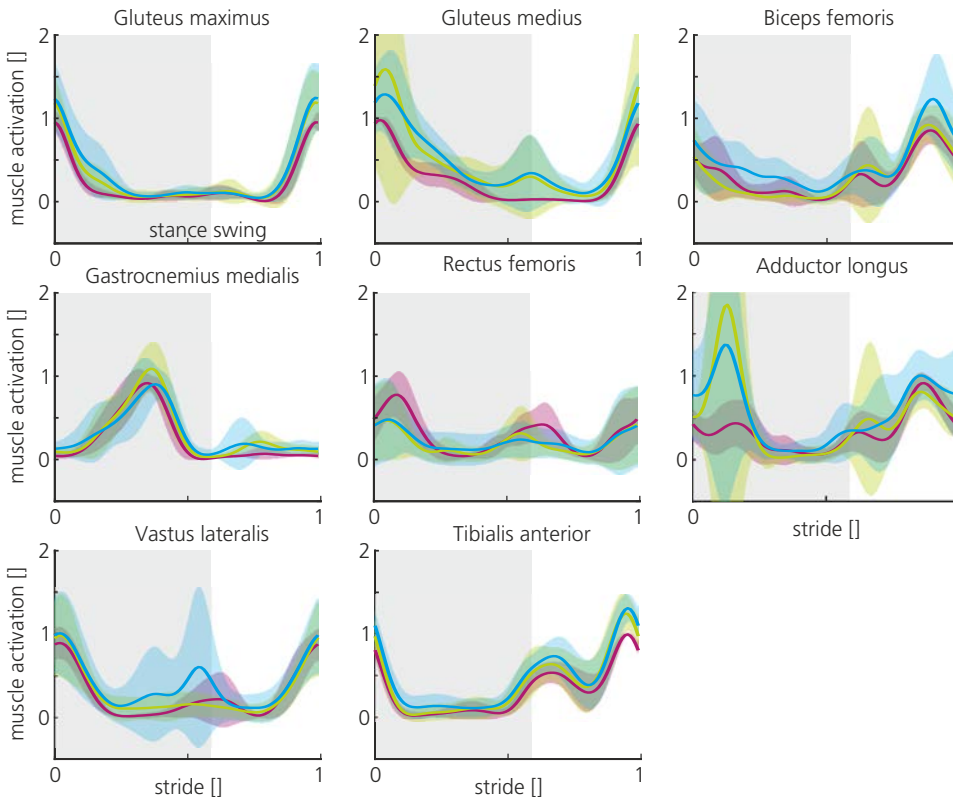


Figure 27: Averaged values and standard deviations across subjects (shaded areas) of the muscle activation patterns from eight subjects of eight muscle groups. The horizontal axis represents one gait cycle where the stance phase is marked with grey. For each subject the EMG data is normalized between zero and one for the normal walking condition. The data is averaged over the subjects. Three conditions are depicted: Normal walking (—), walking with the exoskeleton with the artificial tendons (—), walking with the exoskeleton without the artificial tendons (—).

subject the energy expenditure while walking with the artificial tendons was lower than during each of the trials without the artificial tendons.

### 6.5.3 Muscle activation

Similar to the results found for the energy expenditure, walking with the exoskeleton has a large effect on muscle activation, when compared to normal walking. A large increase is seen at the uniarticular muscles around the thigh. This might be an indication of co-contraction. Co-contraction might indicate a stiffer walking pattern or a less adapted walking pattern. The large reduction in hip torque as expected from the simulation is not reflected in the muscle activation patterns around the hip. The largest positive effect of the artificial tendons is measured in the gastrocnemius muscle. This is what is expected since the moment arm around the ankle is the largest, and the artificial tendon acts parallel with the gastrocnemius muscle and is active during the same part of the gait cycle.

## 6.6 Conclusion

The effect of the artificial tendons on the energy expenditure while walking is much lower than expected from the model optimizations. This limited effect could be caused by: 1.) The learning effect. It takes users more than the measurement time to adapt to walking with the exoskeleton. Thus the still decreasing energy expenditure hides the benefits of adding the artificial tendons; 2.) A significant effect on the gait pattern due to fixation of the exoskeleton to the test person. This could be explained by the increased mass and inertia of the leg as well as the implied constraints; 3.) The supportive torques being lower than expected; 4.) A nonlinear relationship between the reduction in the mechanical work and the reduction in energy expenditure and muscle activation.

## 6.7 Future work

Future research will focus on improving the results by improving the exoskeleton and the evaluation methods. Therefore the following steps will be taken:

- Longer testing that is specifically focused on the identification and minimization of the learning effect in order to (partially) remove it from the results.
- Iterative testing and evaluation of the gait kinematics and kinetics. During iterative steps spring stiffness, moment arms, and slack length of the tendon can be changed and better matched with the results from simulation.

- Minimizing the mass and inertia and improving the freedom of movement while walking with the exoskeleton. This will make it easier for the user to adapt to and walk with the exoskeleton, and decrease the effect of the added mass.

## 7 XPED2: A Passive Exoskeleton with Artificial Tendons

---

*Wietse van Dijk*

*Herman van der Kooij*

*Published as: W. Van Dijk and H. Van Der Kooij, "XPED 2 - A Passive Exoskeleton with Artificial Tendons," IEEE Robot. Autom. Mag., vol. 21, no. 4, pp. 56–61, 2014.*

*Abstract (for indexing purposes only) — Wearable exoskeletons might reduce the human effort during walking. Many of current exoskeletons rely on heavy actuators and/or external power supplies; this has a drawback on their efficiency and operation range. As an alternative, (quasi) passive exoskeletons have been developed. One of the proposed passive exoskeleton concepts is the exotendon concept of van den Bogert. In this concept long elastic cables span multiple joints. The cables can temporary store energy and transfer energy between joints. In simulation, the average absolute joint torque can be reduced by 71%. The simulations are based on the hypotheses that: The exoskeleton does not influence the joint angles and the total joint torques, and a reduction in the human joint torques results in a reduction in the metabolic cost of walking. The goal of this study is to experimentally evaluate the exotendon concept and test the hypotheses underlying it. We implemented the exotendon concept in a lightweight exoskeleton. Experimental results show that the exotendons indeed reduced the average absolute joint torques. However, the exotendons did influence the joint kinematics and the metabolic cost of walking did not decrease. Therefore, the underlying assumptions of the exotendon concept are invalid. We also found that in practice the amount of support given by the exotendons is limited to about 35% of the theoretical optimal support. For higher levels of support the motion is hindered and the support is experienced as uncomfortable by the users of the exoskeleton.*

It has recently been shown that walking with an exoskeleton can reduce the metabolic cost of walking (Malcolm et al., 2013a). For exoskeletons to become useful in daily life, their power consumption is a key factor. The required power is often provided by batteries, which limits the operation time of exoskeletons. For the HAL exoskeleton (Cyberdyne, Tsukuba, Japan) and Ekso (Ekso Bionics, Richmond, CA, USA) the operation time is approximately three hours (Cyberdyne, 2012; Ekso Bionics, 2012).

The high power requirements of exoskeletons contrast with the efficient locomotion found in nature. Human and animal legs possess mechanisms that save energy while in motion. Elastic tendons can temporarily store energy, and multi-articular tendons and muscles can transfer energy between joints (Biewener, 1998;

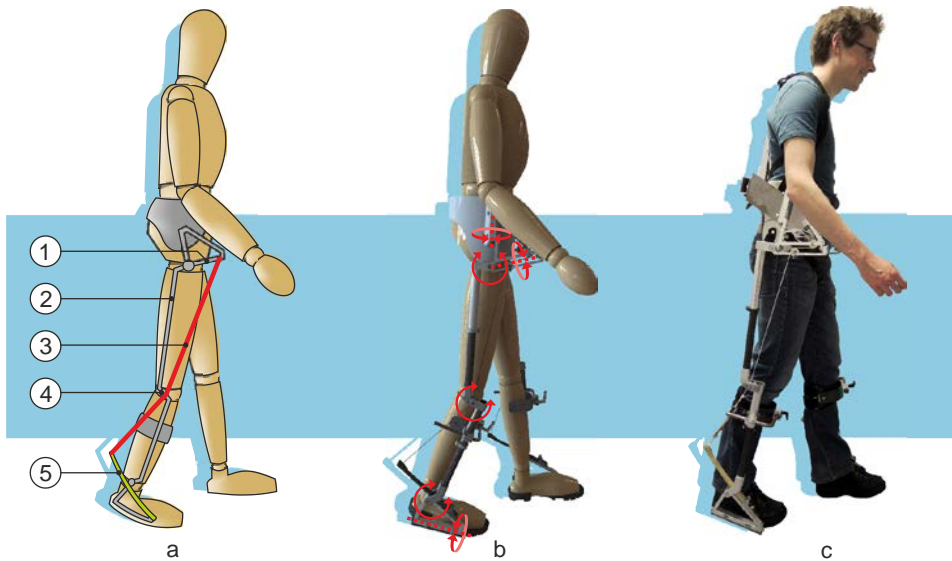


Figure 28a: Working principle: The main functional part of the exoskeleton is the extendon (3), a cable that spans between a lever at the pelvis (1), via a pulley at the knee (4), to a leaf spring at the foot (5). The leaf spring at the foot accounts for the elasticity of the mechanism. Since the cable has an offset from the joint centers, the deformation of the spring, and thereby the force in the cable, depends on the joint angles. In this configuration hip extension and ankle dorsiflexion will tension the cable and hip flexion and ankle plantarflexion will loosen the cable. The movement of the knee has almost no effect on the tension of the cable. For some combinations of joint angles the cable is slack and there will be no force in the cable. The force in the cable multiplied by the offset from the joint gives the moment that the extendon exerts around that joint. The exoskeleton is connected to the human via a rigid frame (2) with connections at the pelvis, shank, and foot segments.

b: CAD-model of the XPED2 exoskeleton. The XPED2 has 6 degrees of freedom per leg: flexion/extension, ab/adduction, and endo/exorotation at the hip; flexion/extension at the knee; plantar/dorsiflexion and pronation/supination at the ankle.

c: Photo of one of the developers wearing the XPED2 exoskeleton. The total mass of the exoskeleton is 6.91 kg.

Ishikawa et al., 2005; Zajac et al., 2002).

Model optimizations of van den Bogert suggest that human joint torque and power can be reduced by placing elastic structures, called exotendons, parallel to the leg (van den Bogert, 2003). These exotendons have a similar function as biological uni-, and multiarticular tendons. Simulations suggest that the human joint torque, the torque provided by the leg muscles, can be reduced by 21% with uni-articular exotendons at the ankle. This reduction increases to 46% if tri-articular exotendons are used that span the hip, knee, and ankle. For more complex configurations with multiple exotendons per leg, the predicted reduction increases to 71%. The hypotheses underlying the exotendon concept are: 1. The exotendons do not influence the joint angles and total joint torques (the sum of the human joint torques and the exoskeleton joint torques), and 2: A reduction in the human joint torques results in a reduction in the metabolic cost of walking.

The first hypothesis has been tested for the hip and ankle separately with uni-articular powered exoskeletons (Kao et al., 2010a; Lewis and Ferris, 2011). These studies show that joint total torque patterns do not change when an external support is provided, but joint angle patterns do change. Two exoskeletons with uni-articular exotendons demonstrated a relative reduction in metabolic cost. Wearing these exoskeletons without the elastic elements increased the walking metabolism, which was only partially compensated when the elastic elements were added to the exoskeleton (e.g. Walsh et al., 2007; Wiggin et al., 2012).

The goal of this study is to experimentally evaluate the exotendon concept of (van den Bogert, 2003). In our study we use tri-articular exotendons as a compromise between predicted reductions and complexity. Our experiment is built up to test the previously mentioned hypotheses underlying the exotendon concept. Based on these hypotheses we expect that our exoskeleton reduces the metabolic cost of walking. This paper first describes the design of the exoskeleton and then describes the experimental evaluation of the exoskeleton.

## 7.1 Design

### 7.1.1 Working principle

The exoskeleton uses a mechanism of springs, cables, lever arms, and pulleys to temporarily store energy and transfer energy between joints. The working mechanism is similar to that of (van den Bogert, 2003) and is described in Figure 28. The characteristics of the support given by the exotendon can be varied. The slack length, lever arm lengths, and spring stiffness of the exotendon were

optimized so that the average absolute human joint torque was minimal. In the optimizations, the human joint torque was the torque observed in a typical gait pattern minus the exotendon torque summed over the hip, knee and ankle (Figure 29).

### 7.1.2 Exoskeleton

The proposed mechanism was realized in the XPED2 exoskeleton (Figure 28). The design is anthropomorphic and has six degrees of freedom per leg. These degrees of freedom were possible through serial hinge joints from the pelvis attachment to the foot attachment. An additional attachment to the human body was made at the shank. The total mass of the exoskeleton is 6.91 kg and is distributed over the pelvis (3.57 kg), the thighs (2x 0.40 kg), the shanks (2x 0.72 kg), and the feet (2x 0.55 kg). The added mass will increase the energy consumption. Given the mass distribution and the empirical relations of (Browning et al., 2007), the estimated increase will be about 14%. The lever arms at the pelvis and the foot and the slack length were adjustable so that the exoskeleton characteristics could be matched to the optimization results. The length of the shank and thigh segments was adjustable and different shoes were available to adjust for subject's size. The tendons were made from Dyneema cable. The elasticity of the system was achieved by making the ankle levers elastic. The levers are of a custom design glass fiber leaf spring with unidirectional fibers.

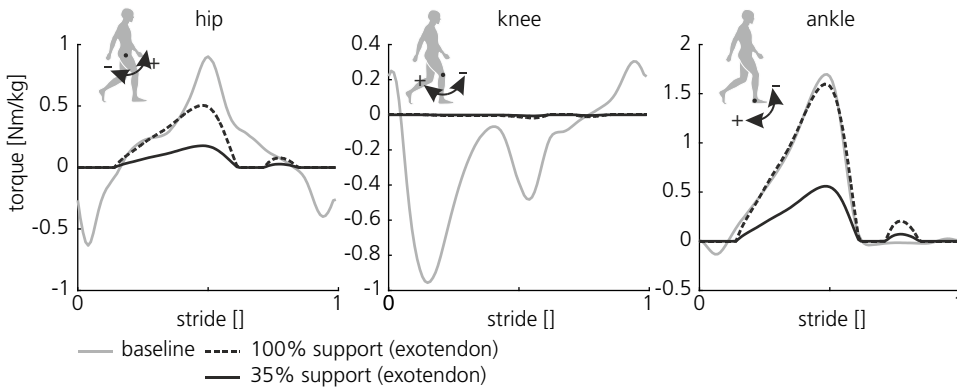


Figure 29: Exotendon optimization results. The torques exerted by the exoskeleton are optimized to match those normally observed in human gait (green lines). The optimization assumes that total torque (human + exotendon) is constant across the different conditions. The optimal (100%) exotendon torques are shown with the dashed blue lines. Preliminary test have revealed that users are uncomfortable if very high torques are exerted on the body. The settings used for the XPED2 exert 35% of the optimal torques (solid blue lines) to ensure that users can walk comfortably with the exoskeleton. The optimizations are done in the sagittal plane since this is the dominant plane for walking.

## 7.2 Experiment

### 7.2.1 Subjects

Six subjects (5 male, 1 female, mean 21 years 3 months (SD: 11 months) of age, 1.80 (0.04) m in height, 72.9 (7.3) kg in weight) volunteered in the study and gave a signed informed consent before participating in the study. Subjects were recruited from the Dutch student population. The subjects were selected if they were in good physical condition without gait abnormalities and if they could fit the exoskeleton.

### 7.2.2 Data recordings

The measurement setup is shown in Figure 30. The metabolic power was recorded using a respiratory measurement system. Motions of the lower body were recorded with markers bilaterally on the foot, shank, thigh and pelvis, and on the right side of the exoskeleton. Ground reaction forces were recorded by a dual belt instrumented treadmill. The forces in the exotendons were recorded with load cells.

### 7.2.3 Protocol

Three walking conditions were evaluated during the experiments: *Baseline*, the

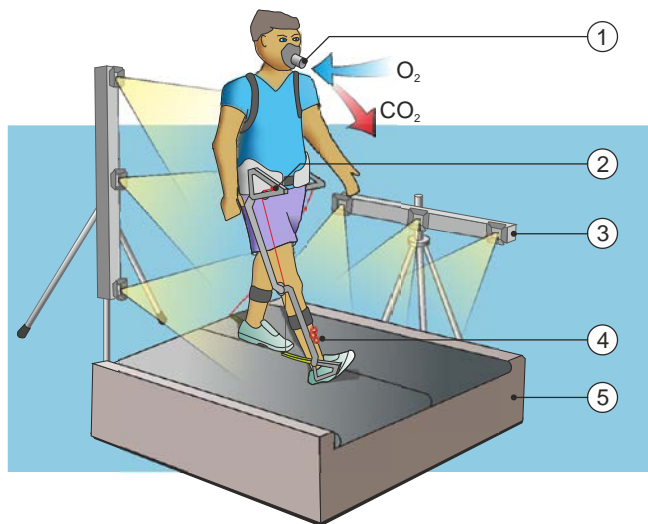


Figure 30: Measurement setup. During the experiments the following measurements were taken. The metabolic power is measured by a respiratory measurement system (1, 2 subjects: K4B2, Cosmed, Pavona, Italy / 4 subjects: Jaeger Oxycon Pro system, Viasys Health Care, Warwick, UK) that measures the gas flow and composition. The force in the cable was measured by load cells at the end of the exotendon (2, LCM200, Futek, Irvine, CA, USA). The kinematics were measured by four trackers (3, VZ4000, Visualeyex, Burnaby, BC, Canada) tracking light emitting markers (4) placed on the exoskeleton and the human. Ground reaction forces were measured with a dual belt instrumented treadmill (5, Y-mill, Forcelink B.V., Culemborg, The Netherlands).

subject walks without the exoskeleton; *No support*, the subject walks with the exoskeleton, but the exotendons are not tensioned; *Support*, the subject walks with the exoskeleton and the exotendons are tensioned, so the user gets support from the exoskeleton. All measurements were performed at a fixed treadmill speed of 1.0 m/s. The subject walked with the exoskeleton during three sessions on separate days. The first two sessions were practice sessions. These sessions were held to minimize the effect of learning that was noted in evaluation of a previous version of this exoskeleton (van Dijk et al., 2011). On these days the subject could practice for 45 minutes at a self-selected speed and at least 10 minutes at the speed of 1.0 m/s. During the first sessions subjects were allowed to take breaks at random intervals. Measurements were taken during the third session. Each session started with fitting the XPED2 to the body and adjusting the settings of the lever arms and slack lengths to their desired values.

During the last sessions five walking trials were conducted: two no support, two support, and one baseline trial. The order of the trials was quasi random. The baseline trial was randomly assigned to the start or the end of the walking trials. The order of the support and no support trials was alternating, with the first trial randomly a support or no support trial. Each walking trial lasted 10 minutes. Additional trials were needed for the inverse dynamics analysis: the recording of a standing pose and identification of anatomical landmarks with a probe. In addition, the metabolic power at rest was recorded for 5 minutes while the subject was sitting in a chair.

#### **7.2.4 Data analysis**

##### ***Kinematics and kinetics***

The kinematic and kinetic analysis was performed for four of the six subjects. Joint kinematics were calculated from the marker data. Joint kinetics were obtained from the marker data, ground reaction forces and exotendon forces with inverse dynamics (Cappozzo et al., 1995) using BodyMech (VUMC, Amsterdam, The Netherlands). The XPED2 is anthropomorphic and we assumed that the mass of the segments of the exoskeleton was rigidly connected to the body parts they were parallel to. A median step was calculated from a two minutes sample taken from the end of each trail. The data was split into individual strides based on the heel-strike events. The heel-strike events were derived from the vertical ground reaction force, measured by the treadmill. The median stride time was calculated for all six subjects. The differences between conditions were compared by the average over the subjects. Statistical analysis was done by a paired t-test.

## Metabolic cost

The metabolic power was calculated from the respiratory data. The following empirical relation for the metabolic power ( $\dot{E}$  [W/kg]) was used (Collins, 2008):

$$\dot{E} = \frac{16.48 \cdot 10^3 \dot{V}_{O_2} + 4.48 \cdot 10^3 \dot{V}_{CO_2}}{m} \quad (40)$$

$\dot{V}_{O_2}$  [L/s] and  $\dot{V}_{CO_2}$  [L/s] are respectively the oxygen uptake and the carbon dioxide production, whereas  $m$  [kg] is the mass of the subject. For all reported metabolic powers, the metabolic power at rest has been subtracted. The differences between conditions were compared by the average over the subjects. Statistical analysis was done by a Wilcoxon signed rank test.

## 7.3 Results

### 7.3.1 Kinetics and kinematics

Figure 31 shows the walking kinetics and kinematics. The exotendons changed the walking kinematics. The maximal ankle dorsiflexion angle during support decreased by  $5.0^\circ$  compared to the no support and  $5.1^\circ$  compared to the baseline condition ( $p < 0.05$ ). The average ankle plantarflexion torque increased in the

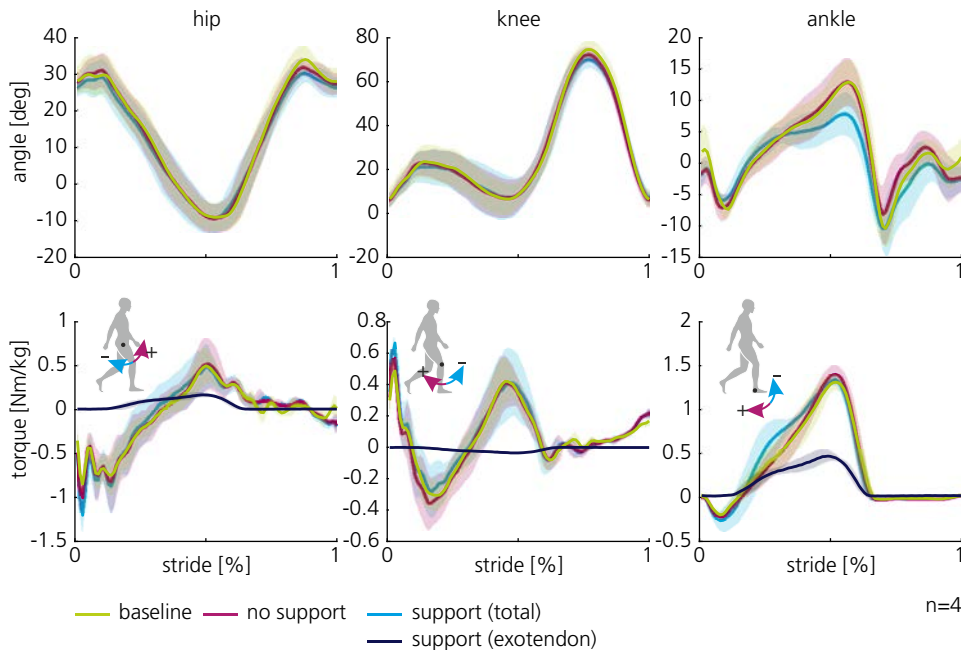


Figure 31: Walking kinetics and kinematics. The lines represent the average over the subjects. The shaded areas are the standard deviations.

support condition by 0.025 Nm/kg compared to the no support condition and 0.022 Nm/kg compared to the baseline condition. This increase was not present for all subjects. The differences in kinematics and kinetics between the conditions were small for the hip and knee. Differences in stride time between the conditions were also small (maximal 1.36%) and not significant ( $p > 0.1$ ).

The measured average absolute human torque was compared to the estimated value from the optimization (Figure 32). The optimization results predict a decrease in the average absolute joint torque of 17.0% for a subject of 70 kg (this value ranges between 16.8 and 18.3% for subjects between 60 and 100 kg). Experimentally we found a reduction of 12.1% in the support condition relative to the no support condition ( $p = 0.089$ ), which could almost entirely be contributed to the ankle torque. The reduction for the ankle only was 29.0% ( $p = 0.057$ ). Apart from the differences between conditions, the human torques in the experiment differ from the human torques in the optimization. Data for the optimization was obtained from different subjects in a different lab causing intra-subject differences.

### 7.3.2 Metabolic cost

The metabolic power of the different subjects is shown in Figure 33. For all subjects the metabolic cost of walking during the baseline condition was the lowest. The

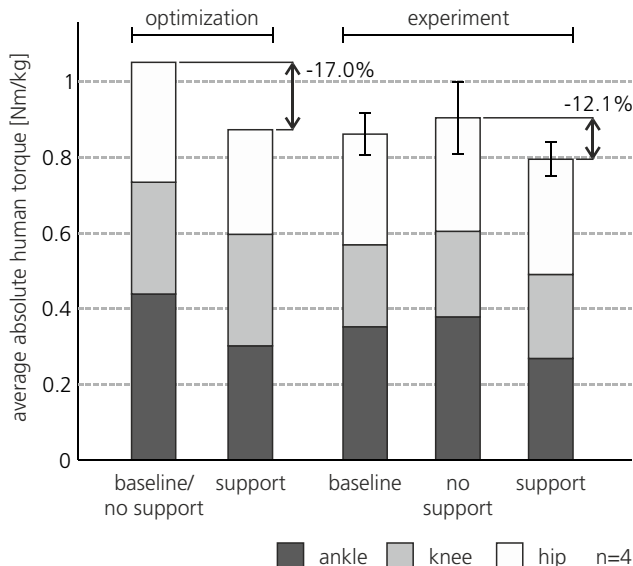


Figure 32: Average absolute human joint torque in different conditions. On the left, the optimization results. The optimization predicts a decrease in average absolute joint torque of 17.0%. Note that the effect of the added weight is not taken into account in the optimization and therefore the baseline and no support condition could not be discriminated. On the right, the experimental results. The difference between the support condition and no support condition is 12.1%.

metabolic cost in the no support condition was significantly higher (21.2%) than in the baseline condition ( $p < 0.05$ ). The added mass explains most of this increase since the estimated increase in metabolism due to the added mass was 14%. In contrast with our predictions, the average metabolic cost in the support condition was 6.1% higher than in the no support condition ( $p = 0.052$ ).

## 7.4 Discussion

We built the XPED2 to test the following hypotheses: 1: The exotendons do not influence joint angles and total joint torques, and 2: A reduction in the human joint torques results in a reduction in the metabolic cost of walking. Although our experiment is based on data from a small number of subjects, we could identify some clear trends. Our experiments demonstrated that deviations from normal walking occur, and thereby we falsified our first hypothesis. The changes in ankle motion were also observed in (Kao et al., 2010a). Still, the exotendons did reduce the average absolute human joint torque. The reduction in average absolute human joint torque did not result in a measurable reduction in the metabolic cost, there was even an indication that the metabolic cost increased. This contradicts with the second hypothesis. However, the effect could have been small and unnoticed. The exotendons did only provide a small amount of support (12.1%). When changing the exotendon parameters or configuration this number might be increased. Given the changes observed in the walking pattern, it is unlikely that 71% reduction in average absolute joint mentioned in (van den Bogert, 2003) is feasible. Preliminary pilot trials taught us that subjects were uncomfortable with higher amounts of support.

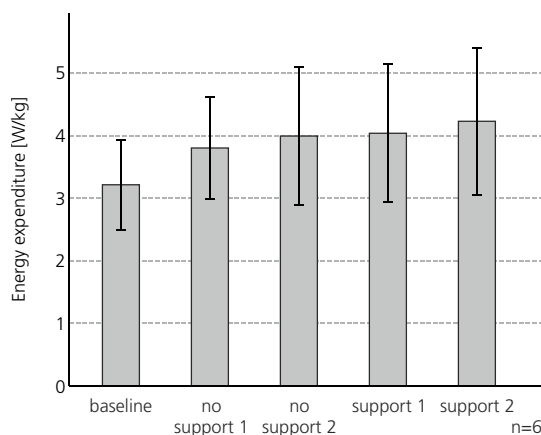


Figure 33: The metabolic power for the different walking conditions. The bars represent the average over the subjects with the standard deviations.

Exoskeleton	Passive?	Number of subjects	Weight and constraints	Support
XPED2 (this chapter)	Yes	6	21.2%	6.1%
XPED1 (previous chapter)	Yes	9	35.9%	-2.1%
Wiggin et al. (2012)	Yes	3	--	-10%
Walsh et al. (2007)	Quasi*	1	24%	-12.9%
Malcolm et al. (2013a)	No	10	14.3%	-17.2%
Sawicki et al. (2009)	No	9	8.3%	-11.5%
Norris et al. (2007)	No	9*	16.2%	-13.9%
Wehner et al. (2013)	No	1	12.8%	-10.2%

Table 16: Comparison of the metabolic cost of walking for different exoskeletons. Quasi-passive means that energy is used for control, but there is no mechanical energy added to the system. \*The results for the young subjects are given.

### 7.4.1 Outlook

Our exoskeleton has shown the contrast between the theory and the experiment and thereby stressed the importance of experimental evaluation of exoskeleton designs. We compared our results to experimental results obtained with other exoskeletons for walking augmentation (Table 16). Although some exoskeletons have shown a (relative) reduction in metabolic cost, there is no general consensus on how to reduce metabolic cost most effectively.

The hypothesis that the metabolic cost reduces when the absolute joint torque reduces is valid for isometric contractions, but in walking there are additional effects that might interfere with this relation. Energy storage and transfer between joints is already partly covered by the human tendons and bi-articular muscles. Adding exotendons might interfere with these energy saving mechanisms. In humans, it has been shown that the Achilles tendon stiffness is optimal in the sense that muscle work during walking is minimal (Ishikawa et al., 2005). In hopping experiments, it has been shown that adding a parallel spring reduced muscle force, but increased muscle work (Farris et al., 2013). The observed changes in kinematics and kinetics might be explained by the fact that the support by the exoskeleton enforces a new equilibrium.

The metabolic cost of walking could be partially explained with the model used by (Donelan et al., 2002). The model predicts that the metabolic cost of walking emerges from the need to compensate for energy losses after impact. This is in line with experimental results of (Malcolm et al., 2013a) where the highest reduction in metabolic cost was observed when the exoskeleton solely provided positive power. This result undermines the passive exoskeleton concept since passive exoskeletons are energy neutral at best. However, it has been shown that relative metabolic cost reductions with a passive exoskeleton are possible (Wiggin et al., 2012). Different from our mechanism, this exoskeleton has a clutch that engages the elastic element. This allows for a better timing of the support, which might be essential to reduce the metabolic cost of walking (Malcolm et al., 2013a; Wehner et al., 2013).

Despite the limited effect of exotendons on the metabolic cost of walking, we see potential for the application of exotendons in exoskeletons. Elastic elements in combination with actuators can lead to smaller power requirements on the actuation side (Hitt et al., 2007), and give the opportunity to place the actuators on a more proximal, and thus more metabolically beneficial, place on the leg (Asbeck et al., 2013). Combined with actuators, exotendons can contribute to elegant and lightweight exoskeleton designs.



# 8 The Achilles Ankle Exoskeleton

---

Wietse van Dijk

Cor Meijneke

Herman van der Kooij

*This chapter is based on the following works:*

C. Meijneke\*, W. van Dijk\*, and H. van der Kooij, “Achilles: An Autonomous Lightweight Ankle Exoskeleton to Provide Push-Off Power,” in *4th IEEE RAS & EMBS International Conference on Biomedical Robotics and Biomechatronics (BioRob)*, 2014. \*Equal contributions

W. van Dijk, C. Meijneke, H. van der Kooij, “Evaluation of the Achilles Ankle Exoskeleton” *IEEE Transactions on Neural Systems and Rehabilitation Engineering* (Submitted)

*Abstract— This chapter presents the Achilles exoskeleton, an autonomous lightweight ankle exoskeleton. The exoskeleton is designed to generate maximal push-off power with minimal added weight to the ankle. This was achieved by using a series elastic actuator. An electromechanical model of the exoskeleton was used to optimize the design for positive power injection. Based on the optimization results, exoskeleton components were selected and dimensioned.*

*Benchmark tests evaluated the performance of the actuator and human experiments evaluated the working of the complete system. The actuator can track the optimized actuator stroke trajectory with a following error that has a RMS of 2.3 mm, it can track force reference signals with amplitudes of 1 N to 100 N with a bandwidth between 8.1 Hz and 20.6 Hz, and outputs a maximum mechanical power of 80.2 W. Based on these results the augmentation factor predicted that the exoskeleton can generate a 33 W decrease in metabolic cost. In contrast with this prediction, in the*

*human experiments we found an increase in metabolic rate for support (21.2 W) and no support (22.7 W) compared to baseline.*

*Our results are compared to those of Malcolm et al. where a reduction in metabolic cost was found. Although the torque provided by the exoskeleton was similar to Malcolm et al. the exoskeleton power and walking speed were lower, which might explain the difference in metabolic cost.*

## 8.1 Introduction

Exoskeletons hold the promise that they can assist people with tasks that require power to perform them. One of the main challenges within this field is to reduce the metabolic cost of walking. Recently, it has been shown that this is possible (Malcolm et al., 2013a; Mooney et al., 2014a).

Although these exoskeletons have shown the potential of the technology, it is still not fully understood how the reduction in metabolic cost arises from the exoskeleton characteristics. The human and the exoskeleton are two (non-linear) dynamical systems that interact. As a result humans adapt their gait when walking with an exoskeleton which causes a change in metabolic cost (Kao et al., 2010a; Sawicki and Ferris, 2008). If the relation between the change in walking conditions and metabolic cost could be known, exoskeleton performance could be estimated on beforehand.

One approach to estimate this relation is through biomechanical models. Biomechanical models have been developed that are capable of generating walking motions and predicting the metabolic cost (Geyer and Herr, 2010; van den Bogert et al., 2011; Wang et al., 2012). These models have to some extent the capability to adapt to new tasks like terrain or speed changes or interaction with exoskeletons (Geyer and Herr, 2010; Song and Geyer, 2012; van Dijk and van der Kooij, 2013). So far these models have not been validated for predicting the metabolic cost for these new tasks.

Another approach is to search for empirical relations (Caputo and Collins, 2014) that estimate the metabolic costs of with wearing an exoskeleton. Experiments with current exoskeletons have shown that the augmentation factor (AF), the exoskeleton control, and the experimental protocol are all important factors in reducing metabolic costs. Besides the measurement of metabolic cost there are secondary measures that give additional insight in how humans adapt to a change in walking conditions.

*Augmentation factor:* The AF estimates the relative change in metabolic cost when walking with an exoskeleton compared to walking without an exoskeleton. This change is called the metabolic advantage. Positive values mean that the metabolic cost of walking with the exoskeleton is lower than normal walking and vice versa. The AF is based on the mass of the exoskeleton and the support the exoskeleton provides. The mass the exoskeleton adds to the legs increases the AF, and the more distally the mass is placed, the larger the increase (Browning et al., 2007). The support of the exoskeleton is the power it provides around the leg joints. These powers can for example be induced by actuators, dampers or springs. The AF increases when the average positive power increases. When the exoskeleton has a net dissipation of energy (the average power is below zero) the AF becomes smaller when the dissipation of energy is larger (Mooney et al., 2014a).

Due to the strong negative effect of added mass on the AF and metabolic cost of walking, walking with many exoskeletons (e.g. Norris et al., 2007; Sawicki and Ferris, 2008; Walsh et al., 2007) did not result in an absolute reduction of the metabolic cost of walking. However, a relative reduction in metabolic cost was found when comparing the unpowered and the powered condition where the added mass in both conditions was the same. The augmentation factor sets constraints on the mass and the support of the exoskeleton if an absolute reduction in metabolic cost of walking is desired.

*Exoskeleton control:* The augmentation factor can roughly explain different experimental results, but does not capture fine differences between exoskeleton designs and control methods. Other studies have investigated how changes in the control of a specific exoskeleton influenced the performance. We mention two examples. Reference (Malcolm et al., 2013a) showed that timing is critical when supporting ankle plantarflexion. By evaluating different onset timings of the support it was possible to find an optimal condition where the reduction in the metabolic cost was the largest. Reference (Cain et al., 2007) compared triggering of the exoskeletal support by a footswitch versus triggering by the EMG signal of the soleus muscle. The EMG triggering resulted in ankle angle patterns more close to normal walking and lower EMG's of the soleus and gastrocnemius.

*Experimental protocol:* The exoskeleton performance depends on the experimental protocol. It has been shown that with the same exoskeleton the reduction of metabolic energy depended on the step length (Sawicki, 2009) and the adaptation time given to subject (Sawicki and Ferris, 2008). For real life applications it would be important to also evaluate the effects of terrain adaptation. This would require an untethered exoskeleton.

*Secondary measures:* The studies mentioned above were mostly focused on directly assessing the human performance. In some studies additional measures were taken to gain insight in the interaction of the dynamical systems lying underneath. Reference (Kao et al., 2010a) shows that the ankle motion changed under influence of the exoskeleton, where the total ankle torque was invariant. To gain deeper insight in how exoskeletal support relates to metabolic cost, the influence on muscle force and work (Farris et al., 2013), and activation (Cain et al., 2007) is investigated.

The knowledge of how metabolic cost is influenced by an exoskeleton could still be expanded. This requires additional knowledge the human and exoskeleton that interact as dynamical systems. With some exceptions (XPED, Witte et al., 2015), the a dynamical model of the exoskeleton is not given. With such a model it would be easier to generalize experimental findings. A dynamical model of the widely used pneumatic actuators is hard to obtain due to their high non-linearity. The use of a precise force controlled actuator would not only make it easy to obtain model of the exoskeleton dynamics, but would also make it easy to evaluate different controllers with one exoskeleton.

Further insight in how humans and exoskeletons interact is possible with new exoskeletons. These exoskeletons should have high power and low weight for a high augmentation factor, be autonomous to allow experiments on different terrains, and have precise force control to be able to model the exoskeleton dynamics and test different controllers. These requirements are in many ways conflicting and require a specialized design.

One of the possibilities to keep the weight down is to buffer energy. An energy buffer is also seen in the human Achilles tendon that works as a catapult during push off. A design analogous to this principle is proposed by (Hitt et al., 2007). The actuator in this design consists out of an electric motor in series with a spring (i.e. a series elastic actuator, SEA). During stance the spring is loaded with the motor and energy is buffered, at late stance the energy is released from the spring and creates the catapult effect. As a result the push-off power can be higher than the motor power. An additional advantage of this SEA is that it enables good force control (Pratt and Williamson, 1995).

To further increase the power-to-weight ratio of the exoskeleton, numerical methods can be used to optimize the exoskeleton design (Wang et al., 2013). This optimization uses a parameterized electromechanical model of the exoskeleton to determine the best choice for the motor, transmission, geometry, and spring



Figure 34: The Achilles exoskeleton

characteristics. Additionally the number of components that interface between the SEA and the human can be kept minimal in weight and number by using function integration.

This chapter describes the design and evaluation of the Achilles exoskeleton (Figure 34). Separate sections will discuss the design methods, benchtop tests that evaluated the performance of the actuator, and human experiments that evaluated the working of the complete system.

## 8.2 Methods

### 8.2.1 Design

#### *Working principle*

The exoskeleton was build up from a linear actuator, that consisted of a rotary electric motor and ball-screw gear, which was suspended in a linkage mechanism between the shank and foot shells. The link, or lever-arm, that was attached to the foot shell was flexible thus introduced the series elasticity (Figure 35).

#### *Mechanical model*

The support torque ( $T_s$ ) was given by the equivalent linear rotational spring stiffness ( $c_s$ ) and the spring deformation angle ( $q_s$ ):

$$T_s(c_s, q_j(t), x_m(t), r_1, r_2, \psi) = c_s \cdot q_s(q_j(t), x_m(t), r_1, r_2, \psi) \quad (41)$$

The spring deformation was a function of the joint angle ( $q_j(t)$ ), the motor stroke trajectory ( $x_m(t)$ ) that were both changing over time ( $t$ ), and the exoskeleton dimensions ( $r_1, r_2$  and  $\psi$ ), and were calculated using trigonometric functions (Figure 35).

The dynamics of the system are given in Figure 35. Throughout the optimization we assumed that we knew the joint angle ( $q_j(t)$ ) and the total joint torque ( $T_j(t)$ ) and used data from (Winter, 1990 data from normal walking) as a reference for the walking pattern. This leaved the design parameters  $r_1, r_2$  and  $\psi$ , and the motor stroke trajectory  $x_m(t)$ . The dynamic equilibrium equations were given by:

$$M_{eq} \ddot{x}_m(t) = \Sigma F(t) = F_m(t) + F_s(t) \tag{42}$$

where  $M_{eq}$  is the equivalent mass combining the reflected mass of the motor and gear inertia.  $F_m$  is equivalent motor force. The force in the spindle  $F_s$  depended on the angle between the actuator axis and lever-arm  $\gamma(x_m(t), r_1, r_2)$  and was given by:

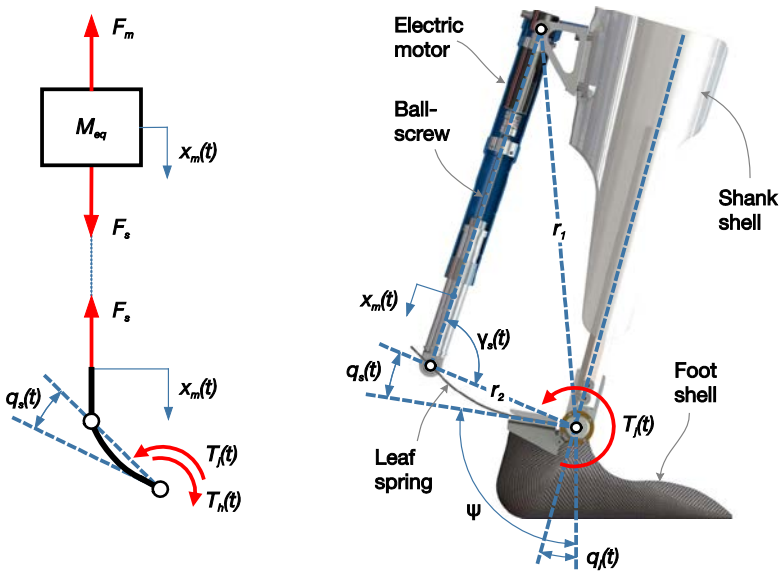


Figure 35 left: A schematic of the system dynamics. Right: The CAD model with a partial cross-section of the actuator (right). The variables are  $x_m(t)$  the stroke of the actuator,  $q_s(t)$  the deflection of the lever-arm,  $q_j(t)$  the joint angle,  $\gamma(t)$  the angle between the actuator axis and lever-arm,  $T_j(t)$  the joint torque,  $T_h$  the torque exerted by the human,  $F_s$  the spindle force, and  $F_m$  the force from the motor. The parameters are  $r_1$  the proximal lever-arm length,  $r_2$  the distal lever-arm length,  $\psi$  the distal lever-arm angle, and  $M_{eq}$  equivalent mass of the drive components. Note that the schematic of the system dynamics gives no clear distinction between rotational and translational components.

$$F_s(t) = \frac{T_s(t)}{r_2 \sin(\gamma(t))} \quad (43)$$

The motor stroke and force  $x_m(t)$  and  $F_m(t)$  were linearly related with the motor angle ( $q_m(t)$ ) and torque ( $T_m(t)$ ) by the transmission ratio of the ball-screw:

$$R_s = \frac{p_s}{2\pi} \quad (44)$$

where  $p_s$  is the pitch of the ball-screw.

### Optimization

The main goal in the actuation system design was to supply the highest amount of support to with the smallest added mass to the ankle. This was achieved by using an optimization process similar to (Wang et al., 2013). The dimensions of the linkage mechanism and stiffness of the flexible lever-arm were optimized for all combinations of preselected motors and gears.

The exoskeleton should provide solely positive power during the push of. The amount of support was therefore captured in the following function:

$$f(\mathbf{z}) = 1 - \frac{\int_0^T \left| \max(P_j(t, \mathbf{o}) - P_s(t, \mathbf{z}) \right| dt}{\int_0^T \left| \max(P_j(t, \mathbf{o})) \right| dt} \quad (45)$$

$P_j(t)$  and  $P_s(t)$  are respectively the total joint power and the exoskeleton joint power and  $\mathbf{z}$  the parameters to be optimized. The support optimization was formulated as the following maximization problem:

$$\text{maximize } f(\mathbf{z}) \text{ subject to } \mathbf{g}(\mathbf{z}) \leq \mathbf{o} \text{ and } \mathbf{lb} \leq \mathbf{z} \leq \mathbf{ub} \quad (46)$$

$\mathbf{g}(\mathbf{z})$  are the electrical and mechanical constraints on the motor and gear.  $\mathbf{lb}$  and  $\mathbf{ub}$  are the respective lower and upper bounds on the parameters. The optimization parameters were given by:

$$\mathbf{z} = \{x_m, r_1, r_2, \psi, c_s\} \quad (47)$$

where  $x_m$  are the stroke trajectory parameters. These parameters represented 16 points equally distributed over the gait cycle. The stroke function of the actuator  $x_m(t)$  was given by smoothed interpolation between these points. The maximization problem was solved by the *fmincon* numerical solver in Matlab

Variable	Description	Constraint equation
$I_m(t)$ $I_m(t)$	Motor current	$\max(I_m(t)) - I_{\max} < 0$
$U_m(t)$ $U_m(t)$	Motor voltage	$\max(U_m(t)) - U_{\max} < 0$
$P_m(t)$ $P_m(t)$	Motor power (electrical)	$\max(P_m(t)) - P_{\max} < 0$
$\dot{q}_m(t)$ $\dot{q}_m(t)$	Motor speed	$\max(\dot{q}_m(t)) - \omega_{\max} < 0$
$F_m(t)$ $F_m(t)$	Motor force	$\max(F_m(t)) - F_{\max} < 0$
$\dot{x}_m(t)$ $\dot{x}_m(t)$	Spindle velocity	$\max(\dot{x}_a(t)) - v_{\max} < 0$
$x_a(t)$ $x_a(t)$	Spindle stroke	$\max(x_m(t)) - \min(x_m(t)) - L_{\max} < 0$

Table 17: Overview of the electrical and mechanical constraints on the system. The maximal current was obtained from the guidelines of the manufacturer:  $I_{\max} = I_{nom} \sqrt{t_{cycle} / t_{I_m > I_{nom}}}$  where  $I_{nom}$  is the nominal current,  $t_{I_m > I_{nom}}$  is the ratio between the cycle time and the time the current is above its nominal value per cycle.

(Mathworks, Natick, MA, US). For comparison, the total mass each motor/gear combination was plotted against the amount of power it supplies to the user.

### *Electrical and mechanical constraints*

The exoskeleton was subject to mechanical and electrical constraints (Table 17). The motor current ( $I_m$ ), voltage ( $U_m$ ) and electrical power ( $P_m$ ) were calculated using the methods of (Wang et al., 2013). The constraint function  $g(\mathbf{z})$  combined the constraint equations of Table 17 and outputs a vector of which all elements were equal or smaller than zero if and only if all constraints were satisfied.

### *Motor gear combinations*

The motors and ball-screw gears that were selected for the optimization are respectively listed in Table 18 and Table 19 along with their relevant specifications. The total mass of each motor/gear combination was calculated by:

$$m_{tot} = m_m + m_{g_1} + \hat{m}_{g_2} (\max(x_m(t)) - \min(x_m(t))) \quad (48)$$

Property	Symbol	RE35	EC32	EC4p22	EC4p22	Unit
Power rating (electrical)	$P_{\max}$	90	80	90	120	[W]
Winding voltage	$U_{\max}$	24	24	24	24	[V]
Nominal current	$I_{\text{nom}}$	3.47	2.44	3.88	4.81	[A]
Motor mass	$m_m$	360	270	125	175	[g]
Rotor inertia	$J_m$	3350	2000	554	891	[g·mm <sup>2</sup> ]
Max speed	$\omega_{\max}$	12000	25000	25000	25000	[rpm]

Table 18: Specifications of preselected motors. Supplier of all listed motor types is Maxon (Maxon Motor ag, Sachseln, Switzerland)

Property	Symbol	SH6x2	SD8x2.5	SD10x2	SD10x4	Unit
Spindle pitch	$p_s$	2	2.5	2	4	[mm]
Max feed velocity	$v_{\max}$	277	260	166	332	[mm/s]
Max spindle load	$F_{\max}$	1500	2600	3500	5400	[N]
Nut mass	$m_{g1}$	25	25	30	40	[g]
Spindle specific mass	$\hat{m}_{g2}$	0.180	0.320	0.510	0.430	[g/mm]
Spindle specific inertia	$\hat{J}_g$	0.07	0.21	0.52	0.38	[g·mm]

Table 19: Specifications of preselected ball-screw gears. Supplier of all listed ball-screw gears is SKF (SKF, Gothenburg, Sweden)

### ***Spring design***

The lever-arm was required to store large amounts of energy. Therefore unidirectional carbon fiber was chosen because of its superior energy density. The spring was cut from a plate with a uniform thickness, hence the design parameters were the thickness and width profile. The correct dimensions were determined using a finite element model of the spring in ANSYS (ANSYS Inc., Cecil Township, PA, US).

### ***Sensors and control electronics***

The exoskeleton used a distributed control architecture that communicated via the EtherCAT protocol running at 1 kHz. A NUC computer with Core i3 processor (Intel, Santa Clara, CA, US) running Linux, and SOEM (SMF Ketels, Drunen, the Netherlands) was used as the EtherCAT master. Matlab/Simulink (MathWorks, Natick, MA, US) with E-box (TU/e, Eindhoven, the Netherlands) was used to program the high level control.

The motors were controlled with EPOS<sub>3</sub> 70/10 EtherCAT motor controllers (Maxon). The motor stroke was recorded with a SCH24-200-D-03-64-3-B incremental encoder (Scancon, Allerød, Denmark). The ankle angle was recorded with an RMB20SC13BC absolute encoder (RLS-Renishaw, Ljubljana, Slovenia). Heel strikes were recorded with a FSR-151AS pressure sensor (IEE, Contern, Luxembourg) under the heel of the foot. EK1100, EL5002, and EL3104 EtherCAT modules (Beckhoff Automation GmbH, Verl, Germany) were used to interface with the incremental encoders and pressure sensors. The motors and computer were powered by respectively a Zippy Compact 5000mAh 8S 25C and a Hacker Top Fuel 5000 6S 20C Lithium-Polymer battery.

### **8.2.2 Exoskeleton control architecture**

The control of the exoskeleton was separated in low-level control and high-level control (Figure 36). The high level control was implemented in Matlab/Simulink and regulates the support torque. The separate components of this controller are described below. The low level control ran on the EPOS<sub>3</sub> motor controllers and regulates the motor current. The velocity loop on the motor controllers was used to implement motor damping to increase the overall control performance. For the walking experiments the controller described below was used. For the benchtop tests only the part of the control architecture that performs the force/torque control (without feed-forward) was used.

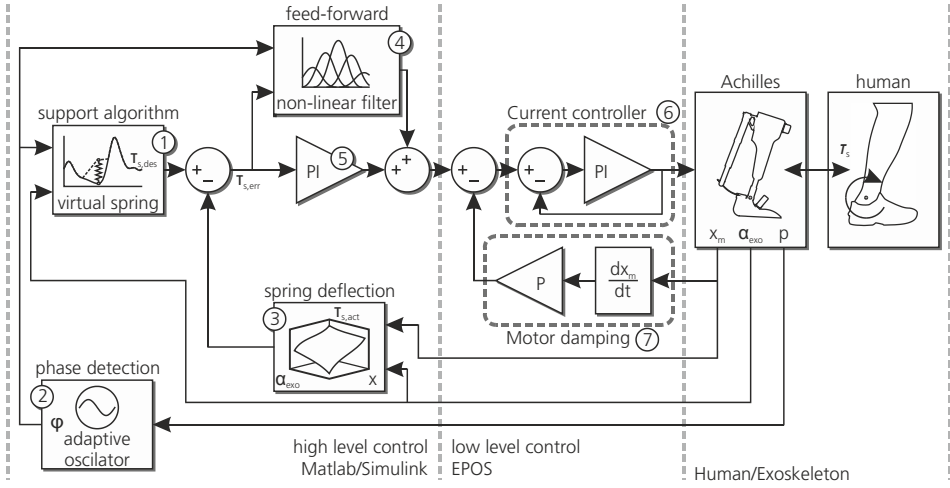


Figure 36: Exoskeleton control architecture. The high level control, implemented in Matlab/Simulink, regulates the support torque ( $\tau_s$ ). The support algorithm (1) calculates the desired support torque ( $\tau_{s,des}$ ) based on the gait phase ( $\varphi$ ), from the phase detection (2), and the joint angle ( $\alpha_{exo}$ ). The actual support torque ( $\tau_{s,act}$ ) is calculated from the spring deflection (3) that is given by the joint angle and the motor stroke ( $x_m$ ). The torque error ( $\tau_{s,err}$ ) is fed to a feed-forward (4) and a PI feed-back controller (5). The low level control, implemented on the EPOS3 motor controllers, regulates the motor current. The current control is performed by a PI feed-back controller (6). The velocity loop of the motor controller is used to add motor damping (7). Finally the motor current induces a support torque ( $\tau_s$ ) that is transmitted to the human.

### Phase detection

The exoskeleton made a continuous estimation of the gait phase with a phase detection algorithm. Inputs to the algorithm were the signals from the pressure sensors ( $p_{left}, p_{right}$ ) under the heels of the orthoses. The normalized gait phase ( $\varphi$ ) and frequency ( $\omega$ ) were learned by an adaptive frequency oscillator (AFO) (Gams et al., 2009). The AFO estimated both signals with a sinusoidal function:

$$\hat{p}_{left} = b + a \cdot \sin(2\pi \cdot \varphi), \quad \hat{p}_{right} = b + a \cdot \sin(2\pi \cdot \varphi + \pi) \quad (49)$$

The estimations were governed by the following set of differential equations:

$$\begin{aligned} \dot{\omega} &= \varepsilon (e_{left} \cos(2\pi \cdot \varphi) + e_{right} \cos(2\pi \cdot \varphi + \pi)) \\ \dot{\varphi} &= 2\pi (\omega + \dot{\omega}) \\ \dot{a} &= \eta (e_{left} \sin(2\pi \cdot \varphi) + e_{right} \sin(2\pi \cdot \varphi + \pi)) \\ \dot{b} &= \eta (e_{left} + e_{right}) \end{aligned} \quad (50)$$

with:

$$e_{left} = p_{left} - \hat{p}_{left} \quad e_{right} = p_{right} - \hat{p}_{right} \quad (51)$$

Additionally a phase offset was learned so that the phase was zero at the heel strike of the left foot. Every time a heel strike had been detected with one of the pressure sensors, the offset value was updated. To prevent abrupt changes in phase estimation the offset value was low pass filtered at 0.2 Hz.

### ***Feed-forward control***

Since human walking is a cyclic motion it was possible to improve the control performance by learning a feed-forward signal based on previous steps. This feed-forward signal was learned as a function of the phase by using a non-linear filter that fits a number of primitives to the signal to be learned (Chapter 5). In our case, these primitives were Gaussian functions.

### ***Support algorithm***

During walking trials the exoskeleton had two operation modes. Zero torque mode where the reference torque in the controller was zero, and a support mode where the reference torque was a supportive torque. A support algorithm similar to (Caputo and Collins, 2014) was used where the support torque was modelled as the torque emerging from the deflection of a virtual spring. The deflection of the spring was the difference between the actual joint angle ( $\alpha_{exo}$  [rad]) and a reference angle ( $\alpha_{ref}$  [rad], Figure 37). The reference angle was given by:

$$\alpha_{ref}(\varphi(t)) = \begin{cases} \alpha_{on} - c_1 (\varphi(t) - \varphi_{on}) & \varphi_{on} < \varphi(t) \leq \varphi_{switch} \\ \alpha_{switch} - c_2 (\varphi(t) - \varphi_{switch}) & \text{if } \left( \begin{array}{l} \varphi_{switch} < \varphi(t) \leq \varphi_{off} \\ \text{and } \alpha_{ref}(t) < \alpha_{meas}(t) \end{array} \right) \\ \alpha_{exo}(t) & \text{otherwise} \end{cases} \quad (52)$$

Where  $\alpha_{on} = \alpha_{meas}(\varphi_{on})$  and  $\alpha_{switch} = \alpha_{ref}(\varphi_{switch})$  at the respectively the last recorded instances of  $\varphi(t) = \varphi_{on}$  and  $\varphi(t) = \varphi_{switch}$ . The desired support torque ( $\tau_s$  [Nm]) was given by:

$$\tau_s = k \cdot (\alpha_{ref} - \alpha_{exo}) \quad (53)$$

Parameter	Value
$\varphi_{on}$	0.37
$\varphi_{on}$	0.48
$\varphi_{on}$	0.65
$c_1$	1.88 rad
$c_2$	0.54 rad
$k$	80-100 nm/rad*

Table 20: Parameters of the exoskeleton support function. \* this parameter is tuned per subject to approximately match the results of (Malcolm et al., 2013a).

where  $k$  [Nm/rad] is the virtual spring stiffness. The constants  $\varphi_{on}$ ,  $\varphi_{switch}$ ,  $\varphi_{off}$ ,  $c_1$  and  $c_2$  (Table 20) were tuned so that the power output of the support algorithm approximately matched the pattern optimized pattern. The virtual spring stiffness  $k$  was tuned per subject to get a maximal support of 0.4 Nm/kg, approximately matching the maximal support used in the study of Malcolm et al. (Malcolm et al., 2013a). By using this parameterization of the support, the amount of mechanical work by the exoskeleton around push-off for each step was approximately the same for every step. The amount of energy stored in the virtual spring was mainly determined by the change in the reference angle between  $\varphi_{on}$  and  $\varphi_{switch}$ , so that

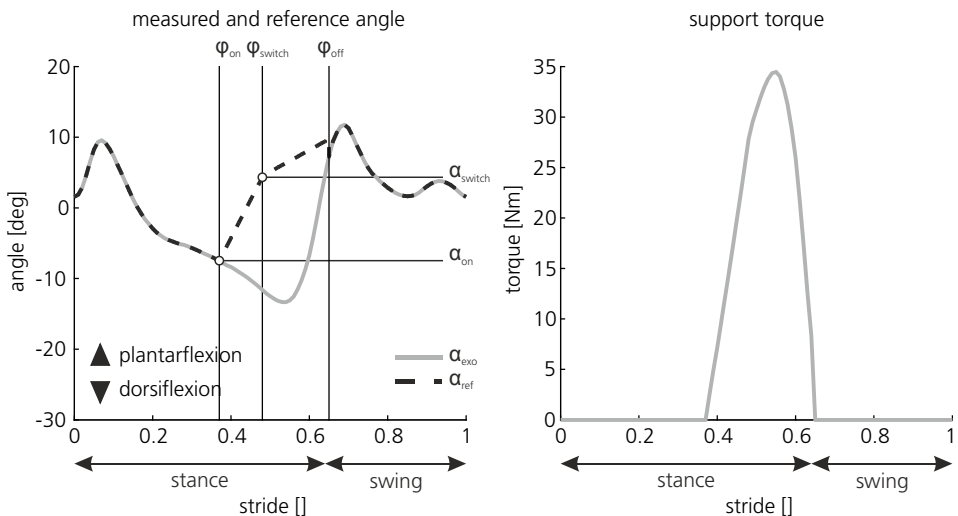


Figure 37 Left: The support torque is represented as the deflection of a virtual spring. The deflection is determined by the ankle angle ( $\alpha_{exo}$ ) at one side and by a reference angle ( $\alpha_{ref}$ ) at the other side. The reference angle is a function of the measured joint angle and the phase. Right: The support torque is given by the deflection multiplied with the stiffness of the virtual spring, in this case a typical value of  $k = 100$  Nm/rad is used.

every step approximately the same amount of energy was stored in the virtual spring. The release of energy after  $\varphi_{switch}$  was mainly determined by the change in the actual joint angle, so that the virtually stored energy was released to the ankle joint. This was favored over following a torque reference pattern, which would have made the amount of mechanical exoskeleton work highly dependent on the angular velocity. The latter approach had led to large step-to-step deviations in preliminary tests.

### 8.2.3 Evaluation

#### *Benchtop testing*

##### *Lever-arm stiffness*

The stiffness of the produced spring was compared to the estimated stiffness. The stiffness is nonlinear and to obtain the exact stiffness characteristic ( $T_s(q_s)$ ) of the spring, a force-travel experiment was performed. The spring was mounted on a table edge using the same mounting components as in the exoskeleton. A platform was connected to the endpoint of the spring via a cable and incrementally loaded with 1, 3, 8, 13, 18, 23, 25 and 35 kg. The travel ( $x_s$ ) of the endpoint was measured with a digital caliper with respect to a reference plate that was fixed to the table.

##### *Stroke tracking*

It was evaluated how well the actuator could track the optimized stroke trajectory. During this test the exoskeleton was mounted such that it could freely move and the optimized stroke trajectory was sent to the controller. The achieved stroke was recorded. The RMS of the tracking error, the difference between the input and output value, was taken as the tracking performance.

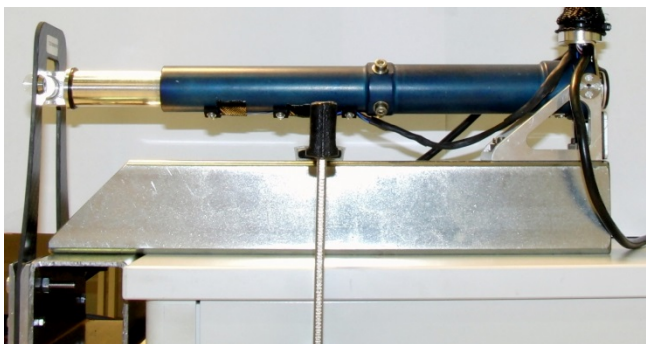


Figure 38: The actuator of the exoskeleton mounted between two rigid endpoints.

### *Force bandwidth*

The force bandwidth gives an indication of how well the actuator could follow a force signal. To test the force bandwidth the series elastic actuator was placed between two fixed endpoints (Figure 38). A sine sweep signal from 1 Hz to 30 Hz was fed to the controller. The amplitude of the signal ranged from 1 N to 100 N with an offset equal to the amplitude (so the maximal force was twice the amplitude and the actuator only exerted plantarflexion torques, which is the intended use). For each amplitude the crossover frequency (at -3dB) was determined.

### *Power*

The mechanical power output of the actuator is evaluated with the same setup as used for the force bandwidth test (Figure 38). The test simulates the loading of the spring during walking. The test starts with no deflection of the spring. From this start point the spring is loaded by sending the maximal allowable input to the actuator. The deflection of the spring is recorded. This gives the force in the spring (see lever arm stiffness) and the speed of the actuator, the product of the two gives the power output of the actuator.

## *Human testing*

### *Subjects*

Seven healthy participants participated in this experiment of which subgroups of four and three subjects participated in different tests. Details are given in Table 21. The Human Research Ethics Committee of the Delft University of Technology approved the study, and all subjects gave written informed consent to participate.

Subject	Age	Length	Mass	M(ale)/ F(emale)	Speed	Kinetics/ Kinematics	AF	Metabolic Cost
unit	years months	m	kg		km/h			
1	20y11m	1.76	76.9	F	4	✓	✓	
2	20y4m	1.72	67.6	F	4	✓	✓	
3	19y11m	1.71	58.8	F	4	✓	✓	
4	19y8m	1.71	68.0	M	4	✓	✓	
5	20y4m	1.74	64.4	F	3.5		✓	✓
6	29y10m	1.78	58.8	F	3.5		✓	✓
7	19y2m	1.78	58.2	F	3.5		✓	✓
mean	21y5m	1.74	64.7	--	--	--	--	--
<i>SD</i>	<i>3y8m</i>	<i>0.03</i>	<i>6.8</i>	--	--	--	--	--

Table 21: Overview of subjects and data recordings. ✓ marks that data is recorded for this subject.

### *Data recordings*

Kinematics and kinetics were measured by recording segment motions and ground reaction forces. Markers placed on the foot and shank segments of one leg were recorded with an optical tracking system (VZ4000, Visualeyex, Burnaby, BC, Canada). Ground reaction forces were recorded with a dual belt instrumented treadmill (Y-Mill, Forcelink B.V., Culemborg, The Netherlands). Kinetics and kinematics of the exoskeleton were recorded by the exoskeleton itself. All kinematic and kinetic data were (re-)sampled at 100 Hz. An open circuit respirometry system (Jaeger Oxycon Pro, Viasys Health Care, Warwick, UK) was used to measure the oxygen consumption ( $\dot{V}_{O_2}$  [l/s]) and carbon dioxide production ( $\dot{V}_{CO_2}$  [l/s]). A synchronization signal was recorded by all measurement systems to synchronize the data except for the respirometry system that was manually synced. Table 21 shows which measurements were taken for which subject.

### *Protocol*

Three measurement trials were used to evaluate the following conditions: *Baseline*, the subject walked without the exoskeleton; *No support*, the subject walked with the exoskeleton while the exoskeleton operates in zero torque mode; *Support*, the subject walked with the exoskeleton while the exoskeleton operates in support mode. The trials were in quasi-random order with the baseline trial always at the beginning or the end of the trials. Each trial had a duration of approximately 12 minutes. Before the measurement trials began, a practice trial was used where the subject could familiarize with the exoskeleton. During the practice trial the virtual spring stiffness was tuned. Additionally the practice trial was intended to wash out learning effects. The kinematics and kinetic analysis required the recording of a standing pose and identification of anatomical landmarks with a probe. The metabolic cost measurements required the recording of the metabolism at rest. This was done in a 5 minute trial where the subject was sitting in a chair.

### *Data analysis*

*Kinetics/kinematics*: The marker and segment trajectories were reconstructed using an extended Kalman filter (Todorov, 2007). The human joint kinematics and kinetics were calculated using inverse dynamics. These results were combined with the exoskeleton kinetics and kinematics. A 90 seconds sample at the end of each trail was used to calculate different measures. A median step was calculated by splitting the data into individual strides. The strides were separated at the heel strike, as detected by the instrumented treadmill.

The exoskeleton and human ankle angle should closely match, otherwise undesired deformations or relative movements are present. The Pearson correlation coefficient was calculated to quantify the relation of the human ankle angle (optical tracking system) and exoskeleton ankle angle (ankle encoder). The work associated with the relative motion between human and exoskeleton was calculated with:

$$W = \int_0^T (\alpha_{exo}(t) - \alpha_{hum}(t)) \tau_s(t) dt \quad (54)$$

Where the interval  $[0, T]$  is one stride cycle and  $\alpha_{hum}$  the (sagittal) human ankle angle calculated from the inverse dynamics.

*Augmentation factor:* The augmentation factor was calculated based on the exoskeleton angle and power using equation (57).

*Metabolic cost:* An empirical relation (Collins, 2008) was used to calculate the metabolic power  $\dot{E}$  [W]:

$$\dot{E} = 16.48 \cdot 10^3 \dot{V}_{O_2} + 4.48 \cdot 10^3 \dot{V}_{CO_2} \quad (55)$$

For all walking conditions the metabolic power at rest has been subtracted. The metabolic advantage is defined as the difference in metabolic power of one condition and the baseline condition ( $\dot{E}_{baseline}$  [W]).

$$\Delta \dot{E} = \dot{E}_{baseline} - \dot{E} \quad (56)$$

## 8.3 Results

### 8.3.1 Design

The actuation system was successfully optimized for all combinations of motors and gearboxes. The resulting support ( $f$ ) and total mass ( $m_{tot}$ ) of each combination is plotted in Figure 39. From the three combinations on the Pareto front, the middle one was chosen for implementation which is a Maxon EC22 4 pole motor with a SH6x2 ball-screw gear. With this drive combination, the actuation system can exert up to 192 W of power around the ankle of an 80 kg person. The full power characteristics are shown in Figure 40. The mass of the motor and gear combination was 218 g.

The optimal components and parameters were implemented in a CAD model which was manufactured. The mass of the Achilles exoskeleton is 1.5 kg per foot and the backpack has a mass of 5.2 kg (Figure 35).

**Augmentation factor**

Based on the optimal performance the theoretical maximal augmentation factor was calculated (Table 22). The augmentation factor (AF [W]) is given by the following empirical relation (Mooney et al., 2014a):

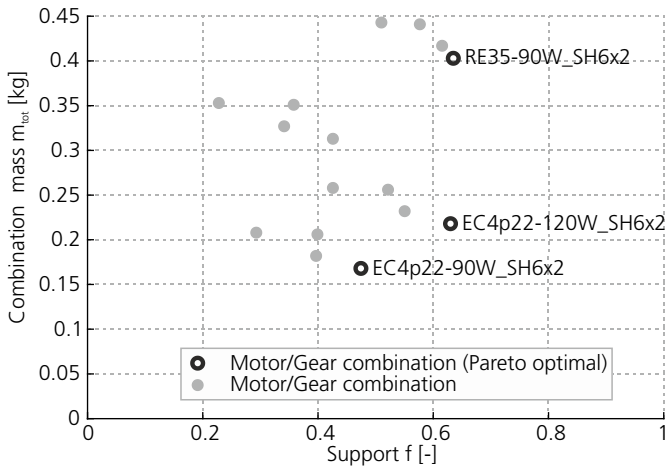


Figure 39: Simulation results of the support given to the user versus total mass of the drive components, where each circle represents an optimization for a motor and gear combination. The three red-thick circles form the Pareto front.

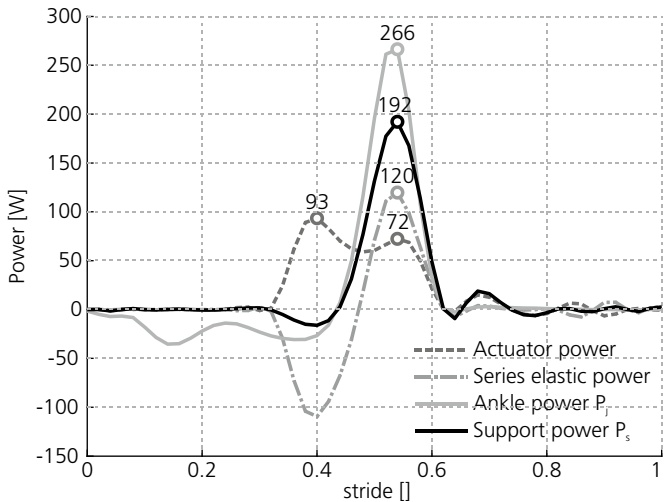


Figure 40: Simulation results of the ankle power as a function of stride with contributions of the motor and spring. The actuator power and the spring power sum up to the support power.

Segment weight	[kg]	$\beta$	Augmentation factor [W]
Waist	6.0	3.3 W/kg	-19.8
Shank	2 x 1.2	5.6 W/kg	-13.4
Foot	2 x 0.3	14.8 W/kg	-8.9
Support	[W]	$\eta$	
p+	35.8	0.41	87.4
p <sub>dis</sub>	0.0	0.41	0
Total			45.3

Table 22: Calculation of the theoretical augmentation factor based on the optimization results and the actual weight of the exoskeleton.

$$AF = \frac{p^+ + p_{dis}}{\eta} - \sum_{i=1}^4 \beta_i m_i \text{ with } p_{dis} = \min(0, p^- + p^+) \quad (57)$$

$p^+$  [W] and  $p^-$  [W] are the average positive and negative mechanical power transferred to the human during one step.  $\eta$  [] is the apparent efficiency that relates exoskeletal power with metabolic power (Sawicki and Ferris, 2008), whereas  $m_i$  [kg] are the exoskeleton's masses connected to the segments and  $\beta_i$  [W/kg] the relative costs of carrying this masses on the foot, shank, thigh, and pelvis segment.

### 8.3.2 Benchtop testing

#### *Lever-arm stiffness*

The predicted and measured lever-arm stiffness is shown in Figure 41. A third-order polynomial was fit through the experimentally obtained data points. The

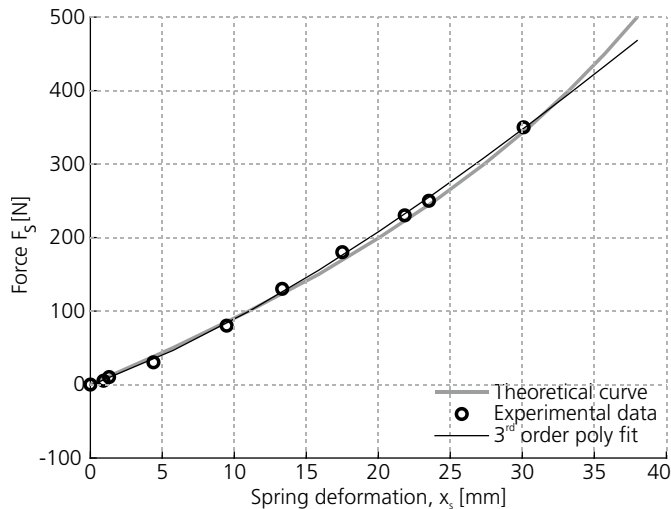


Figure 41: Graph of the force-travel of the lever-arm. The theoretical curve is obtained from the finite element model. The thin line is a 3<sup>rd</sup> order polynomial fit through experimentally obtained data points.

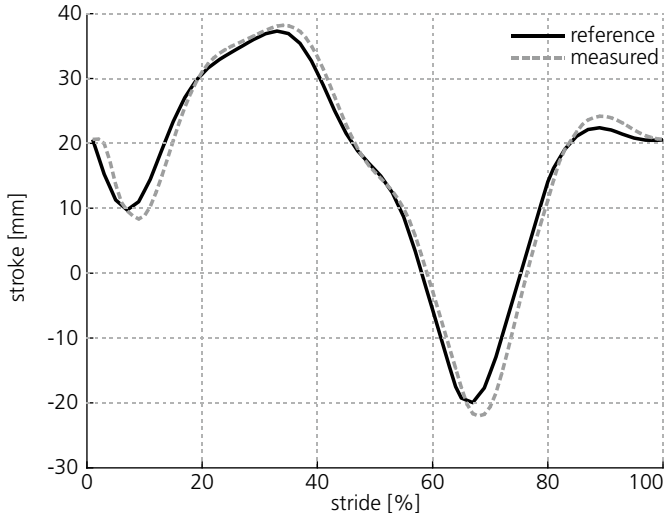


Figure 42: Experimental results of stroke tracking of the actuator. The reference trajectory is the optimized stroke trajectory.

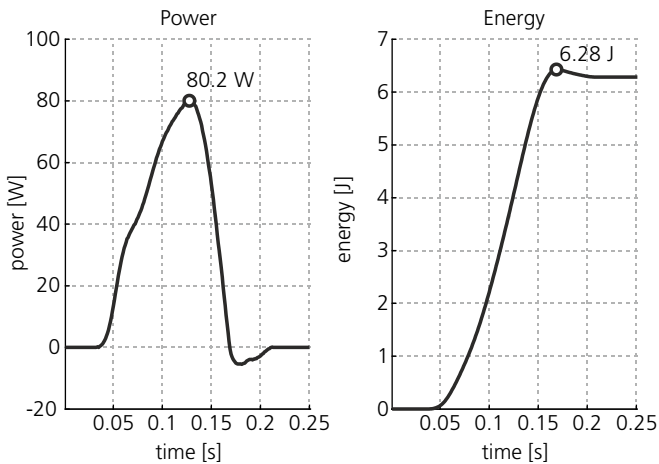


Figure 43 left: Experimental results of the power test. right: The energy stored in the spring. The small decrease after the energy peak is peak is caused by the release of kinetic energy when the motor inertia decelerates.

maximal deflection difference in the evaluated working range of the spring between the predicted stiffness and the measured data was 0.92 mm at a force of 30 N.

### ***Stroke tracking***

Figure 42 shows the tracking performance of the actuator. During this test the actuator tracks the optimized stroke trajectory. The RMS of the tracking error was 2.3 mm.

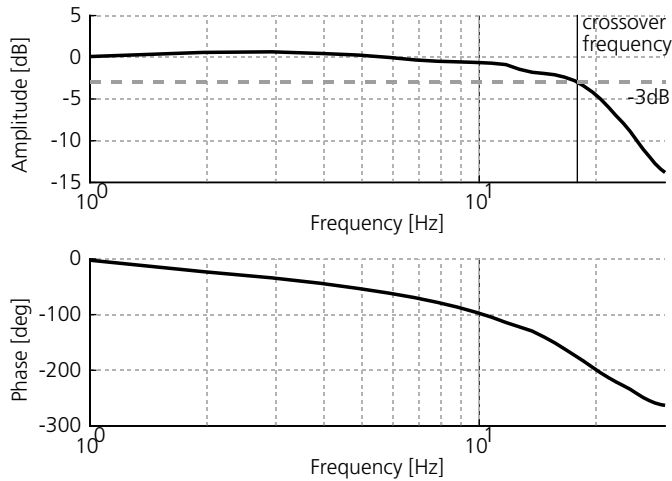


Figure 44: Bode magnitude and Bode phase plot from bandwidth test with an amplitude of 1N. The bandwidth is determined by the point where the magnitude plot crosses the -3dB line.

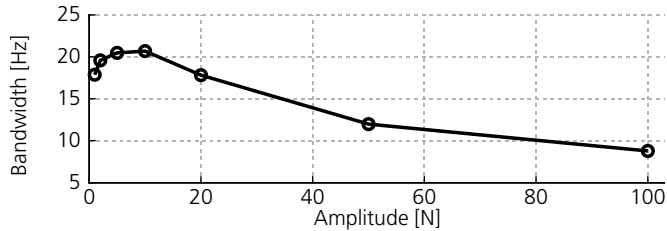


Figure 45: Experimentally determined force bandwidth of the actuator at different force amplitudes.

### **Power test**

The mechanical power of the actuator is shown in Figure 43. The peak power of the actuator was 80.2 W. This is 85.9% of the 93.4 W peak power that was predicted in the simulation. The maximal amount of energy that was stored in the spring is 6.28 J at 34.6 mm deflection. If the average positive power in the augmentation factor is scaled with 85.9% the corrected maximal augmentation factor reduces from 45.3 W (Table 1) to 32.9 W.

### **Bandwidth test**

The force bandwidth was between 8.1 Hz and 20.6 Hz (Figure 44 and Figure 45). The lowest bandwidth was measured at the highest amplitude (100N).

## **8.3.3 Human testing**

### **Ankle kinetics and kinematics**

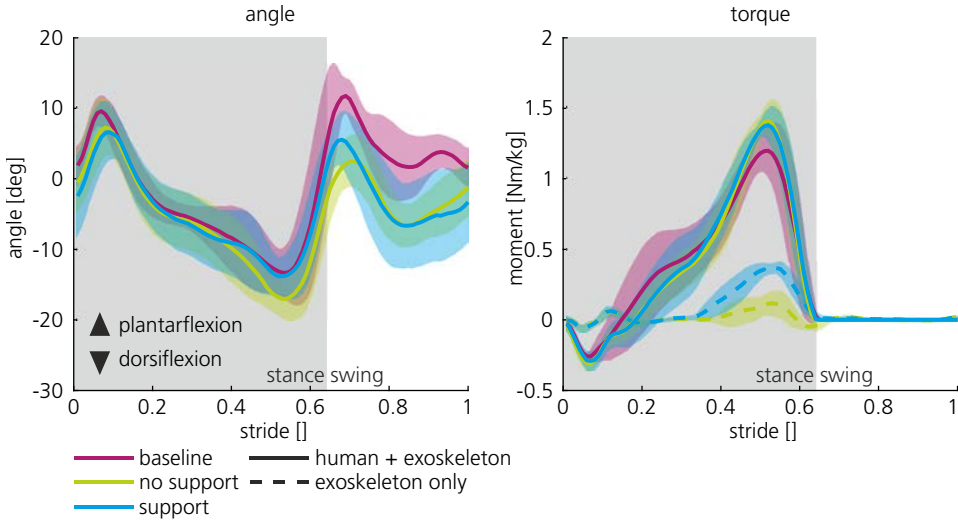


Figure 47: Joint angles and joint torques averaged over the subjects. The torque plots from the exoskeleton only (dashed lines) are obtained from the exoskeleton data.

The ankle angle and torque averaged over the subjects are shown in Figure 47. The maximal torque exerted by the exoskeleton in the no support condition was 0.15 (standard deviation (SD) 0.08) Nm/kg and in the support condition 0.40 (SD 0.02) Nm/kg. The most notable difference in kinematics is the plantarflexion angle around and after toe-off. The maximal plantarflexion angle around toe off is 13.6 (SD 3.2), 3.0 (SD 3.5), and 6.5 (SD 2.8) degrees for respectively the baseline, no support, and support condition. The difference between the baseline and no

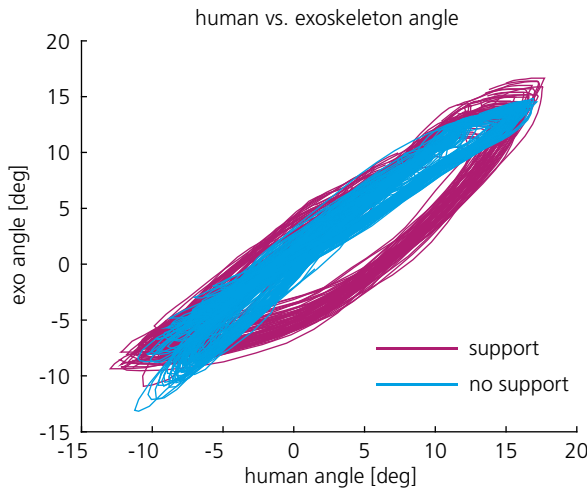


Figure 46: The human angle vs. the exoskeleton angle for a representative subject. All cycles within a 90 second sample are shown.

	Walking speed	Baseline	No support		Support	
subject	v [km/h]	$\dot{E}$ [W]	AF [W]	$\dot{E}$ [W]	AF [W]	$\dot{E}$ [W]
1	4.0	--	-48.5	--	-24.1	--
2	4.0	--	-48.3	--	-24.0	--
3	4.0	--	-46.6	--	-33.2	--
4	4.0	--	-45.4	--	-28.6	--
5	3.5	122.4	-47.4	142.8	-27.4	150.5
6	3.5	144.9	-45.0	186.4	-26.0	164.0
7	3.5	154.3	-44.2	160.5	-27.1	170.6
Mean (SD) 3 subjects	3.5	140.5(16.4)	-45.6 (SD 1.67)	163.2 (SD 21,9)	-26.9 (SD 0.74)	161.7 (SD 10.2)
Mean (SD) 7 subjects	3.8	--	-46.5 (SD 1.67)	--	-27.7 (SD 3.14)	--

Table 23: Augmentation factor and metabolic power (if available) for Achilles. For all conditions the energy metabolic power at rest has been subtracted. The augmentation factor during baseline is zero by definition.

support condition is statistically significant (paired t-test  $p < 0.05$ ).

Differences in the recorded human angle and exoskeleton angle are shown in Figure 46. The correlation between the human ankle angle and the exoskeleton ankle angle in the no support condition ( $r = 0.977$  (SD 0.01)) is significantly higher than for the support condition ( $r = 0.88$  (SD 0.06),  $p = 0.039$  paired t-test). The work associated with these angular differences is 2.16 (SD 0.42) J for the support condition and 0.14 (SD 0.41) J for the no support condition.

### ***Augmentation factor and metabolic power***

The augmentation factor and metabolic power for the different subjects is shown in Table 23. The results of the Achilles exoskeleton are compared to the results of others in Figure 48.

## **8.4 Discussion**

### **8.4.1 Design**

The Achilles exoskeleton is an exoskeleton with a high power-to-weight ratio. The high power-to-weight ratio was achieved by a minimalistic design. The choice for the motor, transmission and spring characteristics was based on optimization results. The spring in the SEA acts as an energy buffer similar to the Achilles tendon. Power losses caused by friction are low due to the use of a ball screw transmission. This largely reduced the required motor power resulting in a weight of the motor and transmission of only 218 g. The elastic element of the SEA and the lever arm function were combined in one leaf spring. This made it possible to make a minimalistic and lightweight design for the interface. Batteries and control

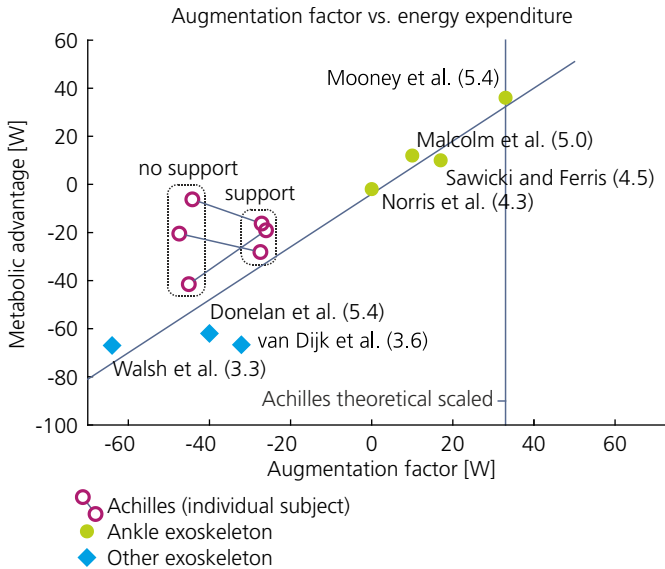


Figure 48: Augmentation factor versus metabolic advantage. Values between brackets are the walking speeds used in the experiments with the exoskeletons. The diagonal line represents the empirical relation found by (Mooney et al., 2014a). The vertical line is the corrected maximal augmentation of Achilles that is based on the actuator power test results. References: Donelan et al. (Donelan et al., 2008; Mooney et al., 2014a); Malcolm (Malcolm et al., 2013a; Mooney et al., 2014a); Mooney et al. (Mooney et al., 2014a); Norris et al. (Norris et al., 2007); Sawicki and Ferris (Mooney et al., 2014a; Sawicki, 2009); van Dijk and van der Kooij (van Dijk and van der Kooij, n.d.); Walsh et al. (Walsh et al., 2007)

electronics are carried on the back where the weight of these components have a much smaller effect on the metabolic cost of walking than if they were placed at the foot or shank.

#### 8.4.2 Actuator performance

The performance of the exoskeleton was assessed in multiple tests that simulated the operation conditions of the exoskeleton. The actual spring stiffness was very close to the spring stiffness in simulation. The actuator was able to track the designed stroke trajectory. The maximal power output in the bench top test was 85.9% of the predicted maximal power output and a corrected maximal augmentation factor is 33 W, which is equal to the result by (Mooney et al., 2014a). The bandwidth of the device is, depending on the amplitude, between 8.1 and 20.6 Hz. We expect this to be sufficient for human walking where frequencies are typical in the in the range up to 6 Hz. Based on the actuator performance we expect the exoskeleton to be capable reducing the metabolic cost of walking.

### 8.4.3 Kinematics and kinetics

The ankle kinematics during stance and total ankle torque are similar for all conditions. In the support and no support condition the plantarflexion angle after toe off is respectively 7.1 and 10.0 degrees smaller than in the baseline condition. This difference is mostly sustained throughout the swing phase. A possible explanation is that the perceived inertia of the exoskeleton is high with respect to the inertia of the foot. This is due to the amplification of the motor inertia through the transmission, and only partly compensated by the exoskeleton control. The high perceived inertia might limit fast plantarflexion just before toe-off, resulting in a smaller plantarflexion angle at toe-off. The effect is less prominent in the support condition, during this condition plantarflexion is supported which might reduce the effect.

The correlation between the human ankle angle and exoskeleton ankle angle is smaller in the support condition than in the no support condition. This makes it likely that the deviation in ankle angle occurs if force is transmitted from the exoskeleton to the human. The deformation can occur from soft tissue deformation at the human side, deformations in the exoskeleton structure or relative movement between the human and the exoskeleton.

### 8.4.4 Augmentation factor and metabolic cost

For all conditions the augmentation factor is below zero, therefore it was not expected that the exoskeleton would offer a metabolic advantage. The augmentation factor predicts that the metabolic power in the support condition would be 18.7 W lower than in the no support condition.

However, for only one of the three subjects the metabolic power was lower. For the other two subjects the metabolic cost was higher. In studies of (Sawicki and Ferris, 2008) and (Malcolm et al., 2013a) a respectively 17 and 10 W increase in augmentation factor led to a measurable reduction in metabolic cost. However, only for the second study this change was significant. The fact no decrease was measured in our experiment might have been caused by the relative low walking speed. Previous studies have shown that the ankle power increases with walking speed (Hansen et al., 2004). It might be possible that reductions in metabolic power with an exoskeleton might be easier to achieve at higher walking speeds, since nominal ankle torques are higher (Sawicki, 2009). Furthermore the relative changes in human angle and exoskeleton angle might be (partially) caused by deformations that induce energy losses, leading to an overestimation of the augmentation factor.

The augmentation factor in our study (-18.7 W) is low given the maximal theoretical augmentation factor (33 W) and the augmentation factor in other studies with similar exoskeletons (10-33 W). The following effects may have contributed to the relative low augmentation factor.

1 Low positive power: The average positive power in the tests with human subjects was low compared to capabilities of the actuator shown in the benchtop tests. This was done deliberately to match the results of (Malcolm et al., 2013a). Reference (Mooney et al., 2014a) have used significant higher powers that will be targeted in future experiments.

2 Exoskeleton weight: Although the foot parts of the exoskeleton was optimized for low weight the backpack of the exoskeleton was not. The relative heavy computer and industrial controllers in the backpack caused the weight of the backpack on its own to decrease the augmentation factor by 19.8 W.

#### **8.4.5 Future work**

Future work will focus on the improving the augmentation factor. On one side this is done by using the actuator closer to its power limits. On the other side this is done by slimming down the backpack by replacing the heavy industrial control components. Once the augmentation factor is improved, the exoskeleton testbed can be used to evaluate different controllers and conditions (e.g. walking on slopes or with a backpack) to further understand how human walking performance can be improved by exoskeletons.

## 9 Conclusions, Discussion, and Future Directions

---

The goal of this dissertation was to improve exoskeletons that reduce the metabolic cost of walking. To achieve this goal, three key challenges were defined. These challenges will form the guidelines for this chapter. The chapter will start with the main conclusions of these three challenges. In the subsequent paragraphs, the three challenges will be discussed in more detail. The chapter ends with a look forward, where future directions of the research field will be indicated.

### 9.1 Conclusions

#### 9.1.1 Challenge 1: Improving knowledge of human–exoskeleton interaction

In this dissertation we explored exoskeletons where a load, in this case walking, is shared between the human and the exoskeleton. The exoskeleton should be designed such that the load sharing between the human and the exoskeleton is optimized. Therefore, a prediction of how the human and exoskeleton interact is required. Based on this prediction, design specifications can be made.

For the XPED and Achilles exoskeletons described in this dissertation, the design specifications were based on the kinematics and kinetics observed in normal walking. Evaluation of the exoskeletons revealed that kinematics, and to a lesser extent also kinetics, were altered by the exoskeleton. These alterations contributed to an incorrect estimation of the metabolic cost of walking. A decrease was predicted, but not measured in experiments for these exoskeletons. I therefore conclude that design specifications of exoskeletons cannot be based solely on the kinetics and kinematics of normal walking.

Alternatively, a prediction of the human exoskeleton interaction can be made on forward simulations. In this dissertation, the muscle-reflex model of Geyer and

Herr (2010) is used to model the human dynamics and muscular control. The exoskeleton dynamics and control were based on the experimental results of Cain et al. (2007). The muscle reflex model can adapt to walking with an exoskeleton. However, the changes in gait kinematics and kinetics of this model, due to the external support, do not yet accurately represent the changes found in experimental data. Consequently, at this time, it cannot be used to predict human-exoskeleton interaction and aid the formulation of exoskeleton specifications.

Different models exist that predict human walking. These models have not been validated for other cases such as walking with an exoskeleton. The models can therefore not be used to predict exoskeletal walking. The current knowledge of human-exoskeleton interaction is mostly empirical and based on studies with previous exoskeletons.

### **9.1.2 Challenge 2: Improving exoskeleton hardware and control**

Generally, exoskeleton performance increases with additional power and decreases with increasing weight. This leads to conflicting requirements since more powerful actuators are generally more heavy than less powerful actuators. In this dissertation, two methods are described that can be used to design powerful, yet lightweight, exoskeletons.

Analogous to muscle-tendon mechanisms found in human and animal legs, passive mechanisms in exoskeletons can temporarily store energy and distribute energy across joints. The Achilles and XPED used springs to reduce, or eliminate, the power required from actuators. However, the performed experiments with these exoskeletons did not show a reduction in metabolic power.

The second method that is proposed to reduce exoskeleton weight, is to select mechanical components and dimensions by using numerical optimization. The interplay between the different exoskeleton components can be captured in an (electro-)mechanical model of which the model parameters can be optimized.

The exoskeleton control should adapt to the human movement which, can induce delays. Since the intended task is walking, the cyclic nature of this task can be used to improve the performance of the controller. Adaptive frequency oscillators and kernel-based non-linear filters can be used to improve force tracking and attenuate undesired effects of the exoskeleton passive dynamics.

### **9.1.3 Challenge 3: Fast and detailed evaluation of exoskeleton concepts**

In this dissertation, exoskeleton performance is primarily evaluated through the measurement of the metabolic cost of walking with and without the exoskeleton. As mentioned above, the relation between metabolic cost and other variables is not exactly known.

These relations can be investigated through experiments in which different conditions (e.g. walking speeds, support levels) are evaluated. In that process, it can thereby be beneficial to measure additional parameters, like gait kinematics and kinetics or muscle activation (EMG).

To evaluate multiple support conditions, versatile exoskeletons are required. The type and amount of support the exoskeleton provides should be well defined in order to generalize the results. On the Achilles exoskeleton, different support algorithms can be implemented with precise force control.

Measuring gait kinematics and kinetics is of special interest. Current measurement protocols are susceptible to noise and measurement errors. These problems increase when walking with an exoskeleton, since joint centers cannot exactly be determined and optical markers might not be visible due to obstruction by the exoskeleton. Current measurement protocols do not explicitly require consistent kinematics and kinetics. This dissertation describes a new method, the Multibody Kalman Filter (MKF), that adds this requirement. It is shown that this method makes more effective use of data redundancy. The MKF eliminates the need to identify joint centers by anatomical landmarks and reduces noise. Furthermore, the MKF allows for real-time data analysis.

## **9.2 Discussion**

### **9.2.1 Improve the knowledge of human–exoskeleton interaction**

It is difficult to predict human–exoskeleton interaction. Exoskeletons are believed to work based on the assumption that sharing a load of a task between the human and the exoskeleton reduces the metabolic cost of performing that task. This is a valid assumption for tasks with a pure dissipative load like cycling. Here, the metabolic cost and the load are coupled via the muscle efficiency (Coyle et al., 1992).

For walking this relation is less obvious. There is a continuous exchange of energies, and loads have been defined in different ways (power, torque, body

weight support). In this dissertation, it is shown that the following characterizations of the exoskeleton support are insufficient to make an estimate of the reduction in metabolic cost:

1. Support definitions based on the superposition principle. The superposition principle assumes that the joint angles and the total torque (human and exoskeleton) are invariant under the load (e.g. van den Bogert, 2003). This implies that the human performance with an exoskeleton can be calculated based on the exoskeleton torques subtracted from the total torques. Chapter 7 has experimentally shown that joint angles, and in a lesser extend total joint torques, can be dependent on the exoskeleton torque. A similar result was found by Kao et al. (2010a). Consequently, using the superposition principle leads to a false estimation of the exoskeleton performance. In case of the XPED exoskeleton, this was a large overestimation of the metabolic advantage given by the exoskeleton.
2. Support definitions based on interaction forces. The exoskeleton performance cannot be understood just from the interaction forces between the human and the exoskeleton. The design of the controller used in the Achilles exoskeleton was based on the results obtained with the exoskeleton of Malcolm et al. (2013a). Both exoskeletons had similar supportive torques. Still, the exoskeletons had different performance results (personal communication).

These findings show that there is no linear relationship between load and metabolic cost. Other experimental studies have confirmed this and have shown that small differences like triggering (Cain et al., 2007) and timing (Malcolm et al., 2013a) of the support have a large influence on the human performance.

This non-linearity is due to different aspects of the muscular dynamics. Bi-articular muscles can transfer power between joints, and tendons can temporary store energy. Farris et al. (2013) have shown that a reduction in joint power does not necessarily lead to a reduction in muscle power. Furthermore, the metabolic cost is dependent on the length and velocities of the muscle fibers (Umberger et al., 2003). As a result, models that describe the load on joint level are not sufficient to describe the relation between load and metabolic cost. In order to do this, models that incorporate the muscular dynamics must be used.

In the ideal case, the human–exoskeleton interaction is predicted through full-scale models of the exoskeleton and human, including the musculoskeletal system. Different studies have shown that human walking dynamics can be simulated (Geyer and Herr, 2010; van den Bogert et al., 2011). In Chapter 3, the muscle-reflex

model was used to simulate walking with an exoskeleton. The model did qualitatively predict some changes in metabolic and muscle activations. To improve this method its validity should be better studied. A main part of this validation would be to compare the model against multiple experimental conditions. Once the validity of the model is known, it might be necessary to refine the model on certain aspects.

Alternatively the human-exoskeleton interaction could be predicted through empirical relations. Efforts have been made to establish these relations. The effect of the added weight to the leg is described by Browning et al. (2007), and the effect of the support power is studied by Mooney et al. (2014a). Based on these relations, general design guidelines for exoskeletons can be formulated. The most important one is that the metabolic cost of walking decreases with the mechanical positive power output of an exoskeleton and increases with the weight of an exoskeleton. However, these relations do not capture the effect of fine differences between support functions, such as the earlier mentioned triggering of the support.

Exoskeleton studies would therefore greatly benefit from expanding this empirical knowledge. This has two additional requirements for exoskeleton design. First the exoskeleton should offer certain flexibility in the support it provides. Secondly, the exoskeleton dynamics should be well described in order to generalize the results.

## **9.2.2 Improving exoskeleton hardware and control**

In this dissertation, different exoskeletons were developed to test specific hypotheses about exoskeleton support. These exoskeletons were subject to the design requirements set in the previous section:

- High power-to-weight ratio
- Exact description of the dynamics
- Flexibility in the provided support

This led to several exoskeleton designs that are described in Chapter 6-8, as well as different design tools that can be generally used to design exoskeletons. The use of passive elements and numerical optimizations focus on increasing the power-to-weight ratio. Transparent control focuses on an exact description of the dynamics. The support strategy focuses on the flexibility of the support and an exact description of the dynamics.

### ***Passive elastic elements***

During walking, there is a continuous exchange of energies. At joint level, high positive and negative power peaks are observed. An exoskeleton that supports walking is likely to have to provide power peaks with the same order of magnitude. If these powers have to be directly provided with actuators, this would require very heavy actuators. However, the average power during walking is much lower than the peak power, and power peaks between joints are not synchronous. This opens the opportunity for buffering energy and redistributing energy across joints.

This can be achieved by passive components such as springs and linkage systems. The use of springs in exoskeleton design has been proposed and applied in different studies. These studies include springs in series with or parallel to a single joint actuator (Hitt et al., 2007; Wang et al., 2011), complete passive exoskeletons with springs in series with a single joint (Wiggin et al., 2011), and springs with a linkage system that spans multiple joints (Elliott et al., 2014; van den Bogert, 2003).

Passive mechanisms were implemented in the XPED and Achilles exoskeletons (Chapter 6-8). The passive mechanism in the XPED exoskeleton was based on the exotendon concept of van den Bogert (2003). In the Achilles exoskeleton, a series elastic actuator at the ankle was used, similar to the concept of Hitt et al. (2007). The configuration of the Achilles was analogous to the Achilles tendon and soleus muscle. Experiments showed that for a given type of support, passive elements can be used to reduce, or even eliminate, the required power from the actuators. This can reduce the weight of the actuators and consequently the exoskeleton. As discussed above, the support provided by these exoskeletons did not result in a reduction of the metabolic cost of walking.

A drawback of the use of passive mechanisms is that they must be tailored for a specific walking pattern. This compromises the flexibility of the provided support. In the XPED exoskeleton, the support was entirely determined by the passive mechanism. The support could only be altered by changing the presets for the lever arm lengths and slack length of the exotendon mechanism. Also for the actively controlled Achilles exoskeleton, the flexibility is compromised. The temporal energy storage works best for a specific walking pattern, and the elastic characteristics of the series elastic actuator determine the bandwidth of the controller (Vallery et al., 2008).

### ***Numerical optimization***

The weight and power of the exoskeleton are determined by the selection and dimensioning of its components. There is considerable interplay between the

exoskeleton components. In other words, choices made for one component directly influence the requirements for other components. This makes it difficult to make design specifications on a component level. The selection and dimensioning of the components should be balanced, such that there are no components that have excessive weight or components that hinder the effectiveness of others.

In this dissertation, a method is described that solves this problem with an optimization routine (Chapter 6-8). The routine assumes that the structure of the exoskeleton is known. Based on this structure, a parameterized (electro-) mechanical model of the exoskeleton is made. The model parameters, like component dimensions or spring stiffness, are optimized using numerical optimization techniques. Optimization criteria can for example be the exoskeleton weight or the maximal power output.

The method assumes known joint angle and torque trajectories. As mentioned earlier, these trajectories are dependent on support and typically not known beforehand (Chapter 7). However, it often suffices to make an estimate on an upper and lower bound of these trajectories. This data can, for example, be obtained from other exoskeleton studies (e.g. Kao et al., 2010a). By simulating with different angle and torque trajectories, it can be verified that the proposed design has enough flexibility in the provided support.

### ***Transparent control by exploiting the cyclic nature of walking***

As mentioned earlier, exoskeleton research benefits from an exact description of the exoskeleton dynamics. Part of this is that the effect of the exoskeleton support can be isolated from other unwanted effects. These unwanted effects include the effect of weight and inertia of the exoskeleton, tracking errors, and friction. These unwanted effects can be identified by studying the transparent mode of the exoskeleton where the support is turned off. Ideally this transparent mode is close to normal walking.

In Chapter 5 describes how the transparent mode can be improved. This method applies to actuated exoskeletons where a controller can be designed to attenuate unwanted effects. Because walking is cyclic, a controller can use information from previous steps to improve its performance in upcoming steps. This dissertation describes a general method that uses adaptive frequency oscillators and kernel-based non-linear filters. This method estimates a repetitive signal by fitting a number of primitive functions on any periodic input signal and can learn and predict this input signal. Furthermore the time derivatives of the predicted signal can be analytically obtained (Gams et al., 2009). This can be used to attenuate the

tracking error and to compensate for the exoskeleton dynamics. The latter requires a model of the exoskeleton dynamics.

The method can also be used improve controller performance on devices other than exoskeletons as long as there is some form of cyclic motion. The sensitivity of the controller to gait changes was not investigated yet. The controller could handle small deviations that occur during treadmill walking of healthy subjects. The performance is likely to drop if deviations become larger, as, for example, happens when walking on uneven terrains.

### ***Support strategy***

The support strategy largely determines the relative change in metabolic cost, that is; the difference between exoskeletal walking with support switched on and off. In this dissertation we have looked at two support strategies: the exotendons of the XPED exoskeletons and the virtual spring of the Achilles exoskeleton.

The XPED support was based on the exotendon concept of van den Bogert (2003). In this concept, different joints are coupled by elastic cables that could temporarily store energy and redistribute energy over the joints. The amount of energy stored in the exotendons is directly dependent on the joint angles. In the Achilles exoskeleton, the ankle push off is supported with a series elastic actuator. The amount of support is determined by deformation of a virtual spring. This deformation is the difference between the actual ankle joint angle and a reference joint angle.

Experiments showed that the support offered by the XPED and Achilles exoskeletons did not result in a relative reduction of the metabolic cost. This was against our hypotheses. In contrast, other exoskeletons studies did find a reduction in metabolic cost. The XPED and Achilles exoskeletons will be compared against those. However, a direct comparison is limited because other exoskeletons might have a significantly different working mechanism of which an exact description is typically missing in the literature. Nevertheless, some general trends can be observed, as will be discussed in the following paragraphs.

### ***Passive exoskeletons***

The XPED is a passive exoskeleton. This group of exoskeletons has been less successful in reducing metabolic cost than active exoskeletons. So far, only one exoskeleton has shown that a relative reduction in metabolic cost is possible (Wiggin et al., 2012). Passive exoskeletons can only redistribute energy. Providing positive power at one point is only possible if negative power is provided at another.

Studies with other exoskeletons suggest that support is most successful if only positive power is provided (Malcolm et al., 2013a; Mooney et al., 2014a).

### *Parametrization of the support*

This dissertation and others have shown that walking with an exoskeleton enforces a new equilibrium that results in different walking kinematics. It is shown that adding parallel assistance to the leg can disturb otherwise-efficient leg dynamics (Farris et al., 2013). The changed walking pattern should therefore be seen as an intrinsic consequence of exoskeleton support, rather than an unwanted side effect that should be avoided. The parameterization of the support should therefore allow for these changes in the walking pattern. For the XPED and Achilles exoskeletons, improvements could be made on this point.

The support of the XPED exoskeletons was highly sensitive to changes in the walking pattern. The force in the extendon, and thereby the support given by the exoskeleton was directly dependent on the joint angles. Changes in the joint angles affected both the timing and the amount of the support. Furthermore, the coupling with the hip motion unintentionally allowed the user to increase and decrease the support with the lean angle of the torso. As a result, the real support of the exoskeleton was very different from the expected support based on the simulation. Others triggered the support with a clutch, which made the support less dependent on the changes in the walking pattern (Wiggin et al., 2011). In the Achilles, the timing issue was addressed by triggering the support based on detected heel strike events.

The support of the XPED and the Achilles exoskeleton was based on the idea that the support was optimal if the joint kinematics during normal walking were maintained during exoskeleton walking. However, the observed changes in the walking pattern, mostly increased plantarflexion, resulted in a decreased support. Other studies suggest that this choice is too conservative. Exoskeletons of Sawicky and Ferris (2008), Malcolm et al. (2013a) and Mooney et al. (2014a) provided high levels of support even when gait changes are present.

The Achilles exoskeleton allows the implementation of different controllers. Still it is difficult to copy results of other exoskeletons since, as mentioned before, a detailed description of the exoskeleton dynamics is not given.

### **9.2.3 Fast evaluation of exoskeleton concepts**

Expanding the empirical knowledge of human–exoskeleton interaction requires many well-conducted experiments. This is only possible if the experiments can be

conducted within a short amount of time. This dissertation describes several techniques that allow for fast evaluation of exoskeleton concepts that will be discussed here.

### ***Exoskeleton platforms***

The development of new hardware is time consuming. In that perspective it would be beneficial to evaluate multiple exoskeleton concepts on one platform. Such a platform should have a certain amount of flexibility to allow the simulation of the mechanics and control of different exoskeleton concepts. Chapter 8 describes an ankle exoskeleton that allows the implementation of different controllers. Chapter 5 explores how existing rehabilitation robots can be used to evaluate new exoskeleton concepts. The chapter describes a controller that increases the transparency of the robot. Synchronous to this controller a controller can be used that simulates the dynamics of the new exoskeleton concept (Koopman and Van Dijk, 2011).

### ***Evaluation techniques***

Performing gait analysis can give insight into how the task is shared between the human and the exoskeleton. There are some key differences between a standard gait analysis setup and gait analysis with an exoskeleton. In standard gait analysis, the subject's healthy, or impaired, gait pattern is analyzed in order to give a good parameterized description of his or hers of gait. In exoskeleton research not only is a description of this gait required. The intention is to actively alter the gait to increase human performance. Based on the results of the gait analysis, the exoskeleton can be tuned.

Current methods for marker-based gait analysis have at least one of the following problems.

1. The gait analysis is not performed real time. If data was available in real time, it would be possible to tune the exoskeleton on the spot.
2. They require palpation of specific anatomical landmarks. These landmarks might be covered by the exoskeleton.
3. They are vulnerable to marker noise and marker occlusion.

The MKF presented in this dissertation addresses all these problems at the same time. The method was compared to a commonly used gait analysis protocol. Both protocols performed equally well in terms of data quality. However, the MKF is less dependent on the skills of the experimenter. It is not dependent on regression equations for joint centers, and could therefore be used to identify bone

abnormalities. With the MKF, the quality of the recorded gait data can be evaluated on the spot, and it can therefore be avoided that experiments have to be done twice. The use of the MKF has large potential, not only for exoskeleton research.

### 9.3 Future directions

In the past, exoskeleton research has mainly been an engineering challenge. For a large part of the exoskeleton research, the single goal was to reduce the metabolic cost of walking. The strict weight and power requirements led to innovative solutions. This is reflected in the large diversity of exoskeletons, which ultimately led to exoskeletons that actually reduced the metabolic cost of walking. Much of this pioneering work has been done and to improve exoskeletons performance their designs need to be further optimized.

This optimization is a difficult task since the influence of changes in the exoskeleton on the metabolic cost of walking is difficult to predict. Furthermore, exoskeletons are very diverse and often not thoroughly evaluated, or evaluated with different protocols. This makes it is difficult to compare exoskeleton results. The often-superficial evaluation of exoskeletons is arguably one of the main deficits in exoskeleton research. Many existing tools can be used to greatly improve our understanding of how exoskeletons exactly work.

#### 9.3.1 Simulation and modelling

To better understand human–exoskeleton interaction there is a large demand for modelling and simulation. The MKF framework is suitable for parameter estimation. In this dissertation, this framework has been used to estimate segment lengths and joint positions. In future work it might also be used to estimate other parameters (e.g. mass distributions) as well. In that case, the MKF might give additional insights in the human and exoskeleton dynamical systems.

Kinematic and kinetic analysis can be expanded with musculoskeletal simulations like computed muscular control (Thelen and Anderson, 2006). This might give additional insights in the changes that occur in the musculoskeletal system and how these changes might be related to changes in metabolic cost (Umberger et al., 2003).

The mentioned models have been used for normal walking. To further develop these models towards a design tool the focus should be on validating these models for altered walking patterns.

### 9.3.2 Design

The exoskeletons that are presented in this dissertation have a design based on classical mechanical engineering methods. Functions are assigned to parts, and the combination of the parts form a linkage mechanism. In Chapter 8 shows how such a mechanism can be optimized. One of the results is that the actuator takes only a small portion of the total weight of the exoskeleton. The majority of the weight is taken by the interface between the actuator and the human.

Alternative interface concepts can further reduce the weight of exoskeletons. For example, the human skeleton could provide a large part of the structural integrity of the exoskeleton. Such ideas have been explored by other researchers. Mooney et al. (2014a) presented an exoskeleton where there is no physical connection between the foot and shank part of the exoskeleton other than a string that transfers the load. Asbeck et al. (2014) present exoskeletons where a soft suit provides anchor points for actuators. All these exoskeletons are very lightweight at the distal part of the leg. Therefore, these weight reduction techniques are essential to further decrease the weight of exoskeletons.

### 9.3.3 Control

This dissertation has shown that the performance of passive exoskeletons can easily be overestimated. This is also partly reflected in the research of Mooney et al. (2014a), which suggests that performance solely increases with positive power. It seems that human performance can best be augmented with active exoskeletons. Passive exoskeletons are likely to be only beneficial in very specific applications (e.g. when supporting a specific subtask of walking (Bregman et al., 2012)).

How these exoskeletons can be controlled best is still open for debate. This dissertation and other research focused on the design of a controller for continuous walking. The general trend is to design a support function. This support function is synchronized with the walking pattern via the detection of discrete events, such as heel-strike. Other strategies exist, such as the EMG feedback algorithm (Sawicki and Ferris, 2008). Small differences in these support functions can have a large effect on the walking metabolism. Consequently, fine-tuning these algorithms can further improve exoskeleton performance. Also, complete new algorithms can be developed in the future. For example, Geyer and Herr (2010) have shown that many walking characteristics can be described with low-level controls. These control rules could form a basis for new, human inspired, exoskeleton controllers.

For real-life applications, an exoskeleton should also be able to handle movements other than continuous walking. This might be achieved by developing in a

universal controller that works for all movements. Another, more likely possibility is that the exoskeleton switches between different controllers based on an intention detection algorithm. For such applications, the adaptive frequency oscillators and non-linear filters of Chapter 5 can play an important role. The adaptive frequency oscillators and non-linear filters can detect deviations from a repetitive signal, and make the controller change to another state.

### **9.3.4 Comparing concepts and parameter sweeps**

The exoskeleton studies described in this dissertation evaluated only a limited number of conditions. To establish empirical relations between walking metabolism and other gait characteristics, more data points are needed. These additional data points can be obtained by performing parameter sweeps, as, for example, has been done to assess the effect of added mass to the leg (Browning et al., 2007). During such a parameter sweep, many conditions are evaluated that are only different by one parameter. Candidate parameters for parameter sweeps are parameters that could easily be generalized across different exoskeletons, or parameters that can directly be used as design input for future exoskeleton designs. A distinction can be made between walking parameters such as walking speed, slope, or step length and support parameters such as amount of energy that is added per step, or the dependency of the support torque on the joint angle (stiffness). The exoskeleton platforms of Chapters 5 and 8 are suitable to perform parameter sweeps to determine the influence of different support parameters.

### **9.3.5 Final thoughts**

The exoskeletons presented in this dissertation did, not yet, reduce the metabolic cost of walking. Other studies with different exoskeletons have shown that such a reduction is possible. These exoskeletons induced a reduction in metabolic cost of 8 percent for walking with a backpack (Mooney et al., 2014a) and a reduction of 6 percent for normal walking (Malcolm et al., 2013a). These are the first exoskeletons for which it was shown that a reduction in metabolic cost is possible and it is likely that this number will increase over time.

Despite these promising results, it is unlikely that the cost of transport, the metabolic cost of the human per travelled distance, of exoskeleton walking can compete with other forms of transportation in the near future. Cycling is for example 2.5 times more efficient than running at the same speed (Davies, 1980).

The use of exoskeletons is therefore likely to be limited to other specific applications where other modes of transportation do not suffice. This includes walking in indoor environments and on rough outdoor terrain. Another significant

application will be the support of specific subtasks of walking that have been affected by trauma or disease.

To achieve these goals, exoskeleton designs should be almost as excellent as the human body they interact with. The difference between a good and a bad exoskeleton can therefore be very subtle. With this dissertation I hope to have provided new tools and insights to identify these subtleties.

# 10 Appendix: MKF and Equations of motion

---

This chapter gives a more in-depth explanation of the workings of the Multibody Kalman Filter (MKF). This chapter is divided into three parts. The first part contains a detailed description of the equations of the MKF. The second part contains the equations of motion used by the MKF. The last part contains the anthropometric measurements that were used for initialization of the filter.

## 10.1 Nomenclature

### 10.1.1 Latin (lower case)

$\bar{a}$	accelerations in global coordinates (linear and angular)
$a_n$	linear acceleration of segment $n$ in global coordinates
$f()$	time update function
$f_{int}$	internal forces and moments
$f_{ext}$	external forces and moments
$g()$	measurement function
$m$	masses
$\bar{p}$	global (inertial) position (location and orientation)
$p_n$	location of segment $n$ in global coordinates
$q$	generalized coordinates
$q_{fix}$	positions (time invariant)
$q_{flo}$	positions (time variant)
$r$	measurement noise
$s$	state vector (MKF)

$\mathbf{u}$	generalized velocities
$\bar{\mathbf{v}}$	velocity in global coordinates (linear and angular)
$\mathbf{v}_n$	linear velocity of segment $n$ in global coordinates
$\mathbf{w}$	process noise
$\mathbf{x}_n$	location of segment $n$ relative to its parent in its own coordinate system
$\mathbf{z}$	measurement vector

**Latin (upper case)**

$A$	$df(\mathbf{x}, \mathbf{w})/d\mathbf{x}'$
$B$	projection of the state update function on the state
$C$	topology matrix
$D$	measurement noise covariance matrix
$G$	$dg(\mathbf{x}, \mathbf{r})/d\mathbf{x}'$
$I$	identity matrix
$J$	rotational inertia matrix in the segment reference frame
$K$	Kalman gain
$O$	zero vector or matrix
$P$	error covariance matrix
$Q$	process noise covariance matrix
$R_i^j$	rotation matrix from segment $i$ to $j$
$S$	acceleration matrix
$T$	velocity matrix
$W$	$df(\mathbf{x}, \mathbf{w})/d\mathbf{w}$

**Greek**

$\alpha_n$	angular acceleration of segment in global coordinates
$\theta_n$	angle of segment $n$ in global coordinates (quaternion)
$\varphi_n$	angle of segment $n$ relative to its parent in its parent coordinate system (quaternion)
$\psi_n$	angular velocity of segment $n$ relative to its parent segment in its own coordinate system
$\omega_n$	angular velocity of segment $n$ in global coordinates

### Operators

- $\dot{\phantom{x}}$  time derivative
- $\tilde{\phantom{x}}$  skew symmetric matrix of a  $3 \times 1$  vector
- $\square \times$  cross product, ( $AB \times C$  might be interpreted as  $\widetilde{ABC}$ )
- $\square \circ$  quaternion product

### Other

- $\square$  vector index
- $\square_{i,j}$  vector sub-index
- $\square_k$  time step  $k$
- $\tilde{\phantom{x}}$  *a priori* estimate of  $\mathbf{x}$  or  $\mathbf{P}$
- $\hat{\phantom{x}}$  *a posteriori* estimate of  $\mathbf{x}$  or  $\mathbf{P}$

## 10.2 The multibody Kalman filter

The MKF is a special application of the extended Kalman, and an extension of the filter developed by Todorov (2007). The MKF performs alternating time and measurement updates. The time update predicts ahead, resulting in an *a priori* estimate (denoted with  $\tilde{\phantom{x}}$ ) of the state and its error covariance matrix. The measurement update corrects the estimates when new measurements are available, resulting in an *a posteriori* estimate (denoted with  $\hat{\phantom{x}}$ ) of the state and its error covariance matrix (Figure 10).

## 10.3 The system state and state updates

The extended state ( $\mathbf{s}$ ) vector is defined by:

$$\mathbf{s} = \begin{Bmatrix} \mathbf{q}_{fix} \\ \mathbf{q}_{flo} \\ \mathbf{u} \\ \mathbf{f}_{int} \\ \mathbf{f}_{ext} \end{Bmatrix} \quad (58)$$

$\mathbf{q}_{fix}$  is a vector with time-invariant spatial variables. These are the model parameters such as segment lengths and local joint orientations of which the value is unknown. Estimation of these parameters is done by modelling them as time-invariant variables in the MKF so they can change until they converge.  $\mathbf{q}_{flo}$  is a vector with time-variant spatial variables (e.g. joint angles).  $\mathbf{u}$  and  $\mathbf{f}_{int}$  are vectors with generalized velocities and forces (e.g. joint velocities and moments).  $\mathbf{f}_{ext}$  is a

vector with external moments and forces acting at the center of mass of each segment in the multibody system (e.g. ground reaction forces).

### 10.3.1 Quasi-state

An extended Kalman filter linearizes the multibody system around the current state  $\mathbf{s}$  through the calculation of Jacobian matrices, which are described below. In our application, the 3D rotations are described with unit quaternions to avoid gimbal locks, which results in a non-minimal set of coordinates and extra constraint equations. To ensure that the filter respects these constraints, we defined a quasi-state ( $\mathbf{s}'$ ) which is minimal and can be used for small state updates, but does not make sense for large state updates.

$$\mathbf{s}' = \begin{Bmatrix} \mathbf{q}'_{fix} \\ \mathbf{q}'_{flo} \\ \mathbf{u} \\ \mathbf{f}_{int} \\ \mathbf{f}_{ext} \end{Bmatrix} \quad (59)$$

The quasi-state is used to perform small state updates leading to a new state ( $\mathbf{s}^+$ ). Matrix  $\mathbf{B}(\mathbf{s})$  is used to project the quasi state onto the real state:

$$\mathbf{s}^+ = \mathbf{s} + \mathbf{B}(\mathbf{s})\mathbf{s}' \quad (60)$$

$\mathbf{B}(\mathbf{x})$  depends on the application. In our application matrix  $\mathbf{B}(\mathbf{x})$  is defined as follows:

$$\mathbf{B}(\mathbf{s}) = \begin{bmatrix} \mathbf{B}_1(\mathbf{q}_1) & & & \mathbf{O} \\ & \ddots & & \\ & & \mathbf{B}_N(\mathbf{q}_N) & \\ \mathbf{O} & & & \mathbf{I} \end{bmatrix} \quad (61)$$

In the case  $\mathbf{q}_i$  describes a 3D rotation (quaternion)

$$\mathbf{B}_n(\mathbf{q}_n) = \frac{1}{2} \cdot \begin{bmatrix} -q_{n2} & -q_{n3} & -q_{n4} \\ q_{n1} & -q_{n4} & q_{n3} \\ q_{n4} & q_{n1} & -q_{n2} \\ -q_{n3} & q_{n2} & q_{n1} \end{bmatrix} \quad (62)$$

For other joint types:

$$\mathbf{B}_i(\mathbf{q}_i) = \mathbf{I} \quad (63)$$

Note that equation (62) is the same as the matrix mapping velocities (3-vector) to quaternions (Schwab and Meijaard, 2006). The different types of joints, the generalized coordinates, and the  $\mathbf{B}(\mathbf{x})$  matrix is described in full detail the section on the equations of motion.

### 10.3.2 Time update

The time update function ( $f(\mathbf{s}_{|k-1}, \mathbf{w})$ ) of the state  $\mathbf{s}_{|k-1}$  is given by:

$$\mathbf{s}_{|k} = \mathbf{s}_{|k-1} + \Delta t \bar{\mathbf{B}}(\mathbf{s}_{|k-1}) f(\mathbf{s}_{|k-1}, \mathbf{w}), \quad \mathbf{w} = \mathbf{N}(\mathbf{O}, \mathbf{Q}) \quad (64)$$

With:

$$f(\mathbf{s}_{|k-1}, \mathbf{w}) = \left\{ \begin{array}{c} \mathbf{O} \\ \mathbf{u}_{|k-1} \\ \bar{\mathbf{M}}(\mathbf{q}_{|k-1})^{-1} \bar{\mathbf{f}}(\mathbf{q}_{|k-1}, \mathbf{u}_{|k-1}, \mathbf{f}_{int|k-1}, \mathbf{f}_{ext|k-1}) \\ \mathbf{w}_{int|k} \\ \mathbf{w}_{ext|k} \end{array} \right\} \quad (65)$$

Where  $\Delta t$  is the time step,  $k$  and  $k-1$  are, respectively, the indices of the current and previous time frame.  $\mathbf{q}_{fix}$  is unchanged because it is time invariant.  $\mathbf{q}_{flo}$  is updated with the velocity.  $\mathbf{u}$  is updated with the acceleration. The acceleration is calculated with the equations of motion.  $\mathbf{f}_{int}$  and  $\mathbf{f}_{ext}$  are updated with the process noise  $\mathbf{w}$ .  $\mathbf{w}$  is assumed to have a normal distribution with zero mean and covariance  $\mathbf{Q}$ . The matrix  $\mathbf{B}$  accounts for the quaternion constraints. The *a priori* estimate of  $\tilde{\mathbf{s}}_{|k}$  is made using the *a posteriori* estimate  $\hat{\mathbf{s}}_{|k-1}$  while assuming zero process noise:

$$\hat{\mathbf{s}}_{|k} = \tilde{\mathbf{s}}_{|k-1} + \Delta t \mathbf{B}(\tilde{\mathbf{s}}_{|k-1}) f(\tilde{\mathbf{s}}_{|k-1}, \mathbf{O}) \quad (66)$$

Note that we have used the quasi state here to update the state. An *a priori* estimate of the error covariance matrix ( $\tilde{\mathbf{P}}_{|k}$ ) is made using the *a posteriori* state estimate  $\hat{\mathbf{s}}_{|k-1}$  and error covariance matrix  $\hat{\mathbf{P}}_{|k-1}$ :

$$\tilde{\mathbf{P}}_{|k} = \mathbf{A}(\hat{\mathbf{s}}_{|k-1}) \hat{\mathbf{P}}_{|k-1} \mathbf{A}(\hat{\mathbf{s}}_{|k-1})^T + \mathbf{W} \mathbf{Q} \mathbf{W}^T \quad (67)$$

With:

$$\mathbf{A}(\mathbf{s}) = \mathbf{I} + \Delta t \frac{d\mathbf{f}(\mathbf{s}, \mathbf{w})}{d\mathbf{s}} \mathbf{B} \quad \text{and} \quad \mathbf{W} = \frac{d\mathbf{f}(\mathbf{s}, \mathbf{w})}{d\mathbf{w}} \quad (68)$$

$\mathbf{A}$  is the identity matrix combined with Jacobian matrix  $\mathbf{A}$  containing the partial derivatives of  $\mathbf{f}(\mathbf{s}, \mathbf{w})$  to the quasi state ( $\mathbf{s}'$ ).  $\mathbf{W}$  is the Jacobian matrix with the partial derivatives of  $\mathbf{f}(\mathbf{s}, \mathbf{w})$  to the process noise ( $\mathbf{w}$ ).  $\mathbf{A}$  was derived by using the following property:

$$\begin{aligned} & \frac{d}{ds'}(\mathbf{f}(\mathbf{s} + \mathbf{B}(\mathbf{s})\mathbf{s}', \mathbf{w})) \\ &= \frac{d\mathbf{f}(\mathbf{s}, \mathbf{w})}{d\mathbf{s}} \cdot \frac{d}{ds'}(\mathbf{s} + \mathbf{B}(\mathbf{s})\mathbf{s}') \\ &= \frac{d\mathbf{f}(\mathbf{s}, \mathbf{w})}{d\mathbf{s}} \mathbf{B}(\mathbf{s}) \end{aligned} \quad (69)$$

### 10.3.3 Measurement update

The measurement function ( $\mathbf{g}(\mathbf{s}, \mathbf{r})$ ) provides a new measurement ( $\mathbf{z}$ ) at each time step. The measurement is a function of the state ( $\mathbf{s}$ ) and the measurement noise ( $\mathbf{r}$ ):

$$\mathbf{z} = \mathbf{g}(\mathbf{s}, \mathbf{r}), \quad \mathbf{r} = \mathbf{N}(\mathbf{O}, \mathbf{D}) \quad (70)$$

Where  $\mathbf{r}$  is assumed to be normally distributed with zero mean and covariance  $\mathbf{D}$ . The measurement Jacobian ( $\mathbf{G}$ ) contains the partial derivatives of  $\mathbf{g}(\mathbf{s}, \mathbf{r})$  to the quasi coordinates ( $\mathbf{s}'$ ):

$$\mathbf{G}(\mathbf{x}) = \frac{d\mathbf{g}(\mathbf{s}, \mathbf{r})}{ds'} \quad (71)$$

Which is the same as:

$$\mathbf{G}(\mathbf{s}) = \frac{d\mathbf{g}(\mathbf{s}, \mathbf{r})}{d\mathbf{s}} \mathbf{B}(\mathbf{s}) \quad (72)$$

It is not required that every time step all signals are measured, this accommodates for missing data. Therefore  $\mathbf{g}(\mathbf{s}, \mathbf{r})$  and  $\mathbf{R}$  may be different for different time steps.

The Kalman gain ( $\mathbf{K}$ ) is calculated as follows:

$$\mathbf{K}_{|k} = \tilde{\mathbf{P}}_{|k} \mathbf{G}_{|k}^T(\tilde{\mathbf{s}}_{|k}) \left( \mathbf{G}_{|k}(\tilde{\mathbf{s}}_{|k}) \tilde{\mathbf{P}}_{|k} \mathbf{G}_{|k}^T(\tilde{\mathbf{s}}_{|k}) + \mathbf{D}_{|k} \right)^{-1} \quad (73)$$

The Kalman gain is used to perform the measurement update resulting in the *a posteriori* estimate of the state and covariance matrix:

$$\hat{\mathbf{s}}_{|k} = \tilde{\mathbf{s}}_{|k} + \mathbf{BK}_{|k} (\mathbf{z}_{|k} - \mathbf{g}(\tilde{\mathbf{s}}_{|k}, \mathbf{O})) \quad (74)$$

$$\hat{\mathbf{P}}_{|k} = (\mathbf{I} - \mathbf{K}_{|k} \mathbf{G}_{|k}(\tilde{\mathbf{s}}_{|k})) \tilde{\mathbf{P}}_{|k} \quad (75)$$

### 10.3.4 Measurements

The MKF can be used for different applications where kinematics and kinetics need to be estimated. We use the filter for gait analysis with an optical marker system and an instrumented treadmill. In our case, the measurement function  $\mathbf{g}(\mathbf{s}, \mathbf{r})$  provides the marker positions ( $\mathbf{g}_m(\mathbf{s}, \mathbf{r})$ ) and ground reaction forces ( $\mathbf{g}_{fp}(\mathbf{s}, \mathbf{r})$ ):

$$\mathbf{g}(\mathbf{s}, \mathbf{r}) = \begin{bmatrix} \mathbf{g}_m(\mathbf{s}, \mathbf{r}) \\ \mathbf{g}_{fp}(\mathbf{s}, \mathbf{r}) \end{bmatrix} \quad (76)$$

with the corresponding measurement Jacobian:

$$\mathbf{G}(\mathbf{s}) = \begin{bmatrix} \mathbf{G}_m(\mathbf{s}) \\ \mathbf{G}_{fp}(\mathbf{s}) \end{bmatrix} \quad (77)$$

The measurement Jacobian for the optical markers ( $\mathbf{G}_m$ ) can be directly derived from the topology matrix ( $\mathbf{C}_m$ ) and velocity matrix ( $\mathbf{T}_m$ ) used in the equations of motion, as will be explained later in the section on the equations of motion.

$$\mathbf{G}_m(\mathbf{x}) = \frac{d(\mathbf{g}_m(\mathbf{s}, \mathbf{r}))}{d\mathbf{s}'} = [\mathbf{C}_m \mathbf{T}_m(\mathbf{q}) \quad \mathbf{O}] \quad (78)$$

The external forces ( $\mathbf{f}_{ext}$ ) are defined around the centers of mass of the multibody system. The force plate measurements are (or can be easily be transformed to) the forces ( $\mathbf{f}^\circ$ ) and moments ( $\boldsymbol{\tau}^\circ$ ) around the origin of the global coordinate frame. This yields the following measurement function:

$$\mathbf{g}_{fp,i}(\mathbf{s}, \mathbf{r}) = \begin{Bmatrix} \mathbf{f}_i^\circ(\mathbf{r}) \\ \boldsymbol{\tau}_i^\circ(\mathbf{s}, \mathbf{r}) \end{Bmatrix} = \begin{bmatrix} \mathbf{I}_3 & \mathbf{O}_3 \\ \tilde{\mathbf{p}}_i(\mathbf{q}) & \mathbf{I}_3 \end{bmatrix} \mathbf{f}_{ext,i} + \mathbf{r} \quad (79)$$

$i$  denotes the number of the force plate.  $\mathbf{p}_i$  is the center of mass position of the segment where the external force is applied in global coordinates. The measurement Jacobian is:

$$G_{f_{\tilde{p},i}}(\mathbf{x}) = \frac{d}{d\mathbf{x}'} \left( \begin{bmatrix} \mathbf{I}_3 & \mathbf{O}_3 \\ \tilde{\mathbf{p}}_i(\mathbf{q}) & \mathbf{I}_3 \end{bmatrix} \mathbf{f}^{ext,i} \right) = \begin{bmatrix} \mathbf{O}_3 & \mathbf{I}_3 & \mathbf{O}_3 \\ -\tilde{\mathbf{f}}_{ext,i}(CT(\mathbf{q}))_i & \tilde{\mathbf{p}}_i(\mathbf{q}) & \mathbf{I}_3 \end{bmatrix} \quad (80)$$

## 10.4 3d multibody dynamics with a minimal set of generalized velocities

### 10.4.1 Introduction

The equations of motion will be derived for systems that have a tree structure (no loops) with hinge, ball, slide or translational joints. To avoid gimbal locks, 3d rotations are described with unit quaternions. Accounting for the quaternion constraints is done in a similar way as accounting for constraints in a non-holonomic system (Kane and Levinston, 1985).

### 10.4.2 Kinematics

The kinematics are described in a recursive way. Throughout this document it is assumed that the multibody system has a tree structure, the terminology of the multibody structure is given in Figure 49. We describe the kinematics of a body  $n$  that is a child of body  $m$ .

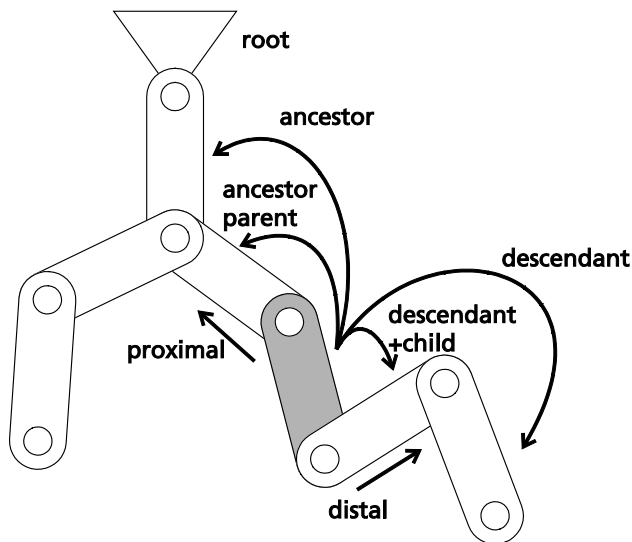


Figure 49: Terminology of a tree structure. The tree structure originates at the root. The tree can split but not reconnect so there are no loops in the structure. The direction towards the root is called proximal; the direction away from the root is called distal. The parent segment is the first segment proximal of a segment. A child segment is the first segment distal of a segment (a segment can have multiple children). Ancestors are all segments proximal of a segment, descendant are all segments distal from a segment.

### The position

The position of a segment ( $\bar{\mathbf{p}}_n$ ) is consist of its location ( $\mathbf{p}_n$ ), a  $3 \times 1$  vector, and its orientation ( $\boldsymbol{\theta}_n$ ), a unit quaternion. The position of segment ( $n$ ) is a function of the position of its parent ( $m$ ) and its position relative to its parent.

$$\bar{\mathbf{p}}_n = \begin{bmatrix} \mathbf{p}_n \\ \boldsymbol{\theta}_n \end{bmatrix} = \begin{bmatrix} \mathbf{p}_m + \mathbf{R}(\boldsymbol{\theta}_n)_1^n \mathbf{x}_n \\ \boldsymbol{\theta}_m \circ \boldsymbol{\varphi}_n \end{bmatrix} \quad (81)$$

$\mathbf{x}_n$  a  $3 \times 1$  vector describing the location of segment  $n$  relative to its parent in its own coordinate system.  $\boldsymbol{\varphi}_n$  is a unit quaternion describing the orientation of segment  $n$  relative to its parent in its parent's coordinate system.  $\mathbf{R}(\boldsymbol{\theta}_n)_1^n$  is the rotation matrix from the global frame to the segment frame.

### The velocity

The velocity of a segment ( $\bar{\mathbf{v}}_n$ ) consists of its linear ( $\mathbf{v}_n$ ) and angular velocity ( $\boldsymbol{\omega}_n$ ), both  $3 \times 1$  vectors. The velocity of segment ( $n$ ) is a function of the velocity of its parent ( $m$ ) and its location and velocity relative to its parent.

$$\begin{aligned} \bar{\mathbf{v}}_n &= \begin{bmatrix} \mathbf{v}_n \\ \boldsymbol{\omega}_n \end{bmatrix} = \begin{bmatrix} \mathbf{v}_m + \frac{d\mathbf{R}(\boldsymbol{\theta}_n)_1^n}{dt} \mathbf{x}_n + \mathbf{R}(\boldsymbol{\theta}_n)_1^n \dot{\mathbf{x}}_n \\ \boldsymbol{\omega}_m + \mathbf{R}(\boldsymbol{\theta}_n)_1^n \boldsymbol{\psi}_n \end{bmatrix} \\ &= \begin{bmatrix} \mathbf{v}_m + \boldsymbol{\omega}_n \times \mathbf{R}(\boldsymbol{\theta}_n)_1^n \mathbf{x}_n + \mathbf{R}(\boldsymbol{\theta}_n)_1^n \dot{\mathbf{x}}_n \\ \boldsymbol{\omega}_m + \mathbf{R}(\boldsymbol{\theta}_n)_1^n \boldsymbol{\psi}_n \end{bmatrix} \end{aligned} \quad (82)$$

In above equation we used the property that:

$$\frac{d\mathbf{R}(\boldsymbol{\theta}_n)_1^n}{dt} = \boldsymbol{\omega}_n \times \mathbf{R}(\boldsymbol{\theta}_n)_1^n \quad (83)$$

$\dot{\mathbf{x}}_n$  and  $\boldsymbol{\psi}_n$  are linear and angular velocity, both  $3 \times 1$  vectors, relative to their parent in the coordinate system of the segment.

### The acceleration

The velocity of a segment ( $\bar{\mathbf{a}}_n$ ) consists of its linear ( $\mathbf{a}_n$ ) and angular velocity ( $\boldsymbol{\alpha}_n$ ), both  $3 \times 1$  vectors. The acceleration is obtained by differentiation of formula(82).

$$\bar{\mathbf{a}}_n = \begin{bmatrix} \mathbf{a}_n \\ \boldsymbol{\alpha}_n \end{bmatrix} = \begin{bmatrix} \mathbf{a}_m + \dot{\boldsymbol{\omega}}_n \times \mathbf{R}(\boldsymbol{\theta}_n)_1^n \mathbf{x}_n + \boldsymbol{\omega}_n \times \boldsymbol{\omega}_n \times \mathbf{R}(\boldsymbol{\theta}_n)_1^n \mathbf{x}_n \dots \\ + 2\boldsymbol{\omega}_n \mathbf{R}(\boldsymbol{\theta}_n)_1^n \dot{\mathbf{x}}_n + \mathbf{R}(\boldsymbol{\theta}_n)_1^n \ddot{\mathbf{x}}_n \\ \boldsymbol{\alpha}_m + \mathbf{R}(\boldsymbol{\theta}_n)_1^n \dot{\boldsymbol{\psi}}_n + \boldsymbol{\omega}_n \times \mathbf{R}(\boldsymbol{\theta}_n)_1^n \boldsymbol{\psi}_n \end{bmatrix} \quad (84)$$

### 10.4.3 Generalized coordinates

We use a set of generalized coordinates ( $\mathbf{q}$ ) for the positions and a set of generalized speeds for the velocities ( $\mathbf{u}$ ). For our derivation of the equations of motion the set of generalized speeds is required to be minimal, the set of generalized positions is not necessarily minimal. Segment positions are a function of the generalized coordinates:

$$\mathbf{x}(\mathbf{q})_n \text{ and } \boldsymbol{\theta}(\mathbf{q})_n \quad (85)$$

The velocities can be functions of  $\mathbf{q}$  and  $\mathbf{u}$ , but to prevent the complexity to get out of hand we assume linear relations for the velocities.

$$\dot{\mathbf{x}}(\mathbf{u}) = \mathbf{X}_n \mathbf{u} \quad \boldsymbol{\psi}(\mathbf{u}) = \boldsymbol{\Psi}_n \mathbf{u} \quad (86)$$

Which is sufficient for many applications, but the proposed method can be extended to allow for non-linear relationships. Definitions for hinge, ball, slide or translational joints are given below. The generalized coordinates and speeds are linked via the following equation:

$$\dot{\mathbf{q}} = \mathbf{B}(\mathbf{q}) \cdot \mathbf{u} \quad (87)$$

#### Velocity

The equation for the velocity (82) can be written as a function of the generalized coordinates:

$$\bar{\mathbf{v}}_n = \begin{bmatrix} \mathbf{v}(\mathbf{q}, \mathbf{u})_m \\ \boldsymbol{\omega}(\mathbf{q}, \mathbf{u})_m \end{bmatrix} + \begin{bmatrix} \boldsymbol{\omega}(\mathbf{q}, \mathbf{u})_n \times \mathbf{R}(\mathbf{q})_1^n \mathbf{x}(\mathbf{q})_n + \mathbf{R}(\mathbf{q})_1^n \dot{\mathbf{x}}(\mathbf{q}, \mathbf{u})_n \\ \mathbf{R}(\mathbf{q})_1^n \boldsymbol{\psi}(\mathbf{q}, \mathbf{u})_n \end{bmatrix} \quad (88)$$

Substituting equations (85) and (86) we can see that the second term is a linear function of  $\mathbf{u}$ .

$$\begin{aligned} \bar{\mathbf{v}}_n &= \begin{bmatrix} \mathbf{v}(\mathbf{q}, \mathbf{u})_m \\ \boldsymbol{\omega}(\mathbf{q}, \mathbf{u})_m \end{bmatrix} + \begin{bmatrix} \boldsymbol{\omega}(\mathbf{q}, \mathbf{u})_n \times \mathbf{R}(\mathbf{q})_1^n \mathbf{x}(\mathbf{q})_n + \mathbf{R}(\mathbf{q})_1^n \mathbf{X}_n \mathbf{u} \\ \mathbf{R}(\mathbf{q})_1^n \boldsymbol{\Psi}_n \mathbf{u} \end{bmatrix} \\ &= \begin{bmatrix} \mathbf{v}(\mathbf{q}, \mathbf{u})_m \\ \boldsymbol{\omega}(\mathbf{q}, \mathbf{u})_m \end{bmatrix} + \mathbf{T}_n(\mathbf{q}) \mathbf{u} \end{aligned} \quad (89)$$

with:

$$\mathbf{T}_n(\mathbf{q}) = \begin{bmatrix} \sum_{i=1}^n (\mathbf{R}(\mathbf{q})_i^i \boldsymbol{\Psi}_i) \times \mathbf{R}(\mathbf{q})_1^n \mathbf{x}(\mathbf{q})_n + \mathbf{R}(\mathbf{q})_1^n \mathbf{X}_n \\ \mathbf{R}(\mathbf{q})_1^n \boldsymbol{\Psi}_n \end{bmatrix} \quad (90)$$

### Acceleration

The acceleration as a function of the generalized coordinates becomes:

$$\bar{\mathbf{a}}_n = \begin{bmatrix} \mathbf{a}(\mathbf{q}, \mathbf{u}, \dot{\mathbf{u}})_m \\ \boldsymbol{\alpha}(\mathbf{q}, \mathbf{u}, \dot{\mathbf{u}})_m \end{bmatrix} + \begin{bmatrix} \dot{\boldsymbol{\omega}}(\mathbf{q}, \mathbf{u}, \dot{\mathbf{u}})_n \times \mathbf{R}(\mathbf{q})_1^n \mathbf{x}(\mathbf{q})_n \dots \\ + \boldsymbol{\omega}(\mathbf{q}, \mathbf{u})_n \times \boldsymbol{\omega}(\mathbf{q}, \mathbf{u})_n \times \mathbf{R}(\mathbf{q})_1^n \mathbf{x}(\mathbf{q})_n \dots \\ + 2\boldsymbol{\omega}_n \times \mathbf{R}(\mathbf{q})_1^n \dot{\mathbf{x}}(\mathbf{q}, \mathbf{u})_n + \mathbf{R}(\mathbf{q})_1^n \ddot{\mathbf{x}}(\mathbf{q}, \mathbf{u}, \dot{\mathbf{u}})_n \\ \mathbf{R}_1^n(\mathbf{q})\boldsymbol{\psi}(\mathbf{q}, \mathbf{u}, \dot{\mathbf{u}})_n + \boldsymbol{\omega}(\mathbf{q}, \mathbf{u})_n \times \mathbf{R}(\mathbf{q})_1^n \boldsymbol{\psi}(\mathbf{u})_n \end{bmatrix} \quad (91)$$

If we again substitute equations (85) and (86):

$$\begin{aligned} \bar{\mathbf{a}}_n &= \begin{bmatrix} \boldsymbol{\omega}(\mathbf{q}, \dot{\mathbf{u}})_n \times \mathbf{R}(\mathbf{q})_1^n \mathbf{x}(\mathbf{q})_n \dots \\ + \sum_{i=1}^n \boldsymbol{\omega}(\mathbf{q}, \mathbf{u})_i \times \mathbf{R}(\mathbf{q})_1^i \boldsymbol{\Psi}_n \mathbf{u} \times \mathbf{R}(\mathbf{q})_1^n \mathbf{x}(\mathbf{q})_n \dots \\ + \boldsymbol{\omega}(\mathbf{q}, \mathbf{u})_n \times \boldsymbol{\omega}(\mathbf{q}, \mathbf{u})_n \times \mathbf{R}(\mathbf{q})_1^n \mathbf{x}(\mathbf{q})_n \dots \\ + 2\boldsymbol{\omega}_n \times \mathbf{R}(\mathbf{q})_1^n \mathbf{X}_n \mathbf{u} + \mathbf{R}(\mathbf{q})_1^n \mathbf{X}_n \dot{\mathbf{u}} \\ \mathbf{R}_1^n(\mathbf{q})\boldsymbol{\Psi}_n \dot{\mathbf{u}}_n + \boldsymbol{\omega}(\mathbf{q}, \mathbf{u})_n \times \mathbf{R}(\mathbf{q})_1^n \boldsymbol{\Psi}_n \mathbf{u} \end{bmatrix} \\ &= \begin{bmatrix} \mathbf{a}(\mathbf{q}, \mathbf{u}, \dot{\mathbf{u}})_m \\ \boldsymbol{\alpha}(\mathbf{q}, \mathbf{u}, \dot{\mathbf{u}})_m \end{bmatrix} + T_n(\mathbf{q})\dot{\mathbf{u}} + \begin{bmatrix} \sum_{i=1}^n \boldsymbol{\omega}(\mathbf{q}, \mathbf{u})_i \times \mathbf{R}(\mathbf{q})_1^i \boldsymbol{\Psi}_n \mathbf{u} \times \mathbf{R}(\mathbf{q})_1^n \mathbf{x}(\mathbf{q})_n \dots \\ + \boldsymbol{\omega}(\mathbf{q}, \mathbf{u})_n \times \boldsymbol{\omega}(\mathbf{q}, \mathbf{u})_n \times \mathbf{R}(\mathbf{q})_1^n \mathbf{x}(\mathbf{q})_n \dots \\ + 2\boldsymbol{\omega}_n \times \mathbf{R}(\mathbf{q})_1^n \mathbf{X}_n \mathbf{u} \\ \boldsymbol{\omega}(\mathbf{q}, \mathbf{u})_n \times \mathbf{R}(\mathbf{q})_1^n \boldsymbol{\Psi}_n \mathbf{u} \end{bmatrix} \\ &= \begin{bmatrix} \mathbf{a}(\mathbf{q}, \mathbf{u}, \dot{\mathbf{u}})_m \\ \boldsymbol{\alpha}(\mathbf{q}, \mathbf{u}, \dot{\mathbf{u}})_m \end{bmatrix} + T_n(\mathbf{q})\dot{\mathbf{u}} + S_n(\mathbf{q}, \mathbf{u}) \end{aligned} \quad (92)$$

Here we have used the property that:

$$\begin{aligned} \dot{\boldsymbol{\omega}}(\mathbf{q}, \mathbf{u}, \dot{\mathbf{u}})_n &= \sum_{i=1}^n \frac{d}{dt} (\mathbf{R}(\mathbf{q})_1^i \boldsymbol{\Psi}_i \mathbf{u}) = \sum_{i=1}^n (\mathbf{R}(\mathbf{q})_1^i \boldsymbol{\Psi}_i \dot{\mathbf{u}} + \dot{\mathbf{R}}(\mathbf{q})_1^i \boldsymbol{\Psi}_i \mathbf{u}) \\ &= \boldsymbol{\omega}(\mathbf{q}, \dot{\mathbf{u}})_n + \sum_{i=1}^n \boldsymbol{\omega}(\mathbf{q}, \mathbf{u})_i \times \mathbf{R}(\mathbf{q})_1^i \boldsymbol{\Psi}_i \mathbf{u} \end{aligned} \quad (93)$$

Please note the special use of the angular velocity function. In  $\boldsymbol{\omega}(\mathbf{q}, \dot{\mathbf{u}})$  we have substituted the generalized velocities ( $\mathbf{u}$ ) with the generalized accelerations ( $\dot{\mathbf{u}}$ ).

#### 10.4.4 Kinematics of the total system

To calculate the motions of all links we define a topology matrix  $\mathbf{C}$  :

$$\mathbf{C} = \begin{bmatrix} \mathbf{C}_{11} & \cdots & \mathbf{C}_{1N} \\ \vdots & \ddots & \vdots \\ \mathbf{C}_{N1} & \cdots & \mathbf{C}_{NN} \end{bmatrix} \quad (94)$$

Where  $N$  is the number of segments in the system,  $\mathbf{C}_{ij} = \mathbf{I}_6$  if  $i = j$  or segment  $i$  is a descendant of segment  $j$ , otherwise  $\mathbf{C}_{ij} = \mathbf{O}_6$ . So the velocities of the multibody system become:

$$\bar{\mathbf{v}} = \mathbf{CT}(\mathbf{q})\mathbf{u} \quad (95)$$

and the accelerations become:

$$\bar{\mathbf{a}} = \mathbf{CT}(\mathbf{q})\dot{\mathbf{u}} + \mathbf{CS}(\mathbf{q}, \mathbf{u}) \quad (96)$$

With:

$$\mathbf{T}(\mathbf{q}) = \begin{bmatrix} \mathbf{T}_1(\mathbf{q}) \\ \vdots \\ \mathbf{T}_m(\mathbf{q}) \end{bmatrix}, \mathbf{S} = \begin{bmatrix} \mathbf{S}_1(\mathbf{q}, \mathbf{u}) \\ \vdots \\ \mathbf{S}_m(\mathbf{q}, \mathbf{u}) \end{bmatrix} \quad (97)$$

#### 10.4.5 Equations of motion

The equations of motion are derived using the virtual power principle:

$$\delta \bar{\mathbf{v}}^T \left( \mathbf{f} - \frac{d}{dt}(\mathbf{M}\bar{\mathbf{v}}) \right) = 0 \quad (98)$$

$\delta \hat{\mathbf{v}}$  can be substituted using (95):

$$(\mathbf{CT}(\mathbf{q})\delta \mathbf{u})^T \left( \mathbf{f} - \frac{d}{dt}(\mathbf{M}\bar{\mathbf{v}}) \right) = 0 \quad (99)$$

Since the generalized speeds are independent of each other we can write:

$$(\mathbf{CT}(\mathbf{q}))^T \left( \mathbf{f} - \frac{d}{dt}(\mathbf{M}\bar{\mathbf{v}}) \right) = \mathbf{O} \quad (100)$$

The first term  $((\mathbf{CT}(\mathbf{q}))^T \mathbf{f})$  are the generalized active forces (Kane and Levinston, 1985). We subdivide this in internal forces ( $\mathbf{f}_{int}$ ) and external moments ( $\mathbf{f}_{ext}$ ). For our application we want to estimate  $\mathbf{f}_{int}$  and use them in their generalized form.

$$\mathbf{f}_{int} + (\mathbf{CT}(\mathbf{q}))^T \left( \mathbf{f}_{ext} - \frac{d}{dt}(\mathbf{M}\bar{\mathbf{v}}) \right) = \mathbf{O} \quad (101)$$

After rewriting and substitution the equations of motion become:

$$\begin{aligned} \mathbf{f}_{int} + (\mathbf{CT}(\mathbf{q}))^T (\mathbf{f}_{ext} - \dot{\mathbf{M}}\mathbf{v} - \mathbf{M}\mathbf{a}) &= \mathbf{O} \\ \mathbf{f}_{int} + (\mathbf{CT}(\mathbf{q}))^T (\mathbf{f}_{ext} - \dot{\mathbf{M}}(\mathbf{q}, \mathbf{u})\mathbf{CT}(\mathbf{q})\mathbf{u} - \mathbf{M}(\mathbf{q})(\mathbf{CT}(\mathbf{q})\dot{\mathbf{u}} - \mathbf{CS}(\mathbf{q}, \mathbf{u}))) &= \mathbf{O} \end{aligned} \quad (102)$$

Where:

$$\begin{aligned} \mathbf{M}(\mathbf{q}) &= \begin{bmatrix} \mathbf{M}_1 & \dots & \mathbf{O} \\ \vdots & \ddots & \vdots \\ \mathbf{O} & \dots & \mathbf{M}_N \end{bmatrix} \text{ with } \mathbf{M}_n = \begin{bmatrix} m_n \mathbf{I}_3 & \mathbf{O} \\ \mathbf{O} & \mathbf{R}(\mathbf{q})_i^n \mathbf{J} (\mathbf{R}(\mathbf{q})_i^n)^T \end{bmatrix} \\ \dot{\mathbf{M}}(\mathbf{q}, \mathbf{u}) &= \begin{bmatrix} \boldsymbol{\Omega}(\mathbf{q}, \mathbf{u})_1 & \dots & \mathbf{O} \\ \vdots & \ddots & \vdots \\ \mathbf{O} & \dots & \boldsymbol{\Omega}(\mathbf{q}, \mathbf{u})_N \end{bmatrix} \mathbf{M} \text{ with } \boldsymbol{\Omega}(\mathbf{q}, \mathbf{u})_n = \begin{bmatrix} \mathbf{O} & \mathbf{O} \\ \mathbf{O} & \tilde{\boldsymbol{\omega}}(\mathbf{q}, \mathbf{u}) \end{bmatrix} \end{aligned} \quad (104)$$

## 10.5 Forward dynamics

To solve the forward dynamics problem the following set of ordinary differential equations can be integrated

$$\begin{Bmatrix} \dot{\mathbf{q}} \\ \dot{\mathbf{u}} \end{Bmatrix} = \mathbf{B}(\mathbf{q}) \begin{Bmatrix} \mathbf{u} \\ \bar{\mathbf{M}}(\mathbf{q})^{-1} \bar{\mathbf{f}}(\mathbf{q}, \mathbf{u}, \mathbf{f}_{int}, \mathbf{f}_{ext}) \end{Bmatrix} \quad (105)$$

With:

$$\begin{aligned} \bar{\mathbf{M}}(\mathbf{q}) &= (\mathbf{CT}(\mathbf{q}))^T \mathbf{M}(\mathbf{q}) \mathbf{CT}(\mathbf{q}) \\ \bar{\mathbf{f}}(\mathbf{q}, \mathbf{u}, \mathbf{f}_{int}, \mathbf{f}_{ext}) &= \mathbf{f}_{int} + (\mathbf{CT}(\mathbf{q}))^T (\mathbf{f}_{ext} - \dot{\mathbf{M}}(\mathbf{q}, \mathbf{u})\mathbf{CT}(\mathbf{q})\mathbf{u} - \mathbf{M}(\mathbf{q})\mathbf{CS}(\mathbf{q}, \mathbf{u})) \end{aligned} \quad (106)$$

And

$$\mathbf{B}(\mathbf{q}) = \begin{bmatrix} \mathbf{B}_1(\mathbf{q}_1) & & & \mathbf{O} \\ & \ddots & & \\ & & \mathbf{B}_N(\mathbf{q}_N) & \\ \mathbf{O} & & & \mathbf{I} \end{bmatrix} \quad (107)$$

## 10.6 Joints

For our application we implemented four types of joints: translational, sliding, rotational and hinge joints.

### 10.6.1 Translational joint

A 3d translation

$$\mathbf{x}_n(\mathbf{q}_n) = [q_{n1} \quad q_{n2} \quad q_{n3}]^T \text{ and } \boldsymbol{\varphi}_n = [1 \quad 0 \quad 0 \quad 0]^T \quad (108)$$

$$\mathbf{X} = \mathbf{I}_3 \text{ and } \boldsymbol{\Psi}_n = \mathbf{O}_3 \quad (109)$$

and

$$\mathbf{B}_n = \mathbf{I}_3 \quad (110)$$

### Sliding joint

A sliding joint along axis  $l$

$$\mathbf{x}_n(q_n) = lq_n \text{ and } \boldsymbol{\varphi}_n = [1 \quad 0 \quad 0 \quad 0]^T \quad (111)$$

$$\mathbf{X} = l \text{ and } \boldsymbol{\Psi}_n = [0 \quad 0 \quad 0]^T \quad (112)$$

and

$$\mathbf{B}_n = 1 \quad (113)$$

### 10.6.2 Ball joint

A 3d rotation. Note that for this type of joint the number of generalized position coordinates is higher than the number of generalized velocity coordinates (Schwab and Meijaard, 2006).

$$\mathbf{x}_n = [0 \quad 0 \quad 0]^T \text{ and } \boldsymbol{\varphi}_n(\mathbf{q}_n) = [q_{n1} \quad q_{n2} \quad q_{n3} \quad q_{n4}]^T \quad (114)$$

$$\mathbf{X}_n = \mathbf{O}_3 \text{ and } \boldsymbol{\Psi}_n = \mathbf{I}_3. \quad (115)$$

and

$$\mathbf{B}_n(\mathbf{q}_n) = \frac{1}{2} \cdot \begin{bmatrix} -q_{n2} & -q_{n3} & -q_{n4} \\ q_{n1} & -q_{n4} & q_{n3} \\ q_{n4} & q_{n1} & -q_{n2} \\ -q_{n3} & q_{n2} & q_{n1} \end{bmatrix} \quad (116)$$

### 10.6.3 Hinge joint

A hinge joint along axis  $l$  with unit length:

	Distance [ ]		Mass [ ]		LongitudinalSagittal r [ ]				Transversal r [ ]		Longitudinal r [ ]	
	F	M	F	M	F	M	F	M	F	M	F	M
Gender <sup>1</sup>												
Thigh <sup>1</sup>	0.212	0.243	0.148	0.142	0.361	0.410	0.369	0.329	0.364	0.329	0.162	0.149
Shank <sup>1</sup>	0.249	0.249	0.048	0.043	0.442	0.446	0.271	0.255	0.267	0.249	0.093	0.103
Foot <sup>1</sup>	0.132	0.148	0.013	0.014	0.401	0.442	0.299	0.257	0.279	0.245	0.139	0.124
Hip width <sup>2</sup>	0.191	0.191										
HAT <sup>1</sup>	0.495	0.486	0.537	0.553	0.551	0.563	0.514	0.532	0.510	0.525	0.428	0.450

Table 24: Anthropometric data used for the initial state of the filter and mass and inertia properties. F = female, M – male. Sources 1: Leva, 1996, 2: Winter, 1990. The measures are normalized to the subject's length and the subject's weight.

$$\mathbf{x}_n = [\mathbf{o} \quad \mathbf{o} \quad \mathbf{o}]^T \text{ and } \boldsymbol{\varphi}_n(q_n) = \begin{Bmatrix} \cos\left(\frac{q_n}{2}\right) \\ l_1 \sin\left(\frac{q_n}{2}\right) \\ l_2 \sin\left(\frac{q_n}{2}\right) \\ l_3 \sin\left(\frac{q_n}{2}\right) \end{Bmatrix} \quad (117)$$

$$\mathbf{X}_n = [\mathbf{o} \quad \mathbf{o} \quad \mathbf{o}]^T \text{ and } \boldsymbol{\Psi}_n(u_n) = \mathbf{l} \quad (118)$$

and

$$\mathbf{B}_n = \mathbf{1} \quad (119)$$

### 10.6.4 Implementation

We have implemented the derivation of equations (105) in a series of Matlab scripts. The  $\mathbf{B}(\mathbf{q})$ ,  $\mathbf{C}$ ,  $\mathbf{M}(\mathbf{q})$ ,  $\mathbf{T}(\mathbf{q})$  and  $\mathbf{S}(\mathbf{q}, \mathbf{u})$  matrices are derived symbolically. The inversion of  $\bar{\mathbf{M}}(\mathbf{q})$  is performed numerically.

## 10.7 Human anthropometrics

The performance of the MKF improves if the initial estimate of the state of the filter is closer to the real state. An initial estimate of the time invariant spatial variables can be made based on anthropometric data. Table 24 shows the anthropometric data that was used to make the initial estimate. Data from the same sources was also use to estimate the mass and inertia properties, these were not estimated by the MKF.



## References

---

- Argo Medical Technologies Ltd, 2010. ReWalk, internet: [www.argomedtec.com](http://www.argomedtec.com).
- Asbeck, A.T., De Rossi, S.M.M., Galiana, I., Ding, Y., Walsh, C.J., 2014. Stronger, Smarter, Softer. *IEEE Robot. Autom. Mag.*
- Asbeck, A.T., Dyer, R.J., Larusson, A.F., Walsh, C.J., 2013. Biologically-inspired soft exosuit. *IEEE Int. Conf. Rehabil. Robot.* 2013, 1–8.  
doi:10.1109/ICORR.2013.6650455
- Baker, R., 2006. Gait analysis methods in rehabilitation. *J. Neuroeng. Rehabil.* 3.  
doi:10.1186/1743-0003-3-4
- Banala, S.K., Agrawal, S.K., Fattah, A., Krishnamoorthy, V., Wei-Li, H., Scholz, J., Rudolph, K., 2006. Gravity-Balancing Leg Orthosis and Its Performance Evaluation. *Robot. IEEE Trans.* 22, 1228.
- Bayona, N.A., Bitensky, J., Salter, K., Teasell, R., 2005. The role of task-specific training in rehabilitation therapies. *Top. Stroke Rehabil.* 12, 58–65.  
doi:10.1310/BQM5-6YGB-MVJ5-WVCR
- Berkeley Bionics, 2010. eLEGS exoskeleton, internet: [berkeleybionics.com](http://berkeleybionics.com) [WWW Document].
- Biewener, A.A., 1998. Muscle-tendon stresses and elastic energy storage during locomotion in the horse. *Comp. Biochem. Physiol. B. Biochem. Mol. Biol.* 120, 73–87.
- Bregman, D.J.J., Harlaar, J., Meskers, C.G.M., de Groot, V., 2012. Spring-like Ankle Foot Orthoses reduce the energy cost of walking by taking over ankle work. *Gait Posture* 35, 148–53. doi:10.1016/j.gaitpost.2011.08.026

- Browning, R.C., Modica, J.R., Kram, R., Goswami, A., 2007. The effects of adding mass to the legs on the energetics and biomechanics of walking. *Med Sci Sport. Exerc.* 39, 515–25.
- Cai, L.L., Fong, A.J., Otoshi, C.K., Liang, Y.Q., Cham, J.G., Zhong, H., Roy, R.R., Edgerton, V.R., Burdick, J.W., 2005. Effects of consistency vs. variability in robotically controlled training of stepping in adult spinal mice, in: *Proceedings of the 2005 IEEE 9th International Conference on Rehabilitation Robotics*. pp. 575–579. doi:10.1109/ICORR.2005.1502028
- Cain, S.M., Gordon, K.E., Ferris, D.P., 2007. Locomotor adaptation to a powered ankle-foot orthosis depends on control method. *J. Neuroeng. Rehabil.* 4, 48. doi:10.1186/1743-0003-4-48
- Cappozzo, A., Catani, F., Croce, U. Della, Leardini, A., 1995. Position and orientation in space of bones during movement: anatomical frame definition and determination. *Clin. Biomech. (Bristol, Avon)* 10, 171–178.
- Cappozzo, A., Della Croce, U., Leardini, A., Chiari, L., 2005. Human movement analysis using stereophotogrammetry. Part 1: theoretical background. *Gait Posture* 21, 186–96. doi:10.1016/j.gaitpost.2004.01.010
- Caputo, J., Collins, S., 2014. A Universal Ankle–Foot Prosthesis Emulator for Human Locomotion Experiments. *J. Biomech. Eng.* 136, 1–10. doi:10.1115/1.4026225
- Centraal Bureau voor de Statistiek, 2014. Mobiliteit in Nederland; vervoerwijzen en motieven (data 2013).
- Cerveri, P., Pedotti, a., Ferrigno, G., 2003. Robust recovery of human motion from video using Kalman filters and virtual humans. *Hum. Mov. Sci.* 22, 377–404. doi:10.1016/S0167-9457(03)00004-6
- Chao, E.Y., Rim, K., 1973. Application of optimization principles in determining the applied moments in human leg joints during gait. *J. Biomech.* 6, 497–510.
- Collins, S.H., 2008. Dynamic walking principles applied to human gait. *Mech. Eng.* The University of Michigan.
- Coyle, E.F., Sidossis, L.S., Horowitz, J.F., Beltz, J.D., 1992. Cycling efficiency is related to the percentage of Type I muscle fibers. *Med. Sci. Sport. Exerc.* 24, 782–788. doi:10.1249/00005768-199207000-00008

- Cyberdyne, 2012. Robot Suit HAL [WWW Document]. URL <http://www.cyberdyne.jp/english/robotsuithal/index.html>
- Davies, C.T., 1980. Effect of air resistance on the metabolic cost and performance of cycling. *Eur. J. Appl. Physiol. Occup. Physiol.* 45, 245–254.
- Davis, R., Ounpuu, S., Tyburski, D., Gage, J., 1991. A gait analysis data collection and reduction technique. *Hum. Mov. Sci.* 10, 575–587.
- De Groote, F., De Laet, T., Jonkers, I., De Schutter, J., 2008. Kalman smoothing improves the estimation of joint kinematics and kinetics in marker-based human gait analysis. *J. Biomech.* 41, 3390–8. doi:10.1016/j.jbiomech.2008.09.035
- Dean, J.C., Kuo, A.D., 2009. Elastic coupling of limb joints enables faster bipedal walking. *J. R. Soc. Interface* 6, 561–73. doi:10.1098/rsif.2008.0415
- Della Croce, U., Leardini, A., Chiari, L., Cappozzo, A., 2005. Human movement analysis using stereophotogrammetry. Part 4: assessment of anatomical landmark misplacement and its effects on joint kinematics. *Gait Posture* 21, 226–37. doi:10.1016/j.gaitpost.2004.05.003
- Delp, S.L., Anderson, F.C., Arnold, A.S., Loan, P., Habib, A., John, C.T., Guendelman, E., Thelen, D.G., 2007. OpenSim: open-source software to create and analyze dynamic simulations of movement. *IEEE Trans. Biomed. Eng.* 54, 1940–50. doi:10.1109/TBME.2007.901024
- Donelan, J.M., Kram, R., Kuo, A.D., 2002. Mechanical work for step-to-step transitions is a major determinant of the metabolic cost of human walking. *J. Exp. Biol.* 205, 3717.
- Donelan, J.M., Li, Q., Naing, V., Hoffer, J. a, Weber, D.J., Kuo, a D., 2008. Biomechanical energy harvesting: generating electricity during walking with minimal user effort. *Science* 319, 807–10. doi:10.1126/science.1149860
- Duprey, S., Cheze, L., Dumas, R., 2010. Influence of joint constraints on lower limb kinematics estimation from skin markers using global optimization. *J. Biomech.* 43, 2858–62. doi:10.1016/j.jbiomech.2010.06.010
- Ekso Bionics, 2012. Ekso product overview.

- Elliott, G., Marecki, A., Herr, H., 2014. Design of a Clutch–Spring Knee Exoskeleton for Running. *J. Med. Device.* 8, 031002. doi:10.1115/1.4027841
- Emken, J.L., Benitez, R., Sideris, A., Bobrow, J.E., Reinkensmeyer, D.J., 2007. Motor adaptation as a greedy optimization of error and effort. *J. Neurophysiol.* 97, 3997–4006.
- Emken, J.L., Reinkensmeyer, D.J., 2005. Robot-enhanced motor learning: Accelerating internal model formation during locomotion by transient dynamic amplification. *IEEE Trans. Neural Syst. Rehabil. Eng.* 13, 33–39. doi:10.1109/TNSRE.2004.843173
- Farris, D.J., Robertson, B.D., Sawicki, G.S., 2013. Elastic ankle exoskeletons reduce soleus muscle force but not work in human hopping. *J. Appl. Physiol.* 115, 579–585. doi:10.1152/jappphysiol.00253.2013
- Ferrari, A., Benedetti, M.G., Pavan, E., Frigo, C., Bettinelli, D., Rabuffetti, M., Crenna, P., Leardini, A., 2008. Quantitative comparison of five current protocols in gait analysis. *Gait Posture* 28, 207–16. doi:10.1016/j.gaitpost.2007.11.009
- Ferris, D., Sawicki, G., Daley, M., 2007. A physiologist’s perspective on robotic exoskeletons for human locomotion. *Int. J. Humanoid Robot.* 4.
- Ferris, D.P., Gordona, K.E., Sawickia, G.S., 2005. An improved powered ankle–foot orthosis using proportional myoelectric control. *Gait Posture* 23, 425–428.
- Galle, S., Malcolm, P., Derave, W., De Clercq, D., 2013. Adaptation to walking with an exoskeleton that assists ankle extension. *Gait Posture* 38, 495–9. doi:10.1016/j.gaitpost.2013.01.029
- Galle, S., Malcolm, P., Derave, W., De Clercq, D., 2014. Enhancing performance during inclined loaded walking with a powered ankle-foot exoskeleton. *Eur. J. Appl. Physiol.* doi:10.1007/s00421-014-2955-1
- Gams, A., Ijspeert, A.J., Schaal, S., Lenarčič, J., 2009. On-line learning and modulation of periodic movements with nonlinear dynamical systems. *Auton. Robots* 27, 3–23.
- Garcia, M., Chatterjee, a, Ruina, a, Coleman, M., 1998. The simplest walking model: stability, complexity, and scaling. *J. Biomech. Eng.* 120, 281–8.

- Geyer, H., Herr, H., 2010. A muscle-reflex model that encodes principles of legged mechanics produces human walking dynamics and muscle activities. *Neural Syst. Rehabil. Eng. IEEE Trans.* 18, 263–273.
- Geyer, H., Seyfarth, A., Blickhan, R., 2006. Compliant leg behaviour explains basic dynamics of walking and running. *Proc. Biol. Sci.* 273, 2861–7. doi:10.1098/rspb.2006.3637
- Gordon, K.E., Ferris, D.P., 2007. Learning to walk with a robotic ankle exoskeleton. *J. Biomech.* 40, 2636–2644.
- Gordon, K.E., Sawicki, G.S., Ferris, D.P., 2006. Mechanical performance of artificial pneumatic muscles to power an ankle-foot orthosis. *J. Biomech.* 39, 1832–1841.
- Gorton, G.E., Hebert, D. a, Gannotti, M.E., 2009. Assessment of the kinematic variability among 12 motion analysis laboratories. *Gait Posture* 29, 398–402. doi:10.1016/j.gaitpost.2008.10.060
- Hansen, A.H., Childress, D.S., Miff, S.C., Gard, S. a, Mesplay, K.P., 2004. The human ankle during walking: implications for design of biomimetic ankle prostheses. *J. Biomech.* 37, 1467–74. doi:10.1016/j.jbiomech.2004.01.017
- Hermens, H.J., Freriks, B., Merletti, R., Stegeman, D., Blok, J., Rau, G., Hägg, G., 1999. SENIAM 8 European Recommendations for Surface Electromyography. Roessingh Research and Development, Enschede.
- Herr, H., 2009. Exoskeletons and orthoses: classification, design challenges and future directions. *J. Neuroeng. Rehabil.* 6, 21.
- Hidler, J., Nichols, D., Pelliccio, M., Brady, K., Campbell, D.D., Kahn, J.H., Hornby, T.G., 2009. Multicenter randomized clinical trial evaluating the effectiveness of the Lokomat in subacute stroke. *Neurorehabil. Neural Repair* 23, 5–13. doi:10.1177/1545968308326632
- Hitt, J., Oymagil, A., Sugar, T., 2007. Dynamically controlled ankle-foot orthosis (DCO) with regenerative kinetics: incrementally attaining user portability. *IEEE Int. Conf. Robot. Autom.* 10–14.
- Hollander, K.W., Sugar, T.G., Herring, D.E., 2005. Adjustable Robotic Tendon Using a “Jack Spring.” 9th Int. Conf. Rehabil. Robot. 2005. ICORR 2005. 113–118. doi:10.1109/ICORR.2005.1501064

- Houck, C.R., Joines, J.A., Kay, M.G., 1995. A Genetic Algorithm for Function Optimization: A Matlab Implementation. North Carolina State University, Raleigh, NC.
- Ishikawa, M., Komi, P. V, Grey, M.J., Lepola, V., Bruggemann, G.-P., 2005. Muscle-tendon interaction and elastic energy usage in human walking. *J. Appl. Physiol.* 99, 603–8. doi:10.1152/jappphysiol.00189.2005
- Jezernik, S., Schärer, R., Colombo, G., Morari, M., 2003. Adaptive robotic rehabilitation of locomotion: a clinical study in spinally injured individuals. *Spinal cord Off. J. Int. Med. Soc. Paraplegia* 41, 657–666. doi:10.1038/sj.sc.3101518
- Johanson, M., 2011. Canadian Man Walks Around the World in 11 Years. *Int. Bus. Times*.
- Kane, T.R., Levinston, D.A., 1985. Dynamics: Theory and applications. McGraw-Hill.
- Kao, P.-C., Lewis, C.L., Ferris, D.P., 2010a. Invariant ankle moment patterns when walking with and without a robotic ankle exoskeleton. *J. Biomech.* 43, 203–9. doi:10.1016/j.jbiomech.2009.09.030
- Kao, P.-C., Lewis, C.L., Ferris, D.P., 2010b. Short-term locomotor adaptation to a robotic ankle exoskeleton does not alter soleus Hoffmann reflex amplitude. *J. Neuroeng. Rehabil.* 7, 33. doi:10.1186/1743-0003-7-33
- Karssen, J.G.D., Wisse, M., 2008. Fall detection in walking robots by multi-way principal component analysis. *Robotica* 27, 249. doi:10.1017/S0263574708004645
- Kerestes, J., Sugar, T.G., 2014. Enhanced running using a jet pack, in: Proceedings of the ASME 2014 International Design Engineering Technical Conferences. ASME, Buffalo, NY, US, pp. 1–7.
- Kerestes, J., Sugar, T.G., Holgate, M., 2014. Adding and subtracting energy to body motion - phase oscillator, in: Proceedings of the 38th Mechanisms and Robotics Conference. Buffalo, NY, US, pp. 2–7.
- Koopman, B., van Asseldonk, E.H.F., van der Kooij, H., 2010. In vivo measurement of human knee and hip dynamics using MIMO system identification, in: EMBC. IEEE, Buenos Aires , pp. 3426–3429.

- Koopman, B., van Asseldonk, E.H.F., van der Kooij, H., 2013. Selective control of gait subtasks in robotic gait training: foot clearance support in stroke survivors with a powered exoskeleton. *J. Neuroeng. Rehabil.* 10, 3. doi:10.1186/1743-0003-10-3
- Koopman, B., Van Dijk, W., 2011. Rendering potential wearable robot designs with LOPES. *ICORR* 2011.
- Krut, S., Benoit, M., Dombre, E., Pierrot, F., 2010. MoonWalker, a Lower Limb Exoskeleton able to sustain Bodyweight using a passive Force Balancer, in: *IEEE International Conference on Robotics and Automation*. Anchorage, Alaska, USA.
- Kuo, A.D., 1998. A least-squares estimation approach to improving the precision of inverse dynamics computations. *J. Biomech. Eng.* 120, 148–59.
- Kuo, A.D., 2002. The relative roles of feedforward and feedback in the control of rhythmic movements. *Motor Control* 6, 129–145.
- Kwa, H.K., Noorden, J.H., Missel, M., Craig, T., Pratt, J.E., Neuhaus, P.D., 2009. Development of the IHMC mobility assist exoskeleton. *Institute of Electrical and Electronics Engineers Inc., The*, pp. 1349–1355.
- Kwakkel, G., Van Peppen, R., Wagenaar, R.C., Dauphinee, S.W., Richards, C., Ashburn, A., Miller, K., Lincoln, N., Partridge, C., Wellwood, I., Langhorne, P., 2004. Effects of augmented exercise therapy time after stroke: A meta-analysis, in: *Stroke*. pp. 2529–2536. doi:10.1161/01.STR.0000143153.76460.7d
- Kwakkel, G., Wagenaar, R.C., Koelman, T.W., Lankhorst, G.J., Koetsier, J.C., 1997. Effects of intensity of rehabilitation after stroke. A research synthesis. *Stroke*. 28, 1550–1556. doi:10.1161/01.STR.28.8.1550
- Leardini, A., Chiari, L., Della Croce, U., Cappozzo, A., 2005. Human movement analysis using stereophotogrammetry. Part 3. Soft tissue artifact assessment and compensation. *Gait Posture* 21, 212–25. doi:10.1016/j.gaitpost.2004.05.002
- Lenzi, T., Member, S., Carrozza, M.C., Agrawal, S.K., 2013. Powered Hip Exoskeletons Can Reduce the User ' s Hip and Ankle Muscle Activations During Walking 21, 938–948.
- Leva, P. De, 1996. Adjustments to Zatsiorsky-Seluyanov's segment inertia parameters. *J. Biomech.* 29, 1223–1230.

- Lewis, C.L., Ferris, D.P., 2011. Invariant hip moment pattern while walking with a robotic hip exoskeleton. *J. Biomech.* 44, 789–93. doi:10.1016/j.jbiomech.2011.01.030
- Lu, T.-W., O'Connor, J.J., 1999. Bone position estimation from skin marker coordinates using global optimisation with joint constraints. *J. Biomech.* 32, 129–134. doi:10.1016/S0021-9290(98)00158-4
- Malcolm, P., Derave, W., Galle, S., De Clercq, D., 2013a. A simple exoskeleton that assists plantarflexion can reduce the metabolic cost of human walking. *PLoS One* 8, e56137. doi:10.1371/journal.pone.0056137
- Malcolm, P., Galle, S., Derave, W., De Clercq, D., 2013b. Powered biarticular exoskeleton with gastrocnemius mimicking configuration produces higher reduction in metabolic cost than soleus mimicking configuration. *Int. Soc. Biomech. XXIVth Congr. Proc.*
- McNeill Alexander, R., 1991. Energy-saving mechanisms in walking and running. *J. exo. Biol.* 160, 55–69.
- Meuleman, J.H., van Asseldonk, E.H., van der Kooij, H., 2013. The effect of directional inertias added to pelvis and ankle on gait. *J. Neuroeng. Rehabil.* 10, 40. doi:10.1186/1743-0003-10-40
- Mooney, L.M., Rouse, E.J., Herr, H.M., 2014a. Autonomous exoskeleton reduces metabolic cost of human walking during load carriage. *J. Neuroeng. Rehabil.* 11, 80. doi:10.1186/1743-0003-11-80
- Mooney, L.M., Rouse, E.J., Herr, H.M., 2014b. Autonomous exoskeleton reduces metabolic cost of human walking. *J. Neuroeng. Rehabil.* 11. doi:10.1186/1743-0003-11-80
- Norris, J.A., Granata, K.P., Mitros, M.R., Byrne, E.M., Marsh, A.P., 2007. Effect of augmented plantarflexion power on preferred walking speed and economy in young and older adults. *Gait Posture* 25, 620.
- Pratt, G. a., Williamson, M.M., 1995. Series elastic actuators. *Proc. 1995 IEEE/RSJ Int. Conf. Intell. Robot. Syst. Hum. Robot Interact. Coop. Robot.* 1, 399–406. doi:10.1109/IROS.1995.525827
- Rauch, H.E., Striebel, C.T., Tung, F., 1965. Maximum likelihood estimates of linear dynamic systems. *AIAA J.* 3, 1445–1450.

- Reinbolt, J.A., Schutte, J.F., Fregly, B.J., Koh, B. II, Haftka, R.T., George, A.D., Mitchell, K.H., 2005. Determination of patient-specific multi-joint kinematic models through two-level optimization. *J. Biomech.* 38, 621–6. doi:10.1016/j.jbiomech.2004.03.031
- Remy, C.D., Thelen, D.G., 2009. Optimal estimation of dynamically consistent kinematics and kinetics for forward dynamic simulation of gait. *J. Biomech. Eng.* 131, 031005. doi:10.1115/1.3005148
- Riener, R., 2012. Technology of the Robotic Gait Orthosis Lokomat, in: Dietz, V., Nef, T., Rymer, W.Z. (Eds.), *Neurorehabilitation Technology*. Springer London, London, pp. 221–232. doi:10.1007/978-1-4471-2277-7
- Riener, R., Lünenburger, L., Jezernik, S., Anderschitz, M., Colombo, G., Dietz, V., 2005. Patient-cooperative strategies for robot-aided treadmill training: First experimental results. *IEEE Trans. Neural Syst. Rehabil. Eng.* 13, 380–394. doi:10.1109/TNSRE.2005.848628
- Rietman, J.S., Goudsmit, J., Meulemans, D., Halbertsma, J.P.K., Geertzen, J.H.B., 2004. *Prosthetics and Orthotics International*. Prosthet. Orthot. Int. doi:10.3109/03093640409167928
- Righetti, L., Buchli, J., Ijspeert, A.J., 2006. Dynamic Hebbian learning in adaptive frequency oscillators. *Phys. D Nonlinear Phenom.* 216, 269–281. doi:10.1016/j.physd.2006.02.009
- Riley, P.O., Paolini, G., Della Croce, U., Paylo, K.W., Kerrigan, D.C., 2007. A kinematic and kinetic comparison of overground and treadmill walking in healthy subjects. *Gait Posture* 26, 17–24. doi:10.1016/j.gaitpost.2006.07.003
- Ronsse, R., Lenzi, T., Vitiello, N., Koopman, B., Van Asseldonk, E., De Rossi, S.M.M., Van Den Kieboom, J., Van Der Kooij, H., Carrozza, M.C., Ijspeert, A.J., 2011. Oscillator-based assistance of cyclical movements: model-based and model-free approaches. *Med. Biol. Eng. Comput.* 1–13.
- Sawicki, G.S., 2009. Powered ankle exoskeletons reveal the metabolic cost of plantar flexor mechanical work during walking with longer steps at constant step frequency. *J. Exp. Biol.* 212, 21–31.
- Sawicki, G.S., Domingo, A., Ferris, D.P., 2006. The effects of powered ankle-foot orthoses on joint kinematics and muscle activation during walking in

- individuals with incomplete spinal cord injury. *J. Neuroeng. Rehabil.* 3, 3. doi:10.1186/1743-0003-3-3
- Sawicki, G.S., Ferris, D.P., 2008. Mechanics and energetics of level walking with powered ankle exoskeletons. *J. Exp. Biol.* 211, 1402–13. doi:10.1242/jeb.009241
- Schwab, A., Meijaard, J., 2006. How to draw Euler angles and utilize Euler parameters, in: *Proc. IDETC/CIE. Philadelphia, Pennsylvania, USA*, pp. 10–13.
- Schwartz, M.H., Rozumalski, A., 2005. A new method for estimating joint parameters from motion data. *J. Biomech.* 38, 107–16. doi:10.1016/j.jbiomech.2004.03.009
- Selinger, J.C., Connor, S.M.O., Wong, J.D., Donelan, J.M., Columbia, B., 2014. Humans continuously optimize energetic cost during walking, in: *Dynamic Walking. Zürich, Switzerland*.
- Song, S., Geyer, H., 2012. Regulating speed and generating large speed transitions in a neuromuscular human walking model. 2012 *IEEE Int. Conf. Robot. Autom.* 511–516. doi:10.1109/ICRA.2012.6225307
- Teasell, R., Bitensky, J., Salter, K., Bayona, N.A., 2005. The role of timing and intensity of rehabilitation therapies. *Top. Stroke Rehabil.* 12, 46–57. doi:10.1310/ETDP-6DR4-D617-VMVF
- Thelen, D.G., Anderson, F.C., 2006. Using computed muscle control to generate forward dynamic simulations of human walking from experimental data. *J. Biomech.* 39, 1107–15. doi:10.1016/j.jbiomech.2005.02.010
- Todorov, E., 2007. Probabilistic inference of multijoint movements, skeletal parameters and marker attachments from diverse motion capture data. *IEEE Trans. Biomed. Eng.* 54, 1927–39. doi:10.1109/TBME.2007.903521
- Umberger, B.R., Gerritsen, K.G.M., Martin, P.E., 2003. A model of human muscle energy expenditure. *Comput. Methods Biomech. Biomed. Engin.* 6, 99–111. doi:10.1080/1025584031000091678
- Umberger, B.R., Martin, P.E., 2007. Mechanical power and efficiency of level walking with different stride rates. *J. Exp. Biol.* 210, 3255–65. doi:10.1242/jeb.000950

- Vallery, H., Duschau-Wicke, A., Riener, R., 2009a. Generalized elasticities improve patient-cooperative control of rehabilitation robots. 2009 IEEE Int. Conf. Rehabil. Robot. 535–541. doi:10.1109/ICORR.2009.5209595
- Vallery, H., Ekkelenkamp, R., Van Der Kooij, H., Buss, M., 2007. Passive and accurate torque control of series elastic actuators, in: IEEE International Conference on Intelligent Robots and Systems. pp. 3534–3538. doi:10.1109/IROS.2007.4399172
- Vallery, H., van Asseldonk, E.H.F., Buss, M., van der Kooij, H., 2009b. Reference trajectory generation for rehabilitation robots: complementary limb motion estimation. IEEE Trans. Neural Syst. Rehabil. Eng. 17, 23–30. doi:10.1109/TNSRE.2008.2008278
- Vallery, H., Veneman, J., Ekkelenkamp, R., Buss, M., van der Kooij, H., 2008. Compliant actuation of rehabilitation robots. IEEE Robot. Autom. Mag. 60–69.
- Van Asseldonk, E.H.F., Veneman, J.F., Ekkelenkamp, R., Buurke, J.H., van der Helm, F.C.T., van der Kooij, H., 2008. The Effects on Kinematics and Muscle Activity of Walking in a Robotic Gait Trainer During Zero-Force Control. Neural Syst. Rehabil. Eng. IEEE Trans. 16, 360.
- Van den Bogert, A.J., 2003. Exotendons for assistance of human locomotion. Biomed. Eng. Online 2, 17. doi:10.1186/1475-925X-2-17
- Van den Bogert, A.J., Blana, D., Heinrich, D., 2011. Implicit methods for efficient musculoskeletal simulation and optimal control. Procedia IUTAM 2, 297–316. doi:10.1016/j.piutam.2011.04.027
- Van den Bogert, A.J., Su, A., 2008. A weighted least squares method for inverse dynamic analysis. Comput. Methods Biomech. Biomed. Engin. 11, 3–9. doi:10.1080/10255840701550865
- Van Dijk, W., 2010. Design of a passive exoskeleton (MSc. Thesis). University of Twente.
- Van Dijk, W., van der Kooij, H., 2013. Optimization of human walking for exoskeletal support. IEEE Int. Conf. Rehabil. Robot. 2013, 1–6. doi:10.1109/ICORR.2013.6650394

- Van Dijk, W., van der Kooij, H., n.d. XPED2: A Passive Exoskeleton with Artificial Tendons. *IEEE Robot. Autom. Mag.*
- Van Dijk, W., van der Kooij, H., Hekman, E., 2011. A passive exoskeleton with artificial tendons: Design and experimental evaluation, in: *Rehabilitation Robotics (ICORR)*, 2011 IEEE International Conference on. pp. 1–6.
- Veltink, P.H., Liedtke, C., Droog, E., van der Kooij, H., 2005. Ambulatory measurement of ground reaction forces. *IEEE Trans. Neural Syst. Rehabil. Eng.* 13, 423–7. doi:10.1109/TNSRE.2005.847359
- Veneman, J.F., Kruidhof, R., Hekman, E.E.G., Ekkelenkamp, R., Van Asseldonk, E.H.F., van der Kooij, H., 2007. Design and Evaluation of the LOPES Exoskeleton Robot for Interactive Gait Rehabilitation. *Neural Syst. Rehabil. Eng.* *IEEE Trans.* 15, 379.
- Voronov, A. V, 2004. The Roles of Monoarticular and Biarticular Muscles of the Lower Limbs in Terrestrial Locomotion. *Hum. Physiol.* 30, 476–484.
- Vukobratovic, M., 2007. When were active exoskeletons actually born? *Int. J. Humanoid Robot.* 4, 459–486.
- Walsh, C.J., Endo, K., Herr, H., 2007. a Quasi-Passive Leg Exoskeleton for Load-Carrying Augmentation. *Int. J. Humanoid Robot.* 04, 487–506. doi:10.1142/S0219843607001126
- Wang, J., Hamner, S., Delp, S., Koltun, V., 2012. Optimizing locomotion controllers using biologically-based actuators and objectives. *ACM Trans. Graph.*
- Wang, S., Meijneke, C., van der Kooij, H., 2013. Modeling, design, and optimization of Mindwalker series elastic joint. *IEEE Int. Conf. Rehabil. Robot.* 2013, 1–8. doi:10.1109/ICORR.2013.6650381
- Wang, S., van Dijk, W., van der Kooij, H., 2011. Spring uses in exoskeleton actuation design, in: *Rehabilitation Robotics (ICORR)*, 2011 IEEE International Conference on. pp. 1–6.
- Wang, S., Wang, L., Meijneke, C., van Asseldonk, E., Hoellinger, T., Cheron, G., Ivanenko, Y., La Scaleia, V., Sylos-Labini, F., Molinari, M., Tamburella, F., Pisotta, I., Thorsteinsson, F., Ilzkovitz, M., Gancent, J., Nevatia, Y., Hauffe, R., Zanow, F., van der Kooij, H., 2014. Design and Control of the MINDWALKER

- Exoskeleton. *IEEE Trans. Neural Syst. Rehabil. Eng.* 4320.  
doi:10.1109/TNSRE.2014.2365697
- Wang, Y., Gao, F., Doyle, F.J., 2009. Survey on iterative learning control, repetitive control, and run-to-run control. *J. Process Control.*  
doi:10.1016/j.jprocont.2009.09.006
- Wehner, M., Quinlivan, B., Aubin, P.M., Martinez-Villalpando, E., Baumann, M., Stirling, L., Holt, K., Wood, R., Walsh, C., 2013. A lightweight soft exosuit for gait assistance. 2013 *IEEE Int. Conf. Robot. Autom.* 3362–3369.  
doi:10.1109/ICRA.2013.6631046
- Wiggin, M.B., Collins, S.H., Sawicki, G.S., 2012. A Passive Elastic Ankle Exoskeleton Using Controlled Energy Storage and Release to Reduce the Metabolic Cost of Walking. *Dyn. Walk.* 2012.
- Wiggin, M.B., Sawicki, G.S., Collins, S.H., 2011. An exoskeleton using controlled energy storage and release to aid ankle propulsion, in: *Rehabilitation Robotics (ICORR)*, 2011 *IEEE International Conference on.* pp. 1–5.
- Winter, D.A., 1990. *Biomechanics and motor control of human movement*, 2nd ed. John Wiley and Sons, Waterloo, Ontario, Canada.
- Witte, K.A., Zhang, J., Jackson, R.W., Collins, S.H., 2015. Design of Two Lightweight , High-Bandwidth Torque-Controlled Ankle Exoskeletons, in: *IEEE International Conference on Robotics and Automation* (submitted).
- Wong, W.Y., Wong, M.S., Lo, K.H., 2007. Clinical applications of sensors for human posture and movement analysis: a review. *Prosthet. Orthot. Int.* 31, 62–75.  
doi:10.1080/03093640600983949
- Yagn, N., 1890. U.S. Patent No. 420179: Apparatus for Facilitating Walking, Running, and Jumping.
- Zajac, F.E., Neptune, R.R., Kautz, S.A., 2002. Biomechanics and muscle coordination of human walking. Part I: introduction to concepts, power transfer, dynamics and simulations. *Gait Posture* 16, 215–32.
- Zeilig, G., Weingarden, H., Zwecker, M., Dudkiewicz, I., Bloch, A., Esquenazi, A., 2012. Safety and tolerance of the ReWalk™ exoskeleton suit for ambulation by people with complete spinal cord injury: a pilot study. *J. Spinal Cord Med.* 35, 96–101. doi:10.1179/2045772312Y.0000000003

- Zeni Jr, J.A., Richards, J.G., Higginson, J.S., 2008. Two simple methods for determining gait events during treadmill and overground walking using kinematic data. *Gait Posture* 27, 710–714.
- Ziegler, M.D., Zhong, H., Roy, R.R., Edgerton, V.R., 2010. Why variability facilitates spinal learning. *J. Neurosci.* 30, 10720–10726. doi:10.1523/JNEUROSCI.1938-10.2010
- Zoss, A.B., Kazerooni, H., Chu, A., 2006. Biomechanical design of the Berkeley lower extremity exoskeleton (BLEEX). *Mechatronics, IEEE/ASME Trans.* 11, 128–138.

# List of figures

---

## ***Introduction***

Figure 1a: Detail of the print “Locomotion” by Robert Seymour (ca. 1830) - Open Access for Scholarly Content, The Metropolitan Museum of Art - Gift of Paul Bird Jr., 1962 ([www.metmuseum.org](http://www.metmuseum.org))

Figure 1b: A patent by Nicholas Yagn describing a “Apparatus for Facilitating Walking, Running, and Jumping” (1891) – reprint from US Patent No. 420179

Figure 1c: First active exoskeleton developed by the Mihailo Pupin Institute - Reprinted with permission from: When were active exoskeletons actually born?, Miomir K. Vukobratovic, International Journal of Humanoid Robotics, Vol 4 Issue No. 3, © 2007 World Scientific

Figure 1d: First exoskeleton that reduces the metabolic cost of walking - Permission for use granted by P. Malcolm

## ***Background***

Figure 4a: Exoskeleton by Malcolm et al. (2013a) - Permission for use granted by P. Malcolm

Figure 4b: Exoskeleton by Mooney et al. - Figure adapted from Mooney et al. (2014b), Creative Commons Attribution License (<http://creativecommons.org/licenses/by/4.0>)

Figure 4c: Exoskeleton by Kao et al. (multiple slightly different versions exist). - Figure adapted from Kao et al. (2010b), Creative Commons Attribution License (<http://creativecommons.org/licenses/by/2.0>)



## Dankwoord / Thanks

---

Ik heb veel goede herinneringen aan dit onderzoek overgehouden, niet in de laatste plaats omdat zoveel mensen zich vaak net zo betrokken voelden bij het onderzoek als ik. Zonder ook hun inzet was dit onderzoek nooit zover gekomen.

Herman van der Kooij, jij hebt heel veel van het exoskelet onderzoek in Enschede en Delft opgezet. Je hebt talent voor het starten van nieuwe projecten en ik ben blij dat ik aan die projecten mijn bijdrage heb mogen leveren. Ik wil je bedanken voor de vele uren die je hebt besteed aan het begeleiden van mijn promotieonderzoek. Je gaf me de vrijheid als ik het alleen af kon, maar was beschikbaar als het nodig was. We hebben veel gediscussieerd en je was altijd zeer betrokken bij het onderzoek. Als het tegenzat dacht je mee over nieuwe oplossingen of motiveerde je me om het toch nog eens te proberen. Als het mee zat hielp je me om er voor te zorgen dat de resultaten werden gepubliceerd.

Frans van der Helm, na mijn masteropleiding in Twente gaf jij me de mogelijkheid om mijn promotie te starten in Delft. Je volle agenda stond het niet toe om ieder detail te bespreken. In onze discussies waren we vaak opzoek naar de kern van het onderzoeksonderwerp. Bedankt voor de inzichten die dit heeft opgeleverd.

Cor Meijneke, tijdens mijn promotie hebben we ontzettend veel samengewerkt. Je bent als technicus binnen de vakgroep, als masterstudent en via DEMO verbonden geweest aan het project. Je een voortreffelijk ontwerper en je hebt vaak laten dat een ontwerp altijd nog iets mooier, slimmer of lichter kan. Je bijdrage ging veel verder dan alleen het ontwerp van exoskeletten, binnen en buiten je masteropdracht heb je meegedacht over het onderzoek, de experimenten, en de toepassing van de technologie. Je was iemand bij wie ik altijd even kon binnenlopen om samen een idee uit te werken. Ook buiten het lab zijn we vrienden. Bedankt.

Veel de experimenten voor mijn onderzoek heb ik in Enschede gedaan. Dit was niet altijd gemakkelijk, maar zonder de hulp van een aantal mensen was het onmogelijk geweest.

Bram Koopman, onze samenwerking begon al tijdens mijn masterstudie met het meten van loopdata. We hebben samen aan het Evryon-project gewerkt. We hebben veel experimenten uitgevoerd met de Lopes en zijn overal naar toe gereisd om onze resultaten te presenteren. Ik vond het fijn om met je samen te werken en te reizen.

Voor het XPED project hebben in Enschede een aantal mensen klaar gestaan om mij te ondersteuning met de experimenten. Als eerste wil ik Thijs Lohuis bedanken. Je hebt me geweldig geholpen bij het uitvoeren van de experimenten. Als ik 's ochtends in Enschede aankwam had jij alle meetapparatuur opgebouwd en je zorgde er altijd voor dat de metingen netjes verliepen. Ik waardeer de precisie waarmee je alle experimenten uitvoerde.

Mark Vlutters, Annerieke Nijman en Jantsje Pasma, ook jullie wil ik bedanken voor jullie hulp bij de experimenten in Enschede.

Hier wil ik ook Hans Koers en Paulien Langelo bedanken. Ik vond het heel fijn dat ik altijd mocht komen logeren als ik weer een paar dagen in Enschede verbleef.

Shiqian, you were my exoskeleton colleague in Delft. Sometimes our projects were moving in different directions and sometimes we worked close together. We did some good work on the sensor fusion. Also you are close to finishing your dissertation. Good luck with the last bit of it.

Brando Maathuis, Chiel Lintzen, Frans Lafeber en Laurent Huberty, het was mij een genoegen jullie te mogen begeleiden tijdens jullie masteropdracht. Bedankt voor jullie inzet voor het onderzoek, en voor de frisse blik op het onderzoek die jullie meebrachten.

Jan van Frankenhuizen en Guus Liqui Lung, bedank voor alle keren dat er nog even snel iets gemaakt moest worden. Jullie houden het lab in beweging.

Ook wil ik alle proefpersonen bedanken die hebben meegeholpen aan het onderzoek. De oproep om mee te doen aan een exoskelet onderzoek leek misschien soms spannender dan het was en ik heb jullie geduld en inspanningsvermogen soms flink beproefd. Alle data die dit heeft opgeleverd is de basis geweest voor veel van de hoofdstukken van dit proefschrift.

I like to thank everybody from the Delft Biorobotics Laboratory for the good mood in the lab. I would like to thank you for the lively lunch discussions, the coffee

breaks, the beer and board games on Friday afternoons that were often a welcome break from all the work.

Als laatste wil ik nog een paar mensen in het bijzonder bedanken. Niet voor hun bijdrage aan dit proefschrift maar voor de belangrijke rol die ze in mijn leven spelen.

Wim en Thea van Dijk jullie zijn erg bescheiden en jullie laten je niet gemakkelijk in het zonnetje zetten. Nu wil ik jullie een keer bedanken voor alle vrijheid die jullie mij hebben gegeven en de steun bij de keuzes die ik maakte. Jullie waren er altijd voor me. Bedankt.

Johan van Dijk, we zijn samen groot geworden. Ik ben heel blij dat we, ook nu we niet in hetzelfde huis wonen en vaak ook niet in dezelfde stad, zo vaak bij elkaar langs komen.

Baukje Koers, het begin van mijn promotie was ook het begin van samenwonen in Oude Leede en Delft. Dat was het beste plan ooit. We hebben sindsdien superveel meegemaakt. Ik ben blij dat je er altijd bij was en ik kijk uit naar alles wat we nog gaan meemaken.



# Publications

---

First Author:

A Passive Exoskeleton with Artificial tendons: Design and Experimental Evaluation

Wietse van Dijk, Edsko Hekman, Herman van der Kooij

*IEEE International Conference on Rehabilitation Robotics 2011 (2011)*

Feed-forward Support of Human Walking

Wietse van Dijk, Bram Koopman, Renaud Ronse, Herman van der Kooij

*IEEE International Conference on Biomedical Robotics and Biomechatronics 2012*

Improving the Transparency of a Rehabilitation Robot by Exploiting the Cyclic Behaviour of Walking

Wietse van Dijk\*, Bram Koopman\*, Edwin van Asseldonk, Herman van der Kooij

\* equal contributions

*IEEE International Conference on Rehabilitation Robotics 2013*

Optimization of Human Walking for Exoskeletal Support

Wietse van Dijk, Herman van der Kooij

*IEEE International Conference on Rehabilitation Robotics 2013*

Achilles: An Autonomous Lightweight Ankle Exoskeleton to Provide Push-Off Power

Cor Meijneke\*, Wietse van Dijk\*, Herman van der Kooij

\* equal contributions

*IEEE International Conference on Biomedical Robotics and Biomechatronics 2014*

XPED2: A Passive Exoskeleton with Artificial Tendons

Wietse van Dijk, Herman van der Kooij

*IEEE Robotics and Automation Magazine* vol. 21, no. 4, pp. 56–61, (2014)

Evaluation of the Achilles Ankle Exoskeleton

Wietse van Dijk, Cor Meijneke, Herman van der Kooij

*Paper submitted to IEEE Transactions on neural Systems and Rehabilitation Engineering*

Real-time Motion Analysis and Parameter Estimation with a Multibody Kalman Filter

Wietse van Dijk, Herman van der Kooij

*in review*

Not first author:

Evaluation of Spring Implementation to Reduce the Required Motor Energy in a Walking Assist Exoskeleton with Linear Actuation (Walking Assist Machine using Crutches)

Frans Lafeber, Wietse van Dijk, Yukio Takeda

*Applied Mechanics and Materials 2012*

Rendering potential wearable robot designs with the LOPES gait trainer

Bram Koopman, Edwin van Asseldonk, Herman van der Kooij, Wietse van Dijk,

Renaud Ronsse

*IEEE International Conference on Rehabilitation Robotics 2011*

Spring uses in exoskeleton actuation design

Shiqian Wang, Wietse van Dijk, Herman van der Kooij

*IEEE International Conference on Rehabilitation Robotics 2011*

## About the author

---

Wietse van Dijk was born on 17 October, 1983 in Goes, the Netherlands. In 2002 he graduated from high school (Atheneum) at the Christelijke Scholengemeenschap Walcheren. He received his bachelor degree in mechanical engineering at the University of Twente in 2006. After this he continued with a master study Mechanical Engineering with a specialization in biomechanical engineering and a master study in Industrial Design Engineering with a specialization in emerging technology design. As part of his master studies he performed an internship at the University of Calgary. In 2009 he started his PhD research at the Delft University of Technology. Part of this research was carried out within the Evryon project sponsored by the European Union. The goal of the project was to develop a novel approach for the design of wearable robots for rehabilitation, assistance, and human augmentation. During his research he received the best student paper award of the 12<sup>th</sup> International Congress on Rehabilitation Robotics and a travel award for the OpenSim Advanced User workshop august 2014. This dissertation presents the final results of his PhD research.



# Propositions

---

1. It cannot be determined in advance if a new exoskeleton concept is successful.
2. The best exoskeleton research is done without actually building an exoskeleton.
- 3a. Reducing your total carbon dioxide production, carbon footprint, is easy but uncomfortable.
- 3b. Reducing your total carbon dioxide production during walking, with an exoskeleton, is difficult but comfortable.
4. An exoskeleton does not need an own skeleton.
5. The danger of artificial intelligence is not recognizing it.
6. Editing Wikipedia is a bigger contribution to science than writing articles for scientific journals.
7. A nuance is more valuable than a proposition.



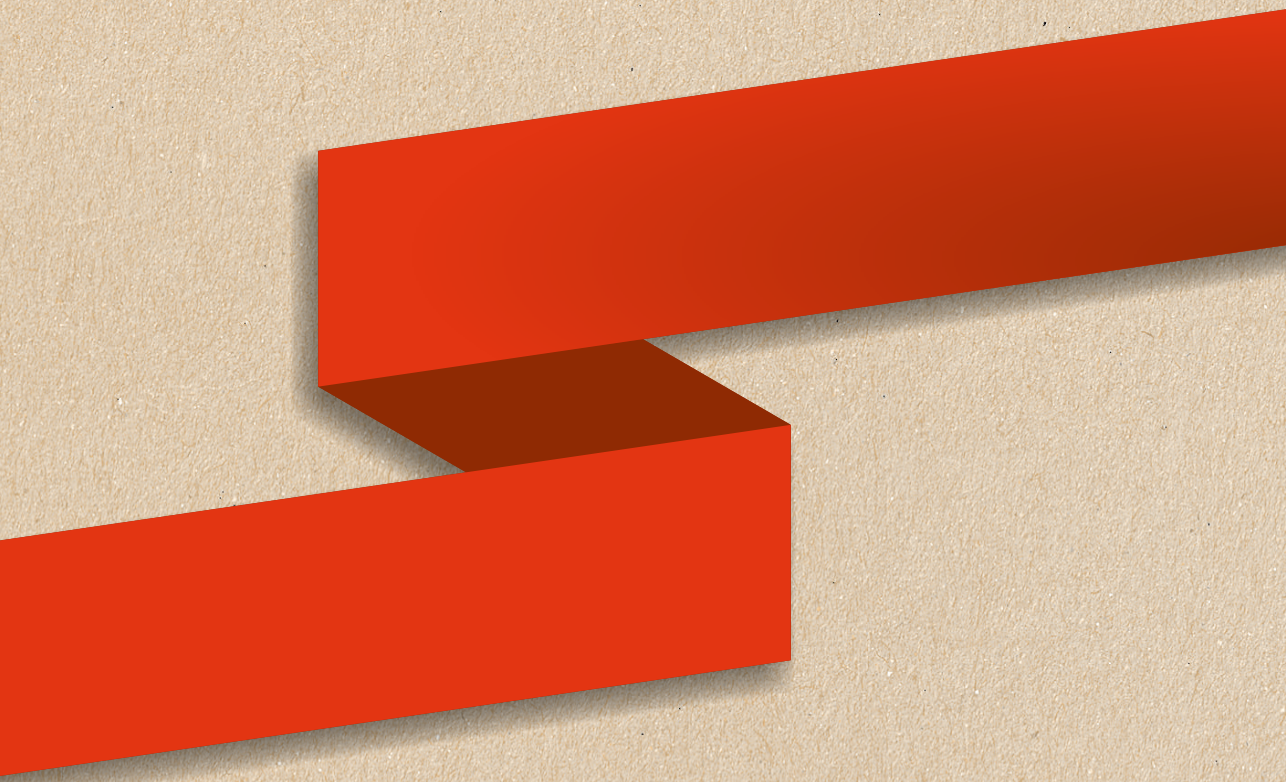
# Stellingen

---

1. Van te voren is niet te bepalen of een nieuw exoskeletconcept goed is.
2. Het beste exoskelet onderzoek doe je zonder een exoskelet te bouwen.
- 3a. Het reduceren van je CO<sub>2</sub> voetafdruk is makkelijk maar oncomfortabel
- 3b. Het reduceren van je CO<sub>2</sub> uitstoot tijdens het lopen, met een exoskelet, is moeilijk maar comfortabel
4. Een exoskelet heeft geen eigen skelet nodig.
5. Het gevaar van kunstmatige intelligentie is het niet (h)erkennen ervan.
6. De wetenschap zou er bij gebaat zijn als men in plaats van artikelen te schrijven voor wetenschappelijke tijdschriften Wikipedia zou aanvullen.
7. Een nuance is waardevoller dan een stelling.







ISBN: 978-94-6186-463-5